

PERFORMANCE ENHANCEMENT OF P3HT:PC₆₁BM
ORGANIC SOLAR CELLS VIA ACETIC ACID TREATMENT
APPROACH

LIM LIH WEI

FACULTY OF SCIENCE
UNIVERSITI MALAYA
KUALA LUMPUR

2022

**PERFORMANCE ENHANCEMENT OF P3HT:PC₆₁BM
ORGANIC SOLAR CELLS VIA ACETIC ACID
TREATMENT APPROACH**

LIM LIH WEI

**THESIS SUBMITTED IN FULFILMENT OF THE
REQUIREMENTS FOR THE DEGREE OF DOCTOR OF
PHILOSOPHY**

**DEPARTMENT OF PHYSICS
FACULTY OF SCIENCE
UNIVERSITI MALAYA
KUALA LUMPUR**

2022

UNIVERSITI MALAYA
ORIGINAL LITERARY WORK DECLARATION

Name of Candidate: **LIM LIH WEI**

Matric No: **17003161/3 (NEW) SHC140098 (OLD)**

Name of Degree: **DOCTOR OF PHILOSOPHY**

Title of Project Paper/Research Report/Dissertation/Thesis (“this Work”):

PERFORMANCE ENHANCEMENT OF P3HT:PC₆₁BM ORGANIC SOLAR CELLS VIA ACETIC ACID TREATMENT APPROACH

Field of Study: **PHYSICS (ORGANIC SOLAR CELLS)**

I do solemnly and sincerely declare that:

- (1) I am the sole author/writer of this Work;
- (2) This Work is original;
- (3) Any use of any work in which copyright exists was done by way of fair dealing and for permitted purposes and any excerpt or extract from, or reference to or reproduction of any copyright work has been disclosed expressly and sufficiently and the title of the Work and its authorship have been acknowledged in this Work;
- (4) I do not have any actual knowledge nor do I ought reasonably to know that the making of this work constitutes an infringement of any copyright work;
- (5) I hereby assign all and every rights in the copyright to this Work to the University of Malaya (“UM”), who henceforth shall be owner of the copyright in this Work and that any reproduction or use in any form or by any means whatsoever is prohibited without the written consent of UM having been first had and obtained;
- (6) I am fully aware that if in the course of making this Work I have infringed any copyright whether intentionally or otherwise, I may be subject to legal action or any other action as may be determined by UM.

Candidate’s Signature

Date: 24th May 2022

Subscribed and solemnly declared before,

Witness’s Signature

Date: 24th May 2022

Name:

Designation:

PERFORMANCE ENHANCEMENT OF P3HT:PC₆₁BM ORGANIC SOLAR CELLS VIA ACETIC ACID TREATMENT APPROACH

ABSTRACT

In this work, an acid acetic solution treatment was developed to improve the performance of the organic solar cells (OSCs) based on bulk heterojunctions regioregular poly(3-hexylthiophene-2,5-diyl) (P3HT):[6, 6]-Phenyl-C₆₁-butyric acid butyl ester (PC₆₁BM). After the deposition of active layer using spin-coating technique, additional treatment step where the solution of the diluted acetic acid with different concentrations (5 %, 10 %, 25 %, 50 %, 75 % and 100 %) was spun on top of the active layer. Current density-voltage (J-V) characteristics under light illumination was used to characterise the photovoltaic effects of the devices. The untreated device showed typical photovoltaics effect with current density (J_{sc}) of 2.0 mA/cm², open circuit voltage (V_{oc}) of 0.58 V, 46 % fill factor (FF) and 0.53 % power conversion efficiency (PCE). All the devices that were treated with acetic acid treatment showed significant enhancement in the J_{sc} and PCE outputs. The highest values of J_{sc} and PCE of the devices occurred at 50 % acetic acid concentration treatment. At this acid concentration, J_{sc} of 11.0mA/cm² with PCE up to 2.04 % can be achieved. On the other hand, V_{oc} remains constant as 0.58 V whereas FF decreased to 32 % due to drastic increase in J_{sc} . It can be seen that the rise of J_{sc} with V_{oc} remain constant in Region III will make the slope of the J-V curve decreases correspondingly, leading to less “squareness” of J-V curve, therefore a lower FF . Hence, this inexpensive and simple technique have demonstrated that acid treatment greatly increased the J_{sc} of the devices and consequently, the PCE of the devices are enhanced up to three folds. In addition, the effect of acid acetic solution treatment on the device physics of polymer solar cells has been investigated through Schottky diode method, Cheung & Cheung method and Norde’s function to provide fundamental insight into electrical parameters of the OSCs. SCLC approach was performed to explain the enhancement of

the current produced by OSC devices treated with acetic acid. The results indicate that the concentration of traps in the treated devices become lower compared to the untreated device. However, optical spectroscopy characterisations of the untreated and treated thin films exhibited similar pattern without any shift in the spectra suggesting that the acid treatment did not alter the molecular packing of the P3HT and PC₆₁BM in the bulk heterojunction system. FESEM measurements revealed that the impurity particles on the active layer have been removed and visible cavities on the surface can be seen after it went through the treatment. The etching effect of the acetic acid may not only create cavities on the surface of active layer but at the same time dissolved the particles/impurities to provide clean surface. Therefore, purification on the active layer surface might have taken place. The reduction of the impurities results in lower series resistance and barrier height which in turn caused the enhancement performance of the OSCs.

Keywords: Organic Solar Cells, Organic Photovoltaics, Acetic Acid Treatment, P3HT:PC₆₁BM, Performance Enhancement

PENINGKATAN PRESTASI P3HT: PC₆₁BM SEL SURIA ORGANIK MELALUI PENDEKATAN RAWATAN ASID ACETIK

ABSTRAK

Dalam karya ini, satu rawatan baru iaitu rawatan asid asetik telah dikemukakan dan digunakan pada sel suria organik berdasarkan heterosimpang pukul *regioregular poly(3-hexylthiophene-2,5-diyl) (P3HT):[6, 6]-Phenyl-C61-butyric acid butyl ester (PC₆₁BM)* untuk meningkatkan prestasi peranti. Selepas pemendapan lapisan aktif, langkah rawatan tambahan yang mana larutan asid asetik yang telah dicairkan, disalutputar di atas lapisan aktif. Ciri-ciri ketumpatan arus-voltan ($J-V$) di bawah pencahayaan digunakan untuk mengenal pasti kesan fotovoltai peranti. Peranti yang tidak dirawat menunjukkan kesan fotovoltai dengan ketumpatan arus (J_{sc}) 2.0 mA/cm² dan voltan litar terbuka (V_{oc}) 0.58 V, 46 % faktor pengisian (FF) dan 0.53 % kuasa kecekapan penukaran (PCE). Semua peranti yang telah menjalani rawatan asid asetik menunjukkan peningkatan dalam J_{sc} dan PCE . Kedua-dua J_{sc} dan PCE yang maksimum berlaku pada rawatan dengan 50 % kepekatan asid asetik. Pada kepekatan asid ini, J_{sc} berjumlah 11.0 mA/cm² dengan PCE bernilai 2.04% dapat dicapai. V_{oc} tetap stabil pada 0.58 V sementara FF menurun menjadi 32 % kerana peningkatan J_{sc} secara drastik. Jelasnya kenaikan J_{sc} dengan V_{oc} kekal malar pada *Region III* akan menyebabkan kecerunan lengkung $J-V$ menurun dan ini menyebabkan kepada ketidaksempurnaan "bentuk segi empat" pada lengkung $J-V$ dan seterusnya menyebabkan FF yang lebih rendah. Maka dengan teknik yang mudah dan mudah ini dapat meningkatkan J_{sc} dengan mendadak dan seterusnya meningkatkan PCE peranti sehingga tiga kali ganda. Tambahan pula, kesan rawatan larutan asid asetik pada fizik peranti sel suria polimer telah disiasat secara terperinci melalui kaedah diod Schottky, kaedah Cheung & Cheung dan fungsi Norde untuk memberikan gambaran asas mengenai sifat elektrik *OSC*. Pendekatan *SCLC* dapat menjelaskan arus yang lebih tinggi yang dihasilkan dalam *OSC* yang dirawat dengan asid asetik. Keputusan menunjukkan

bahawakepekatan perangkap dalam peranti yang telah dirawat dengan asid asetik menjadi lebih rendah berbanding dengan peranti yang tidak dirawat. Walau bagaimanapun, peningkatan prestasi elektrik tidak dapat dijelaskan dengan pengukuran optik spektroskopi. Corak yang serupa tanpa anjakan pada semua spectrum pengukuran yang tersebut menunjukkan bahawa proses rawatan asid asetik tidak mengubah molekul P3HT dan PC₆₁BM dalam sistem. Imej-imej daripada *FESEM* menunjukkan bahawa zarah-zarah kotoran/partikel pada lapisan aktif telah dikeluarkan dan kaviti dapat dilihat pada permukaan lapisan aktif setelah melalui rawatan larutan asid asetik. Kesan kakis asid asetik dipercayai bukan sahaja dapat menghasilkan kaviti pada permukaan lapisan aktif tetapi pada masa yang sama melarutkan zarah-zarah kotoran/partikel bagi menghasilkan permukaan yang bersih. Oleh itu, penghapusan zarah-zarah kotoran/partikel telah merendahkan rintangan bersiri dan *barrier height* pada *OSC* dan seterusnya menyebabkan peningkatan prestasi pada *OSC*.

Kata Kunci: Sel Suria Organik, Fotovoltaik Organik, Rawatan Asid Asetik, P3HT:PC₆₁BM, Peningkatan Prestasi

ACKNOWLEDGEMENTS

This thesis is dedicated to my family, my wife and my daughter. First and foremost, I wish to show my deepest appreciation to my father, Lim Sun Hing, my mother, Yee Kam Foong, my brother, Lim Lee Yoong, my sister, Lim Yee Tying for their concerns, understanding, moral and financial supports as well as encouragements that have enabled me to persist in my work until the end. This work would have been impossible without their unconditional loves. I am extremely grateful for their patient and tolerant on me throughout the pursuance of my Ph. D. degree. Special dedication to my wife, Kika Abe and my daughter Lim Xiao Li. Your arrivals in my life gives me the motivation to continue and never give up on my Ph.D. You have made me stronger, better and more fulfilled than I could have ever imagined.

Besides that, I would like to express my sincere gratitude to my supervisor, Associate Professor Dr. Khaulah Sulaiman and co-supervisor Dr. Azzuliani Binti Supangat for their invaluable guidance, encouragements, advices and assistances given to me throughout the entire progress of this work. Moreover, I am gratefully and deeply appreciate their patient and tolerant on me (especially Associate Professor Dr. Khaulah Sulaiman) for my mistakes, misbehaviours and inefficiency throughout the entire work. I am sorry to cause you so much troubles and inconveniences during these years.

I would also like to express millions thanks to all the members of Low Dimensional Materials Research Centre especially Professor Datin Dr. Saadah Abdul Raman, Professor Dr. Wan Haliza Abd. Majib, Dr. Huang Nay Ming, Dr. Woon Kai Lin, the laboratory assistants, Mr. Muhammad Aruf and Mdm. Norlela Mohamed Shahardin for their kind supports, advices and guidance. Not forgetting to express my gratitude to my seniors especially Dr. Goh Boon Tong and Dr. Gan Wee Chen and my fellow colleagues especially Dr. Chua Chong Lim, Dr. Yeoh Keat Hoe, Dr. Chong Su Sin, Dr. Rahman

Ismiel, Mr. Lee Yen Sian and Dr. Lim Lian Kuang for their companionship, assistances, moral supports, suggestions and understanding which making my working environment interesting and constructive.

Last but not least, I would like to acknowledge University of Malaya and Department Physics for offering the Ph. D. degree to me which allow me pursue my dream. I would also like to acknowledge the Ministry of Higher Education (MOHE) for awarded me the MyPhD scholarship under MyBrain15 program. The scholarship provided 3 years funding for my pursuance of PhD degree which I greatly appreciate.

Universiti Malaya

TABLE OF CONTENTS

ABSTRACT	iii
ABSTRAK	v
ACKNOWLEDGEMENTS	vii
TABLE OF CONTENTS	ix
LIST OF FIGURES	xii
LIST OF TABLES	xv
LIST OF SYMBOLS AND ABBREVIATIONS	xvi
CHAPTER 1: INTRODUCTION	1
1.1 Background.....	1
1.2 Brief History of Organic Photovoltaic Cell.....	3
1.3 Advantages of Organic Solar Cells.....	6
1.3.1 Simple manufacturing process & lower manufacturing cost	6
1.3.2 Low weight & flexibility	7
1.3.3 Tailoring Molecular Properties	7
1.3.4 Short energy payback times & low environmental impact	8
1.3.5 Multiple Uses and Applications	8
1.4 Disadvantages of Organic Solar Cells	9
1.4.1 Disadvantages.....	9
1.5 Objectives	9
1.6 Thesis Organisation	10
CHAPTER 2: LITERATURE REVIEW	11
2.1 Overview.....	11
2.2 Oxygen Plasma Treatment on Indium-tin-oxide (ITO).....	11

2.3	Chemical/Metal Additives Doping in Polymer Blended Solution	12
2.4	Solvent Post-treatment Method on PEDOT:PSS.....	14
2.5	Thermal Post-treatment Method on PEDOT: PSS	17
2.6	Slow Solvent Vapour Treatment on Active Layers.....	17
2.7	Thermal Post-treatment Method on Active Layers	18
2.7.1	Ultraviolet-Ozone Treatment on Active Layers	19
2.7.2	Post Polar Solvent Treatment Method on Active Layers	20
2.8	Summary.....	21
 CHAPTER 3: METHODOLOGY.....		23
3.1	Overview.....	23
3.2	Device Fabrication.....	23
3.2.1	Solution Preparation	23
3.2.2	Substrates Preparation	25
3.2.3	Thin Film Deposition	27
3.2.4	Active Layer Treatment.....	27
3.2.5	Al Electrode Deposition	27
3.3	Thin films/Devices Characterisation Methods	29
3.3.1	Ultraviolet-Visible-Near-Infrared (UV-Vis-NIR) Spectroscopy	29
3.3.2	Field Emission Scanning Electron Microscopy (FESEM).....	30
3.3.3	X-Ray Diffraction (XRD).....	30
3.3.4	Raman Spectroscopy	32
3.3.5	Thickness Measurement	33
3.3.6	J-V Characteristics Measurement.....	34
 CHAPTER 4: ACID ACETIC SOLUTION TREATMENT ON P3HT:PC₆₁BM ORGANIC SOLAR CELLS		35

4.1	Overview.....	35
4.2	Fabrication of ITO/PEDOT:PSS/P3HT:PC61BM/Al Devices	42
4.3	Current-density Curves of the Fabricated Devices under Light Illumination	43
4.4	Investigation of Electrical Properties via Schottky Diode Method	49
4.5	Alternative Methods to Determine Electric Properties from Dark I-V Curves	60
4.5.1	Cheung & Cheung Method.....	60
4.5.2	Norde's function.....	68
4.6	Space Charge Limited Conduction (SCLC) Explanation.....	72
4.7	Ultraviolet - Visible (UV-Vis) Absorption Measurements	80
4.8	Raman Spectroscopy Measurements	82
4.9	X-Ray Diffraction (XRD) Measurements	83
4.10	Field Effect Scanning Electron Microscopy (FESEM) Measurements.....	86
4.11	Investigation of Degradation Process of the Fabricated Devices	88
4.12	Versatility of Acetic Acid Treatment on Other Materials	91
CHAPTER 5: CONCLUSION.....		96
5.1	Conclusion	96
5.2	Future Works	99
REFERENCES.....		101
LIST OF PUBLICATIONS AND PAPERS PRESENTED		108

LIST OF FIGURES

Figure 3.1	: Schematic diagram of pre-patterned ITO substrates.....	27
Figure 3.2	: Selected samples of P3HT:PC ₆₁ BM in solution form and thin film.....	28
Figure 3.3	: Flow chart of thin film deposition and treatment process.....	29
Figure 3.4	: Schematic diagram of the electrical measurement on photovoltaic device.....	35
Figure 4.1	: Photons with energy, $h\nu$ equal or larger than the band gaps, E_g (acceptor) or E_g' (donor) excited the electrons from the HOMO to the LUMO leaving holes behind in the HOMO. Electrons are collected at the anode and holes transported to the cathode.....	38
Figure 4.2	: Equivalent circuit for (a) ideal and (b) practical solar cells, J_{ph} is the photoinduced current density, J_d is the current density of the diode, R_s and R_{sh} are the series and shunt resistance, respectively, J is the current flow in the external load and V is the applied voltage (image taken from (Qi & Wang, 2013)).....	39
Figure 4.3	: The current-voltage curve (J-V curve) of an organic solar cell under dark condition (dash line) and illuminated (full line).....	40
Figure 4.4	: The power-voltage curve (P-V curve) of an organic solar cell under illuminated radiation.....	40
Figure 4.5	: (a) Device structure of ITO/PEDOT:PSS/P3HT:PC ₆₁ BM/Al and (b) Diagram of the fabricated device with connection leg.....	43
Figure 4.6	: The J-V characteristics of the untreated and acetic acid treated ITO/PEDOT:PSS/P3HT:PC ₆₁ BM/Al organic solar cells.....	45
Figure 4.7	: The J_{sc} output and PCE of the untreated and acetic acid treated ITO/PEDOT:PSS/P3HT:PC ₆₁ BM/Al organic solar cells.....	47
Figure 4.8	: The plot of open circuit, V_{oc} and fill factor, FF versus acid concentration.....	49
Figure 4.9	: The current-voltage (I-V) curves of the devices measured in the dark condition at room temperature (300K).....	51
Figure 4.10	: The turn-on voltage by extrapolating I-V curves of the OSC devices in the dark condition. The extrapolation lines in red indicates the turn-on voltage.....	52

Figure 4.11	:	The ohmic region (region I) of the dark I-V curve on the natural logarithmic (ln) scale.....	56
Figure 4.12	:	The linear fitted results for the untreated and acetic acid solution treated devices in the Ohmic region in the dark condition.....	57
Figure 4.13	:	Ideality factor, n versus acetic acid concentration plot of the untreated and acetic acid solution treated devices.....	58
Figure 4.14	:	The linear fitting of $\frac{dV}{d(\ln I)}$ vs I graphs in the linear region for the untreated and acetic acid solutions treated devices.....	62
Figure 4.15	:	Series resistance, R_s versus acetic acid concentration plot for the untreated and acetic acid solutions treated devices extracted from linear fitting of $\frac{dV}{d(\ln I)}$ vs I plots.....	64
Figure 4.16	:	Ideality factor, n versus acetic acid concentration plot for the untreated and acetic acid solutions treated devices extracted from linear fitting of $\frac{dV}{d(\ln I)}$ vs I plots.....	64
Figure 4.17	:	The linear fitting of $H(I)$ vs I graphs in the linear region for the untreated and acetic acid solutions treated devices.....	66
Figure 4.18	:	Series resistance, R_s versus acetic acid concentration plot for the untreated and acetic acid solutions treated devices extracted from linear fitting of $H(I)$ vs I plots.....	68
Figure 4.19	:	Barrier height, Φ_{bo} versus acetic acid concentration plot for the untreated and acetic acid solutions treated devices extracted from linear fitting of $H(I)$ vs I plots.....	68
Figure 4.20	:	The polynomial fitting of $F(V)$ vs V graphs in the linear region based on the Norde's function, for the untreated and acetic acid solutions treated devices.....	70
Figure 4.21	:	Series resistance, R_s versus acetic acid concentration plot for the untreated and acetic acid solutions treated devices determined from Norde's function.....	71
Figure 4.22	:	Barrier height, Φ_{bo} versus acetic acid concentration plot for the untreated and acetic acid solutions treated devices determined from Norde's function.....	72
Figure 4.23	:	Log J versus V plot for the untreated and acetic acid solutions treated devices under light illumination.....	74
Figure 4.24	:	Log J versus V plot for the untreated and acetic acid solutions treated devices under dark condition. Red circle indicates differences which showed in Figure 4.21 as enlarged plot.....	75

Figure 4.25	:	Enlarged plot on the red circle area of Figure 4.20 (Log J versus V plot for the untreated and acetic acid solutions treated devices under dark condition).....	75
Figure 4.26	:	Log J versus log V plot of OSCs with pristine and acetic acid solutions treated P3HT:PC ₆₁ BM active layers in dark condition..	76
Figure 4.27	:	The trap-filling limit voltage, V _{TFL} and concentration of traps, N _t of the untreated and acetic acid solutions treated devices plot against acid concentration.....	81
Figure 4.28	:	UV-Vis spectrum of the untreated and acid treated P3HT:PC ₆₁ BM organic thin films. The pristine films of P3HT and PC ₆₁ BM are also displayed.....	82
Figure 4.29	:	Raman spectroscopy measurements of untreated and acid treated P3HT:PC ₆₁ BM organic thin films.....	84
Figure 4.30	:	The X-ray diffraction (XRD) spectra of the untreated and acetic acid treated P3HT:PC ₆₁ BM organic thin films.....	85
Figure 4.31	:	P3HT crystallites in the blend films with a-axis orientation where main chain parallel and side chain perpendicular to the substrate.....	86
Figure 4.32	:	Field Effect Scanning Electron Microscopy (FESEM) images on the surface of untreated and acid treated P3HT:PC ₆₁ BM organic thin films. The bar-scale is 1 μm.....	88
Figure 4.33	:	The performance of untreated and acid treated P3HT:PC ₆₁ BM organic solar cells for eleven days.....	90
Figure 4.34	:	Normalized absorption spectra of PC ₆₁ BM, BHBT ₂ and BHBT ₂ :PC ₆₁ BM thin films. (Inset) PC ₆₁ BM and BHBT ₂ molecular structure.....	93
Figure 4.35	:	The diagram of device construction of ITO/PEDOT:PSS/BHBT ₂ :PC ₆₁ BM/Al organic solar cell and active layer consists of blended BHBT ₂ :PC ₆₁ BM.....	94
Figure 4.36	:	The J-V characteristics of the untreated and acetic acid treated ITO/PEDOT:PSS/BHBT ₂ :PC ₆₁ BM/Al organic solar cells.....	95

LIST OF TABLES

Table 1.1	: The chronological developments of OPVC.....	6
Table 3.1	: The pre-patterned ITO substrates specifications manufactured by Luminescence Technology Corp.....	26
Table 3.2	: Scan parameters of KLA Tencor P-6 Surface Profilometer.....	34
Table 4.1	: Description of acetic acid treated active layer utilised in ITO/PEDOT:PSS/P3HT:PC ₆₁ BM/Al devices.....	42
Table 4.2	: Photovoltaic properties of ITO/PEDOT:PSS/P3HT:PC ₆₁ BM/Al organic solar cells.....	46
Table 4.3	: Summary of the series resistant, R _s and shunt resistant, R _{sh} of the untreated and acetic acid solution treated OSCs.....	49
Table 4.4	: The turn on voltage and rectification ratio of OSC.....	53
Table 4.5	: The electrical poperties extracted from the Ohmic region of the dark I-V curve with the natural logarithmic scale.....	58
Table 4.6	: Ideality factor, <i>n</i> , series resistant, R _s and shunt resistant, R _{sh} determined from the $\frac{dV}{d(\ln I)}$ vs <i>I</i> graphs based on the Cheung and Cheng method, for the untreated and acetic acid solutions treated devices.....	63
Table 4.7	: Series resistance, R _s , shunt resistance, R _{sh} and barrier height, Φ_{bo} determined from linear fitting of H(<i>I</i>) vs <i>I</i> graphs based on the Cheung and Cheung method.....	67
Table 4.8	: The electrical properties for the untreated and acetic acid solutions treated devices extracted from polynomial fitting of F(<i>V</i>) vs <i>V</i> graphs.....	71
Table 4.9	: The trap-filling limit voltage, V _{TFL} and concentration of traps, N _t of the untreated and acetic acid solutions treated devices extracted from double-logarithmic of the J-V.....	80
Table 4.10	: Summary of Raman spectroscopy measurements of untreated and acid treated P3HT:PC ₆₁ BM organic thin films.....	84
Table 4.11	: The summary of the performance for the untreated and acid solution treated ITO/PEDOT:PSS/BHBT ₂ :PC ₆₁ BM/Al organic solar cells.....	96

LIST OF SYMBOLS AND ABBREVIATIONS

CO ₂	:	Carbon Dioxide
DC	:	Direct Current
PV	:	Photovoltaic
CdTe	:	Cadmium Telluride
CIGS	:	Copper Indium Gallium Selenide
OPV	:	Organic Photovoltaic
OPVC	:	Organic Photovoltaic Cell
Pt	:	Platinum
AgBr	:	Silver Bromide
AgCl	:	Silver Chloride
Se	:	Selenium
MgPc	:	Magnesium Phthalocyanine
DSSC	:	Dye Sensitized Solar Cell
TiO ₂	:	Titanium Dioxide
Ru	:	Ruthenium
Me-PTC	:	N-type Perylene Tetracarboxylic Derivative
H ₂ Pc	:	P-type Metal-free Phthalocyanine
EQE	:	External Quantum Efficiency
V _{oc}	:	Open Circuit Voltage
J _{sc}	:	Short Circuit Current Density
FF	:	Fill Factor
PCE	:	Power Conversion Efficiencies
D8	:	Polymer Donor
Y6	:	Small Molecule Acceptor

ITO	:	Indium-tin-oxide
PEDOT:PSS	:	Poly(3,4-ethylenedioxythiophene):poly(styrene sulfonate)
PDIN	:	Perylene Diimide
Ag	:	Silver
μ_h	:	Hole Mobility
μ_e	:	Electron Mobility
OSCs	:	Organic Solar Cells
P3HT	:	Poly(3-hexylthiophene-2,5-diyl)
PC ₆₁ BM	:	[6, 6]-phenyl-C ₆₁ -butyric Acid Butyl Ester
BHBT ₂	:	2, 2'-Bithiophene End-Capped Dihexyloxy Phenylene Pentamer
O ₂	:	Oxygen
HOMO	:	Highest Occupied Molecular Orbital
LUMO	:	Lowest Unoccupied Molecular Orbital
h ν	:	Photon Energy
E _g	:	Acceptor Band Gaps
E _g '	:	Donor Band Gaps
J-V	:	Current Density-voltage
J	:	Current Density
V	:	Voltage
J _{ph}	:	Photo-generated Current Density
J _d	:	Current Density of Diode
Fe ₃ O ₄	:	Iron (II, III) Oxide Nanoparticles
ZnO	:	Zinc Oxide
SWCNT	:	Single Wall Carbon Nanotube
CNT	:	Carbon Nanotube
F4-TCNQ	:	2, 3, 5, 6-tetrafluoro-7, 7, 8, 8-tetracyanoquinodimethane

PCPDTBT	:	Poly[2, 6(4, 4-bis-(2-ethylhexyl)-4H-cyclopenta[2, 1-b: 3, 4-b0]-dithiophene)-alt-4, 7-(2, 1, 3-benzothiadiazole)]
PET	:	Polyethylene Terephthalate
EG	:	Ethylene Glyco
ZnPc	:	Zinc Phthalocyanine
C ₆₀	:	Fullerene C ₆₀
DMSO	:	Dimethyl Sulfoxide
EMIMBF ₄	:	1-ethyl-3-methylimidazolium Tetrafluoroborate
ME	:	Methoxyethanol
BHJ	:	Bulk Heterojunction
R _s	:	Series Resistance
Wt. %	:	Weight Percent
2-CE	:	2-chloroethanol
Vol. %	:	Percentage by Volume
PTB7-Th	:	Poly[4, 8-bis(5-(2-ethylhexyl) thiophen-2-yl)benzo[1, 2-b: 4, 5-b']dithiophene-co-3-fluorothieno[3, 4-b] thiophene-2-carboxylate]
PC ₇₁ BM	:	Phenyl-C71-butyric Acid Methyl Ester
PL	:	Photoluminescence
CT	:	Charge-Transport
T _g	:	Glass Transition Temperature
UV	:	Ultraviolet
PC ₇₀ BM	:	[6,6]-Phenyl C70-Butyric Acid Methyl Ester
PTB7	:	Thieno[3, 4-b]-thiophene/benzodithiophene
XPS	:	X-Ray Photoelectron Spectroscopy
V _{bi}	:	Built-in Voltage
R _{sh}	:	Shunt Resistance

UV-Vis	:	Ultraviolet-Visible
FESEM	:	Field Emission Scanning Electron Microscopy
XRD	:	X-Ray Diffraction
DI	:	Deionised
SiO ₂	:	Silicon Oxide
R _a	:	Mean Roughness
R _{max}	:	Maximum Roughness Depth
rpm	:	Revolutions Per Minute
Al	:	Aluminium
PbS	:	Lead (II) Sulphide
CCD	:	Charge-Coupled Device
ID/IG	:	Ratio of the Intensity of D-Raman Peak And G-Raman Peak
2D	:	Two Dimensional
SMU	:	Source/Measure Unit
AM 1.5 G	:	Air Mass 1.5 Global
GPiB	:	General Purpose Interface Bus
I-V	:	Current-Voltage
I	:	Current
RR	:	Rectification Ratio
<i>n</i>	:	Ideality Factor
Φ_{bo}	:	Zero Bias Barrier Height
R _s	:	Series Resistance
R _{sh}	:	Shunt Resistance
SCLC	:	Space Charge Limited Current/Conduction
ln	:	Natural Logarithmic
q	:	Electron Charge

k	:	Boltzmann Constant
T	:	Temperature
K	:	Kelvin
A	:	Effective Area
A^*	:	Richardson Constant
I_0	:	Saturation Current
m	:	Slope
m_e	:	Electron Rest Mass
m^*	:	Effective Mass
h	:	Planck's Constant
η_A	:	Absorption Efficiency
η_{ED}	:	Exciton Dissociation Efficiency
η_{CT}	:	Charge Transfer Efficiency
η_{CC}	:	Carrier Collection Efficiency
$H(I)$:	Cheung and Cheung Function
Ω	:	Ohm
$F(V)$:	Norde's Function
γ	:	Dimensionless Arbitrary Integer
V_0	:	Corresponding Voltage of $F(V_0)$
$F(V_0)$:	The Minimum Point of $F(V)$ Versus V Plot
Log	:	Logarithmic
L	:	Thickness
n_f	:	Free Charge Carriers Density
n_{tot}	:	Total Charge Carriers Density
V_{TFL}	:	Trap-Filling Limit Voltage
N_t	:	Concentration of Traps

ϵ_0	:	Permittivity of Free Space
ϵ_t	:	Dielectric Constant of Semiconductor
n_t	:	Trapped Carriers Density
N_V	:	Effective Density of States in Valence Band
E_F	:	Fermi Level
E_i	:	Trap Energy
$h(E)$:	Energetic Distribution of Localised States
TFSCLC	:	Trap-Filling Space Charge Limited Current
nm	:	nanometer
C	:	Carbon
S	:	Sulfur
H	:	Hydrogen
λ	:	Wavelength
d	:	Lattice Constant/Interplanar Distance
μm	:	micrometer
H ₂ O	:	Water Molecule
NMR	:	Nuclear Magnetic Resonance Spectroscopy
FTIR	:	Fourier Transform Infrared Spectroscopy

CHAPTER 1: INTRODUCTION

1.1 Background

As global energy demand is expected to rise rapidly and conventional shrinking fossil-based resources remaining the dominant source, the search of alternative energy resources is one of the mankind's primary challenge for the long term future growth and development. Furthermore, the combustion of fossil fuel produces greenhouse gases such as carbon dioxide (CO₂) is thought to be responsible for the global warming or greenhouse effect. Therefore, alternative energy resources or technologies which are sustainable, reliable, cheap, efficient and have minimal environmental impact is expected to gain a lot of focus. Solar photovoltaic cell is one of the renewable energy technology which is able to provide clean and sustainable energy power much needed by mankind for developments. A photovoltaic solar cell is an electrical device that converts the light energy directly into direct electric current (DC) by taking advantage of the photoelectric effect. Generally, solar photovoltaic cells can be classified into three generations. The first generation solar cells are called traditional, conventional or inorganic (silicon wafer-based) solar cells. They are made of crystalline silicon wafers such as monocrystalline or polycrystalline silicon wafers. They are currently the commercially predominant photovoltaic (PV) technology as a result of their relatively high efficiency and stability. However, they are considered rigid and require complex fabrication techniques which increase the manufacturing complexity and cost.

Second generation solar cells are often called thin film solar cells. Amorphous silicon solar cells, cadmium telluride (CdTe) solar cells and copper indium gallium selenide (CIGS) solar cells are classified into this category. Compared to the first generation solar cells which normally use wafers of up to 200 μm , thin film solar cells are made of semiconductor layers with only a few micrometers thick. This allows thin film solar cells

to be low weight and flexible. The exploitations of using less material in fabrication and lower cost manufacturing processes allow the manufacturers to manufacture and sell the second generation solar panels at a much lower cost. As a result, second generation solar cells are commercially significant in building integrated photovoltaics, utility-scale photovoltaic power stations or in small stand-alone power system. Nevertheless, second generation solar cells tends to have lower efficiency. In addition, the production of second generation solar cells still involve complex fabrication techniques and high energy consumption still associated with the manufacture of this type of solar cells. Furthermore, the second generation solar cells are based on rare earth elements and this becomes a price limiting factor.

Basically, inorganic based solar cells like first and second generation solar cells are more efficient and have longer lifespan. However, these solar cells are energetically and economically costly than conventional means of producing energy (for example, power plants using fossil fuels) due to the complex fabrication techniques, tremendous amount of energy consumption in production and high material costs. Therefore, there is a need to improve on the solar cells already commercially available or even innovate new technologies by making solar energy more efficient, less expensive, ecofriendly and to develop more and different uses so that it can be used by more and more people. Based on this motivation, third generation solar cells emerged as one of the most promising and have been attracting considerable interest and research from the scientists around the world. At present, most of the third generation of solar cells (often referred as emerging photovoltaics) which include a variety of thin film technologies are still in the development or research phase and not commercially available yet. Organic photovoltaic (OPV) is the third generation of rapidly developing solar technology. In contrast to inorganic photovoltaic cells, organic photovoltaic cell (OPVC) is a type photovoltaic cell that uses small organic molecule compounds such as dyes and pigments or semi-

conductive organic polymers as active layer for light absorption and charge transport to generate electricity from light through the photovoltaic effect. This technology has the potential to provide electricity at a lower cost than first and second generation solar technologies. It is particularly promising in the building-integrated PV market because a variety of absorbers can be used to create colored or semitransparent OPV devices. However, efficiency limitations as well as long-term reliability constraints continuously become significant barriers for the organic solar cells to be commercially viable. Nonetheless, its inefficiency and stability drawbacks, along with the low production cost promise and increasing efficiency, making it a popular field in photovoltaics research.

In the following sections, a brief history of the organic solar cells (OSCs) will be described. The advantages and disadvantages of the OSCs as well as the objectives of this research will be discussed. The last section in this chapter is the thesis organization which provides an overview of the remaining structure of the thesis.

1.2 Brief History of Organic Photovoltaic Cell

The invention of the solar/photovoltaic cell can be traced back to the discovery of the photovoltaic effect. The photovoltaic effect is usually attributed to the French experimental physicist Alexander Edmond Becquerel. Alexander Edmond Becquerel discovered photocurrent in 1839 when a platinum (Pt) electrode coated with silver bromide (AgBr) or silver chloride (AgCl) was illuminated in aqueous solution (Green, 2002). However, the importance of the photovoltaic effect was not realized until forty years later, when the phenomenon of photoconductivity was first observed in 1873 by the British electrical engineer Willoughby Smith and also by William Grylls Adams, professor of natural philosophy at King's College, London with his student Richard Evan

Day in 1876. Both worked on selenium (Se) (Adams & Day, 1877; Smith, 1873) . Since then, the solar cells have appeared.

In general, the history of organic photovoltaic cells can be traced back to the early 20th century. Anthracene was the first organic compound whose photoconductivity was observed by Alfredo Pochettino in 1906 and by Max Volmer in 1913 (Moore & Silver, 1960; Spanggaard & Krebs, 2004). These observations marked the beginning of this field. In the 1950s, the first solar cells were made, consisting mainly of organic dyes, chlorophyll, and related compounds. In 1958, Kearns and Calvin, working with magnesium phthalocyanine (MgPc), were able to measure 200 mV photovoltage (Kearns & Calvin, 1958). The first polymer-based solar cells appeared in the 1980s, but these simple photovoltaic devices typically offer limited power conversion efficiencies well below 0.1 %. An important breakthrough came in 1986 when Ching W. Tang discovered donor-acceptor based cells that dramatically increased efficiency to about 1 % (Tang, 1986). In 1991, Brian O'Regan and Michael Grätzel jointly discovered a type of dye-sensitized solar cell (DSSC), or more commonly known as a Grätzel cell, by sensitizing a semiconductor film made of nanometer-sized particles of titanium dioxide (TiO₂). Ruthenium (Ru) complex (O'Regan & Grätzel, 1991). In the same year, the first dye-based solar cell was produced by Hiramoto (Hiramoto, Fujiwara, & Yokoyama, 1991). He made bilayer and triple-layer cells using n-type perylenetetracarboxylic acid-derived pigments (Me-PTC) and p-type metal-free phthalocyanine (H₂Pc) to produce organic p-n heterojunction. The first polymer/C60-based solar cell (or so-called fullerene-based solar cell) was successfully produced in 1993 by Niyazi Serdar Sariciftci (Sariciftci et al., 1993). In fact, to date, this fullerene-based organic solar cell is the most efficient organic solar cell among other types of organic solar cells. In 1995 the first polymer/polymer-based solar cell was invented by Yu and Hall (Halls et al., 1995; Spanggaard & Krebs, 2004; Yu & Heeger, 1995). At present, the development of organic photovoltaic cells has

increased significantly. Intensive research by researchers from all over the world flows into this area. Organic photovoltaics have recently achieved efficiencies of more than 10 % (Kumari, Lee, Kang, Chen, & Yang, 2017; You et al., 2013; J. Zhao et al., 2016). New OPV companies like Heliatek, InfinityPV, OPVIUS GmbH etc. established and innovative products are marketed. In 2018, the tandem structure OPV created by Meng et al. achieved a record efficiency for organic photovoltaic of 17.3 %. The researchers carefully selected several organic semiconductors that able to absorb almost the entire sunlight spectrum absorption with high external quantum efficiency (EQE > 75 %) as well as well-aligned energy levels of the organic semiconductors to reduce the charge recombination in the cell. Therefore, high open circuit voltage, V_{oc} (1.642 V), high short circuit current, J_{sc} (14.35 mA/cm²), high fill factor, FF (73.7 %) as well as high power conversion efficiency, PCE (17.36 %) has been achieved (Meng et al., 2018). Researchers have developed acceptors with small molecules that, due to their good energy resistance, can also have high voltages in open circuits. By combining a small molecule acceptor (Y6) with a polymer donor (D18), Liu et al. have fabricated organic solar cells in the laboratory with a structure of ITO/PEDOT:PSS/D18:Y6/PDIN/Ag giving high efficiencies over 18 % with a V_{oc} of 0.859 V, a J_{sc} of 27.70 mA/cm² and a FF of 76.6 %. The cell achieved over 80 % in EQE at 460-740 nm, with a maximum of 87 % at 540 nm indicating efficient photocurrent generation. The balanced charge carrier transport ($\mu_h/\mu_e = 1.06$ where μ_h is the hole mobility and μ_e is the electron mobility) accounts for the high FF. Their bimolecular recombination results showed reduced charge recombination in the device facilitated the charge transport thus improved J_{sc} and FF. The organic solar cells with a PCE of 18.22 % is considered the highest efficiency achieved from organic solar cells to date (Q. Liu et al., 2020).

Table 1.1: The chronological developments of OPVC.

Year	Achievement	Reference
1839	Alexander Edmond Becquerel discovered the photovoltaic effect.	(Green, 2002)
1873	Willoughby Smith observed the photoconductivity of selenium.	(Smith, 1873)
1906	Alfredo Pochettino observed the photoconductivity in anthracene.	(Spanggaard & Krebs, 2004)
1950s	Organic dye, chlorophyll and related compounds photovoltaic devices started to emerge.	(Spanggaard & Krebs, 2004)
1958	Kearns & Calvin et al. measured photovoltage of 200mV in MgPc device.	(Kearns & Calvin, 1958)
1986	Bilayer heterojunction OPVC was invented by Ching W. Tang et al.	(Tang, 1986)
1991	First dye/dye based OPVC was fabricated by Hiramoto et al.	(Spanggaard & Krebs, 2004)
1992	First fullerene based OPVC was invented by Niyazi Serdar Sariciftci et al.	(Spanggaard & Krebs, 2004)
1995	Yu & Hall invented first polymer/polymer based solar cells.	(Spanggaard & Krebs, 2004)
2005	Kuwat Triyana et al. reported a tandem OPVC with an efficiency of 1.38%.	(Triyana, Yasuda, Fujita, & Tsutsui, 2005)
2009	Kwanghee Lee and Alan J. Heeger et al. fabricated 6.1 % power conversion efficiencies (PCE) & near 100 % internal quantum efficiency fullerene based OPVC.	(Park et al., 2009)
2013	First certified polymer solar cell efficiency above 10% was reported by You et al.	(You et al., 2013)
2016	Zhao et al presented organic solar cells (OSCs) with PCE up to 11.7 %	(J. Zhao et al., 2016)
2016	Kumari et al's ternary organic solar cells achieved PCE of 12.1 %	(Kumari et al., 2017)
2018	A record efficiency for organic photovoltaics of 17.3 % was achieved by the tandem structure by Meng et al.	(Meng et al., 2018)
2020	The organic solar cells with a PCE of 18.22 % is considered the highest efficiency achieved from organic solar cells to date is fabricated by Liu et al.	(Q. Liu et al., 2020)

1.3 Advantages of Organic Solar Cells

1.3.1 Simple Manufacturing Process & Lower Manufacturing Cost

Organic solar cells are relatively easy to manufacture compared to silicon-based solar cells due to the molecular nature of the materials used. The molecules (which are larger than atoms) used in organic solar cells are easier to work with and present versatility in their production methods such as solution processes (paints or inks), roll-to-roll

technology, high throughput printing techniques, evaporation method and et cetera making large scale production possible. These methods do not have high energy and temperature demands as conventional silicon based solar cells resulting in low production cost. The organic active layers can be deposited as thin films that are much thinner than silicon cells (on the order of several hundred nanometers). The reduction in the use of materials can further reduce the cost production significantly.

1.3.2 Low Weight & Flexibility

Organic solar cells can be lightweight and flexible compared to their heavy and rigid counterparts. These characteristics are important for small autonomous sensors or devices. They are potentially disposable and inexpensive to fabricate allowing them to have versatile applications. A variety of portable and even roll form devices are possible, and their light weight and flexibility make storage, installation and transportation easier.

1.3.3 Molecular Properties Adjustment

A key advantage of the organic semiconductors used in the manufacture of organic solar cells is the capability to tailor the properties of molecules in order to fit versatile applications. Through molecular modifications (e.g. by modifying functional group and the length of polymers), bandgap, the molecular mass and ability to generate charges can be changed allowing for electronic tunability. Moreover, organic molecules can be combined with inorganic molecules to create new unique formulations which making the printing of the organic solar cells in any desirable color or pattern possible.

1.3.4 Short Energy Payback Times & Low Environmental Impact

The ease of utilising organic materials, versatile production methods, possible large scale production, low consumption of fabrication materials resulting low production cost of organic solar cells. The energy required to manufacture an organic solar cell is much lower than the amount of energy required for a conventional inorganic cells. As a result, the energy conversion efficiency of organic solar cells need not be as high as energy conversion efficiency of conventional inorganic cells. All these factors have shorten the energy payback time of organic solar cells and contribute a low environmental impact. The widespread usage of organic solar cells could contribute to an increase in the use of solar energy worldwide and make renewable energy friendlier to average consumers.

1.3.5 Multiple Uses and Applications

The abovementioned versatility of production methods, low weight and flexibility characteristics as well as tunable molecular properties enable organic solar cells to exist in various forms, portable and highly useful on curved building/object surfaces and wide-ranging applications. Organic solar cells also exhibit potential in applications on walls, windows, roof top, flexible electronics etc. due to the translucency of organic solar cells.

Organic solar cells are not currently seen as a replacement for silicon cells in the energy conversion field. Nevertheless, their applications are more targeted towards specific implementations such as recharging surfaces on camping tents/bags for smart phones, laptops or to power small portable devices such as digital cameras, MP3 players and cellphones.

1.4 Problem Statement of Organic Solar Cells

1.4.1 Disadvantages

Organic solar cells have drawbacks and it is not a mature technology. The major disadvantages of organic photovoltaic cells are their low efficiency (only 5 % average efficiency compared to 15 % average efficiency for silicon cells), low stability and low strength. Relatively poor extraction and generation of charges carriers limits the organic solar cells efficiency. The low carrier mobility of organic semiconductors greatly limits the organic solar cells efficiency. In addition, device architecture, absorption spectrum, and position of the energy levels with respect to vacuum factors can affect the efficiency of organic solar cells too. Furthermore, the performance of organic solar cells can be strongly affected by the active layer morphology and polymer microstructure (Vandewal, Himmelberger, & Salleo, 2013). Organic moieties are volatile entities that will easily react with other molecules such as moisture and oxygen. Consequently, they change or degraded causing loses of original properties and strength. As with any new technology, there are many major obstacles that must be overcome before the final product can be brought to market. Nonetheless, the organic solar cells inefficiency and stability problems along with its promise of low costs production and gradually increased efficiency making it a popular field in photovoltaic research.

1.5 Objectives

Organic solar cells offer great technology potential as an alternative renewable source of energy. The search for cheap renewable energy sources is the driving motivation for the new approaches in the development of low-cost photovoltaic cells. Therefore, four main objectives are being focused in this research in order to search and develop a new

approach to fabricate and characterise an efficient and cost effective organic solar cells.

Below are the details of these four main objectives:

1. To fabricate and examine bulk heterojunction organic solar cells based on poly(3-hexylthiophene-2,5-diyl):[6, 6]-phenyl-C61-butyric acid butyl ester (P3HT:PC₆₁BM),
2. To investigate the effects of acetic acid solution treatment on the surface morphology, light absorption spectroscopy and Raman spectroscopy of the P3HT:PC₆₁BM active layer,
3. To examine the influence of acid acetic solution treatment on the photovoltaic parameters for the devices under AM 1.5 and intensity of 100 mW/cm² simulated solar illumination,
4. To obtain correlation between the enhancement in the photovoltaic performance and the physical parameters using Schottky junction approach for the devices in the dark.

1.6 Thesis Organisation

The first chapter has covered basic background of organic solar cells: solar cells classification, brief history, advantages and disadvantages of organic solar cells. Chapters 2 covers the literature review of the treatment methods which have performed by researchers throughout the global. Chapter 3 describes the methodology of the experiments and characterisation methods. Chapter 4 discusses the results and analysis after the P3HT:PC₆₁BM organic solar cells gone through the acid treatment. Finally the conclusion of the research and offers recommendations for improvements to this work are presented in Chapter 5.

CHAPTER 2: LITERATURE REVIEW

2.1 Overview

As mentioned in Chapter 1, one of the challenging hurdle that prevent organic solar cells from commercialise in the market is their low efficiencies. Currently, the average efficiency of the P3HT:PC₆₁BM organic solar cells fabricated in laboratory is still less than 5 % efficient (Campoy-Quiles et al., 2008; Chen, Nakahara, Wei, Nordlund, & Russell, 2011; Chi, Qu, Wang, & Wang, 2014; Dang, Hirsch, & Wantz, 2011; Kim et al., 2006; Ma, Yang, Gong, Lee, & Heeger, 2005; Vanlaeke et al., 2006). Due to this reason, the efficiency of the organic solar cells still need to be greatly improved for commercial applications. There are a lot of methods have been tried to enhance the performance of the organic solar cells. Generally, those methods can be performed in the pre-production stage such as oxygen plasma treatment on ITO or postproduction stage such as slow solvent treatment and thermal annealing on photoactive layers. The following sections will discuss about some of the common practices of organic solar cells treatments being used in organic solar cells fabrication by researchers throughout the globe.

2.2 Oxygen Plasma Treatment on Indium-Tin-Oxide (ITO)

The electronic properties of organic/metallic interfaces are a major problem in organic electronic devices. A metal with a suitable work function is preferred to use as the anode of the organic solar cells either for electron injection into or extraction out of the photoactive layer. One of the biggest challenge for these organic devices is the relatively poor charge extraction at the anode which is normally indium-tin-oxide (ITO). ITO is renowned for its use in organic devices due to its semitransparency, high conductivity and capability of carrier injection into the organic layer in thin film form (Hashimoto & Hamagaki, 2006). Oxygen (O²) plasma treatment has been introduced to treat the surface

of ITO in the OPVC processing for performance enhancement. This technique has previously been used to improve electron extraction in bulk heterojunction organic solar cells and electron injection in organic light emitting diodes (Hashimoto & Hamagaki, 2006). The ITO work function could be improved by plasma treatments to fulfill a better match between the anode energy levels and the highest occupied molecular orbital (HOMO) of the hole conducting material. The improvement of the short-circuit photocurrent density suggests that the increase in the work function of ITO plays a role in increasing the hole injection ability at the interface. It can be attributed to alteration of the oxidation structure on the ITO surface in addition to the removal of organic contaminants. A large increase in photocurrent and fill factor (FF) was observed in the devices upon modification by the O₂ plasma resulting in a net increase in power conversion efficiency (PCE). The injection current density improves with the plasma treatment verified by the decline in the series resistance. The increase in FF for plasma treated devices may be due to the overall decrease in series resistance obtained from the slope of the current density versus voltage (J-V) curves for the voltage condition, $V > V_{oc}$.

2.3 Chemical/Metal Additives Doping in Polymer Blended Solution

González et al. doped the blended P3HT:PC₆₀BM with different concentrations of iron (II, III) oxide nanoparticles (Fe₃O₄) able to bring up the PCE of the OSCs from 3.05 % to 3.37 % which was an improvement of 11 %. The FF also showed 12 % of improvement (from 56.5 % to 63.5 %) after the low doping concentration of Fe₃O₄. They attributed the enhancements were due to lower recombination current which increased effective lifetime of exciton. The occupancy of heavy atoms offered the system an increase of spin-orbit coupling which increased the efficiency of the exciton intersystem crossing process in the

devices. This indicates that a longer effective exciton lifetime is achievable and thereby a lower recombination current. They also stated that the increase in performance cannot be attributed to the changes in morphology or crystallinity (González et al., 2015).

The research group of Oseni et al. has done the investigation on P3HT:PC₆₁BM blend active layers containing zinc oxide (ZnO) doped single wall carbon nanotube (ZnO:SWCNT) nanocomposite at various concentrations. They observed enhanced photocurrents and improvement in power conversion efficiencies (PCE) as high as 31 % for P3HT:PC₆₁BM blend with ZnO:SWCNT (Oseni et al., 2018). They postulated that the improvement is a result of the creation of efficient charge percolation paths in the photoactive layer and improved photon harvesting. Nevertheless, ZnO doping level should not be too high in the ZnO:SWCNT synthesis for efficient photon collection. This is because the higher concentration of ZnO will stimulate the agglomeration of carbon nanotubes (CNT) which will obstruct charge transport mechanism in the photoactive layer. Therefore, the overall performance of the ZnO:SWCNT doped devices at loading concentration more than 6 % is very low.

Scientists in Germany introduced molecular dopant of 2, 3, 5, 6-tetrafluoro-7, 7, 8, 8-tetracyanoquinodimethane (F4-TCNQ) into blends of poly[2, 6(4, 4-bis-(2-ethylhexyl)-4H-cyclopenta[2, 1-b: 3, 4-b0]-dithiophene)-alt-4, 7-(2, 1, 3-benzothiadiazole)] (PCPDTBT) and [6, 6]-phenyl-C₆₁-butyric acid methyl ester (PC₆₁BM) through co-solution in the concentrations range of 0 % to 1 %. They demonstrated that the mobility and conductivity of the holes increased with the doping concentration. The open circuit voltage, V_{oc} and short circuit current, J_{sc} of the corresponding solar cells can be improved by doping at 0.5 %, resulting in improved power conversion efficiencies. The performance improvement is discussed in terms of trap filling owing to the increase of carrier density as well as the decline in recombination which is related to the increase in

mobility. The doping caused increase in the current from 9.42 to 10.31 mA/cm² and an enhancement in the overall solar cell efficiency from 3.28 % to 3.62 %. (Veysel Tunc et al., 2012)

2.4 Solvent Post-treatment Method on PEDOT:PSS

In 2011, Kim et al. adopted optimized solvent post-treated PEDOT:PSS films on glass and polyethylene terephthalate (PET) substrates as anode for small molecule based organic solar cells without using ITO successfully generated roughly same power conversion efficiency as that of the solar cell with an ITO anode. They first mixed PEDOT:PSS solutions with ethylene glycol (EG). The formulations were filtered and spin-coated on glass and PET substrates. The spin coated PEDOT:PSS films were subsequently annealed on a hot plate at 120 ° C for 15 min in ambient atmosphere. After thermal annealed, the samples were immediately immersed and cooled in an EG bath for 0-30 minutes. After that, the samples were again thermal annealed at 120 ° C for 15 minutes. The removal of residual water in the PEDOT:PSS film by substrate pre-heating has greatly enhanced the performance of solar cells with a decrease in the series resistance of the solar cell. The highest conductivity of 1418 Scm⁻¹ has been obtained for a single layer PEDOT:PSS film. By using this ITO-free, highly conductive PEDOT:PSS film, small molecule based organic solar cells with a bulk heterojunction zinc phthalocyanine (ZnPc):fullerene C₆₀ (ZnPc:C₆₀) have been produced on glass and PET substrates and realised PCE of 2.54 % and 1.95 % respectively. They claimed this method caused a reduction in the insulating PSS of conductive polymer layer along with the rearrangements and conformational changes of the PEDOT:PSS polymer chains when exposed to a high boiling point solvent, treated in the solvent bath or mixed with the high boiling point solvent.

According to Luo et al., PEDOT:PSS can be improved by addition of polar solvent, dimethyl sulfoxide (DMSO) into the PEDOT:PSS solution. Moreover, they performed post-treatment of PEDOT:PSS thin films with a mixture of DMSO and ionic liquid, 1-ethyl-3-methylimidazolium tetrafluoroborate (EMIMBF₄) which in turn is much more effective than direct addition of DMSO to the PEDOT:PSS solution. It is shown that both DMSO addition and post-treatment induced morphological changes where an interconnected network of elongated PEDOT grains is generated subsequently leading to higher electrical conductivity. In contrast, for those films post-treated in the presence of EMIMBF₄, an interconnected network of short and circular PEDOT grains with increased polaron density is created. With DMSO post-treatment, elongated PEDOT grains (mainly in the bipolaron state) can be observed. The application of EMIMBF₄ in the post-treatment triggers the formation of a network with short, circular PEDOT grains (Luo et al., 2013).

Hu et al. investigated the effects of poly(3, 4-ethylenedioxythiophene): poly(styrene sulfonate) (PEDOT:PSS) films treated with methoxyethanol (ME) on the performance of bulk heterojunction (BHJ) poly(3-hexylthiophene):[6,6]-phenyl-C₆₁-butyric acid methyl ester (P3HT:PC₆₁BM) OSCs and the effects were compared with the PEDOT:PSS films treated with dimethyl sulfoxide (DMSO). Various concentrations of methoxyethanol (ME) and dimethyl sulfoxide (DMSO) were added to the PEDOT:PSS solutions. They alleged that the enhanced conductivity of the treated PEDOT:PSS improved the short circuit current, J_{sc} and reduced the series resistance, R_s of the organic solar cells. However, the enhanced conductivity and surface roughness of the treated PEDOT:PSS thin films also induced the large leakage current and sacrificed the device fill factor FF. The open circuit voltage, V_{oc} was almost constant although slightly reduced voltage was observed. Their device with the PEDOT:PSS treated with 10 weight percent (wt. %) of ME and DMSO (1:1) exhibits performance characteristics with J_{sc} of 10.88 mA/cm², V_{oc} of 0.62

V, FF of 67 %, which results in PCE of 4.52 %. By comparison, the pristine device performed with V_{oc} of 0.64, J_{sc} of 8.25 mA/cm², FF of 0.66 and PCE of 3.48 %. (Z. Hu, Zhang, & Zhu, 2014).

Jang et al. succeeded in increasing the electrical conductivity of poly(3,4-ethylenedioxythiophene):poly(styrene sulfonate) (PEDOT:PSS) films by post-treatment with an alcohol-based solvent which is called 2-chloroethanol (2-CE) and improved the OSCs performance. They spin coated PEDOT:PSS thin film which has added 5 percentage by volume (vol %) DMSO and annealed the thin film at 140 °C in ambient air as a reference sample. For the 2-CE treatment, 2-CE was applied on the PEDOT:PSS thin films without additives for 3 minutes and then spun to remove the remaining liquid. Thermal annealing is carried out to completely dry the solvent. The OSCs based on the bulk heterojunction (BHJ) of poly[4, 8-bis(5-(2-ethylhexyl) thiophen-2-yl)benzo[1, 2-b:4, 5-b']dithiophene-co-3-fluorothieno[3, 4-b] thiophene-2-carboxylate] and phenyl-C71-butyric acid methyl ester (PTB7-Th:PC₇₁BM) were fabricated onto PEDOT:PSS thin films. Based on their results, the PEDOT:PSS thin film which has been treated with 2-CE produced notably better performance (PCE = 9.04 %) than the thin film that added DMSO (PCE = 7.63 %). Their direct-current (DC) conductivity measurements of the samples achieved 762.1 Scm⁻¹ which was 70 % higher than that of the control film that added DMSO. The PEDOT-to-PSS ratio was remarkably reduced for the 2-CE-treated thin film, showing that the 2-CE post-treatment eliminated the insulating PSS component from the polymer matrix. The photoluminescence (PL) intensity was lower when the 2-CE treatment was applied compared to the case when DMSO was added, which indicates that greater PL quenching due to better exciton dissociation occurred in the active layer of the 2-CE-treated PEDOT:PSS. In addition, the 2-CE-treated PEDOT:PSS anode exhibited lower charge-transport resistance than the DMSO-added film, as demonstrated by impedance spectroscopy (Jang et al., 2020).

2.5 Thermal Post-treatment Method on PEDOT:PSS

Thermal annealing of the poly(3,4-ethylenedioxythiophene): poly(styrenesulfonate) (PEDOT:PSS) layer is by far the most direct and easiest method to improve the performance of OSCs. This step can be considered as a compulsory step in OSCs fabrication if the devices involved are utilising PEDOT:PSS. Kim et al. annealed the PEDOT:PSS layer at high temperatures (200-230 °C) proved to have increased the J_{sc} of the P3HT:PC₆₁BM OSCs slightly but decreased FF. They proposed that these effects were caused by variations in conductivity and surface roughness of the PEDOT:PSS layers with thermal annealing temperature. They observed the work function was decreased with an increase in annealing temperature whilst remaining high enough to provide an ohmic contact with P3HT (Kim, Ballantyne, Nelson, & Bradley, 2009).

Friedel et al. conducted studies on the thermal annealing effects on PEDOT:PSS based on various of annealing temperature ranged from 120 and 400 °C. They found out the optimum annealing temperature of PEDOT:PSS for their OSCs is at 250 °C. They concluded that the performance enhancement is associated with loss of water from the PSS shell of the PEDOT:PSS grains. For annealing temperatures above 260 °C, device performance was dramatically reduced. This was associated with chemical decomposition leading to loss of sulfonic acid groups causing a breakdown in device performance (Friedel et al., 2009).

2.6 Slow Solvent Vapour Treatment on Active Layers

Slow solvent vapor treatment is one of the treatment that effect the surface morphology of the organic solar cells active layer. Generally, the treatment was performed by utilising the vapour of the solvent which used to dissolve the active materials to slowly treat the surface of the active layer in a confine area full with evaporating solvent vapour.

Container was used to confine the vapour inside the container and samples were put inside the container to allow the vapour slowly and continuously treated the surface of the active layer. Slow solvent vapour treatment produced rougher surface morphology suggests the formation of the inter-penetrating P3HT:PCBM molecular network. It is also suggesting the treatment able to increase the crystallinity of the active layer due to the decelerated release of the residual solvent during the solidification of the blend film improves the self-organization of the active layer. The observed improvement in the electrical characteristics of the slow solvent vapor treatment cells is caused by the favorable change on the polymer morphology of the blend P3HT:PCBM films. Notably, the series resistance (R_s) of the slow solvent vapour treatment devices is markedly reduced. The slow solvent vapour treatment films exhibit better crystallinity, optical absorption and polymer morphology than the as-cast films. The power conversion efficiency of such fabricated solar cells was improved (Guo et al., 2008).

2.7 Thermal Post-treatment Method on Active Layers

Thermal annealing is a well-known method to optimize the important OPVC parameters. A large number of experimental studies have investigated the role of thermal annealing in the effect of charge photogeneration in organic donor/acceptor blend films and these observations to an increase in the crystallinity of the material. Geminate recombination has been associated with thermal annealing in several reports, although a number of other explanations for the effect of annealing on device performance have been suggested in the literature. The crystallinity of P3HT increased with thermal annealing, which leads to stronger interactions between the chains and thus increases the mobility of holes. It is believed that this crystallisation process stimulated the formation of distinct P3HT phases and PCBM aggregates in the blend film due to more orderly packing of the

polymer chains. Hence, phase segregation is improved upon thermal treatment. The higher photocurrents measured as a resultant of the change of morphology upon thermal annealing have most often been ascribed to the increment in charge carrier mobility. An alternative possibility for the increase in photocurrent is a reduction in geminate recombination losses, thereby increasing the efficiency of charge-transport CT-state dissociation into the free charge carriers. Annealing at higher temperatures causes a deterioration of device performance, characterized by a fall in both J_{sc} and FF and a corresponding increase in V_{oc} . This may be due to an increased mixing of the components upon reaching the glass transition temperature, T_g of the blend, leading to a degradation of the transport properties in the blend or deterioration of the contact with the electrodes. No change in spectral shape was observed after device annealing. This indicates that the enhanced photocurrent generation is mainly due to the improved charge carrier mobilities, rather than to improve light harvesting. The increase in fill factor and decrease in series resistance is consistent with improved transport properties in the blend films upon annealing (Dittmer et al., 2000; Kim et al., 2005).

2.7.1 Ultraviolet-Ozone Treatment on Active Layers

Hu et al. have performed the ultraviolet (UV)-ozone treatment on ITO surface and the influence of the treatment to their fabricated bulk heterojunction organic solar cells based on the blend of poly(3-hexylthiophene-2,5-diyl) (P3HT) and [6,6]-phenyl C_{61} butyric acid methyl ester ($PC_{61}BM$) was investigated. They found that the devices with the UV-ozone treatment for 5 minutes on ITO substrates show the better performance, compared with the devices without this treatment. Their device J_{sc} increased from 2.68 mA/cm^2 to 4.13 mA/cm^2 and the FF of the treated device enhanced from 32.2 % to 38.8 % leading to improvement of the power conversion efficiency from 0.62 % to 1.08 %. They claimed

that the enhancement of OSC after gone through the UV–ozone treatment on ITO surface were the removing carbon atoms from the ITO surface and increase the surface oxygen concentration, thereby raise the work function of the ITO. The Fermi level of ITO substrate became close to the HOMO of P3HT due to UV–ozone treatment on ITO substrate therefore the J_{sc} could be enhanced due to the lowered hole potential barrier between HOMO of P3HT and the Fermi level of ITO after UV–ozone treatment (T. Hu et al., 2009).

Cheng et al. have applied detergent, UV-ozone and combination of detergent + UV-ozone treatments on ITO surface. They claimed that the ITO surface cleaned by detergent for 5 minutes and by UV-ozone for 20 minutes results in significant increase in the work function value from the untreated ITO which is 4.82 eV to 5.22 eV. The combination treatment successfully increased the power conversion efficiency for their organic solar cell from 1.1 % to 2.12 % (Y.-T. Cheng et al., 2010).

2.7.2 Post Polar Solvent Treatment Method on Active Layers

Several independent groups have found that treatments with polar solvents such as acetonitrile, ethanol, methanol, or mixed solvents that applied on organic solar cells prior to the metal electrodes deposition can notably enhance performance of the device. It is believed that the positive effects of solvents on the device performance optimize the phase separation in bulk heterojunctions (BHJ) active layers or perhaps even changed the interface between the BHJ active layer and the poly(3,4-ethylenedioxythiophene):poly(styrenesulfonate) (PEDOT:PSS) layer. Polar solvents are also thought to modify the crystallinity within P3HT-containing BHJ solar cells. Zhou et. al. have tried to use methanol solvent to treat their polymer: fullerence BHJ solar cells based on a low-bandgap donor material thieno[3, 4-b]-thiophene/benzodithiophene

(PTB7) and [6,6]-phenyl C₇₀-butyric acid methyl ester (PC₇₀BM). Their devices exhibited concurrent increases in short-circuit current (J_{sc}), open circuit voltage (V_{oc}), and fill factor (FF), resulting in a significant increase in power conversion efficiency (PCE). Treatment with methanol did not cause significant changes in the morphology and roughness of the film. There was also no visible change in the film thickness confirmed by profilometry and no obvious change in the absorption spectrum of the PTB7:PC₇₀BM film after methanol treatment, indicating that there was no surface reconstruction of the PTB7:PC₇₀BM mixture after methanol treatment. X-ray photoelectron spectroscopy (XPS) results showed that the effect of methanol treatment on the chemical composition of the PTB7:PC₇₀BM film surface was negligible. Methanol treatment induced passivation of surface traps, lowered series resistance, accelerated as well as elevated charge extraction, increased hole mobility and reduced charge recombination due to increase of built-in voltage (V_{bi}) and/or decrease of trap density. All these improvements resulted in the observed increase in J_{sc} and FF. (X. Liu, Wen, & Bazan, 2012; Zhou et al., 2013). The shunt resistance (R_{sh}) increased and the series resistance (R_s) decreased after polar solvent treatment indicate that better diode characteristics were obtained after simple ethanol treatment.

2.8 Summary

In this chapter, various of approaches and strategies have been carried out by researchers aiming at improving the overall performance of OSCs have been discussed. These approaches have been performed either on the electrodes of the OSC or on the active layer of the OSC as well as whole device was under treatment for example thermal annealing method. By any means, these methods have their own disadvantages such as require sophisticated equipment/instrument, complex and complicated processes, delicate

controls of variables/environment etc. This in turn will increase the cost of fabrication of the OSC. However, the biggest issue is that all of these methods that has been discussed in this chapter are not able to enhance the performance of OSC significantly. Furthermore, the problem of these treatments are being too specialised to perform on certain material which has limited the usage of these methods on other organic semiconductors that are being used to fabricate OSC. Although the efficiency of OSCs has recorded a new milestone in recent years (T. Liu et al., 2021; Xiao et al., 2021; Xie et al., 2018; Y. Zhang et al., 2018), further improvement in both efficiency and stability are yet required for their real-world application and possible commercialization of these devices. There is none research work that used different concentration of acetic acid solutions as a treatment to the surface of active layer to enhance the performance of OPV. However, there is one study that can be related to this research where the researchers have used different concentration of acetic acid as solvent additive to fabricate the bulk heterojunction active layers based on P3HT:PCBM blend through electrospray fabrication of OPV devices (X.-Y. Zhao et al., 2014). They claimed that the organic solvent with strong polarity as acetic acid can be the conductivity booster for electrospray fabrication of OPV devices due to electrical conductivity of solvent plays the most critical role because it directly affects the droplet diameter and subsequently the film nanostructure and morphology. Therefore for their work, they added acetic acid in the mixed solvent for the purpose of film nanostructure and morphology and not for OPV devices treatment.

CHAPTER 3: METHODOLOGY

3.1 Overview

In this chapter, the processes involved in the device fabrication including substrate preparations, solution preparations, thin films deposition, active layer treatments and electrodes deposition will be presented in details. The characterisations of the device such as J-V characteristics measurements, Ultraviolet-Visible (UV-Vis) spectroscopy, Raman spectroscopy, X-Ray Diffraction (XRD), Field Emission Scanning Electron Microscopy (FESEM) will be described in detail.

3.2 Device Fabrication

3.2.1 Solution Preparations

Regioregular poly (3-hexylthiophene-2, 5-diyl) (P3HT) and [6, 6]-Phenyl-C₆₁-butyric acid butyl ester (PC₆₁BM) with purity > 99 % were purchased from Sigma Aldrich. Both PC₆₁BM and P3HT were used as received without further purification. PC₆₁BM and P3HT were weighted using an analytical balance with a weight ratio of 1:1 then dissolved in 1, 2-dichlorobenzene (DCB). The concentration of the solution was 20 mg/ml and allowed it to stir overnight at room temperature. One of the reason that regioregular P3HT and PC₆₁BM were chosen to be the donor and acceptor for the OPV in this research is because the couple of these two organic semiconductors in thin film can efficiently harvest almost the entire visible light wavelength from 300 nm to 700 nm. The UV-Vis absorption results in chapter 4.7 show that pristine P3HT thin film absorb well between 400 nm and 650 nm while pristine PC₆₁BM thin film dominated the absorption below 400 nm. The absorbance of the blended P3HT:PC₆₁BM organic thin films are the superposition of the absorbance of the pristine P3HT and PC₆₁BM thin films that cover almost entire visible light spectrum made them ideal candidates for OPV. Besides that,

PC₆₁BM is a fullerene derivative with high electron mobility (Devižis, Hertel, Meerholz, Gulbinas, & Moser, 2014; He, Du, Zhang, Xiao, & Ding, 2013). P3HT is among the polythiophene family which is a kind of conducting polymer. It is the excitation of the π -orbit electron in P3HT that gives the photovoltaic effect in the blend. The blended P3HT:PC₆₁BM organic thin films is the most efficient fullerene derivate based donor-acceptor copolymer so far due to their balanced charge carrier mobility in the blends (Laquai, Andrienko, Mauer, & Blom, 2015; Mauer, Kastler, & Laquai, 2010). Furthermore, P3HT and PC₆₁BM can dissolve well in several volatile solvents such as chloroform, DCB etc.to form homogenous thin film through spin coating technique. These two organic semiconductors also commercially available in Malaysia and can be purchased easily therefore made them accessible as main materials for OPV research for this study.

Poly (3,4-ethylenedioxythiophenepoly (styrene sulfonate) (PEDOT:PSS) aqueous solution having the viscosity of 15-60 mPas and conductivity of 850 Scm⁻¹ was purchased from H. C. Starck. It is used as received without further purification.

The treatment acid solutions used in this research work were diluted acetic acid solutions. Acetic acid with purity > 99.5 % was purchased from Sigma Aldrich. Acetic acid was diluted using deionised (DI) water to different volume percentage. Six different volume percentage/concentration of the diluted acetic acids were prepared – 5 %, 10 %, 25 %, 50 %, 75 % and 100 %. The percentage indicating the percentage by volume (vol. %) of a solution. A 5 % aqueous solution of acetic acid indicates that 50 μ l of acid acetic was diluted by 950 μ l DI water to make 1 ml of solution. Therefore, a 50 % acetic acid solution means that 500 μ l of acid acetic was diluted by 500 μ l DI water to make 1 ml of solution. 100% acid acetic acid solution represents pure acetic acid without dilution.

3.2.2 Substrates Preparations

Translucent glass substrates coated with indium-tin-oxide (ITO) are used as the base support for the organic solar cells. These ITO coated glass substrates was manufactured by Luminescence Technology Corp. The ITO substrates were pre-patterned as displayed in Figure 3.1. The ITO substrates specifications are given in Table 3.1 below:

Table 3.1: The pre-patterned ITO substrates specifications manufactured by Luminescence Technology Corp.

Thickness of ITO	1200~1600Å
Resistance of ITO	9~15 Ω/sq
Transparency of ITO	> 84 % (at 550 nm)
Components	Polished soda lime glass
Size	200 mm × 250 mm
Thickness of Glass	0.7 mm
Thickness of Silicon Oxide (SiO ₂)	≥ 200 Å
Mean Roughness (R _a)	< 6nm
Maximum Roughness Depth (R _{max})	< 35nm

The ITO substrates gone through a cleaning process before being used to fabricate the organic solar cells. The ITO substrates were sequentially cleaned with acetone, isopropanol, deionised water and finally dried with nitrogen gas. The ITO-coated substrate were then treated with 35 W oxygen plasma for 5 min to increase the adhesion of PEDOT:PSS to the ITO surface.

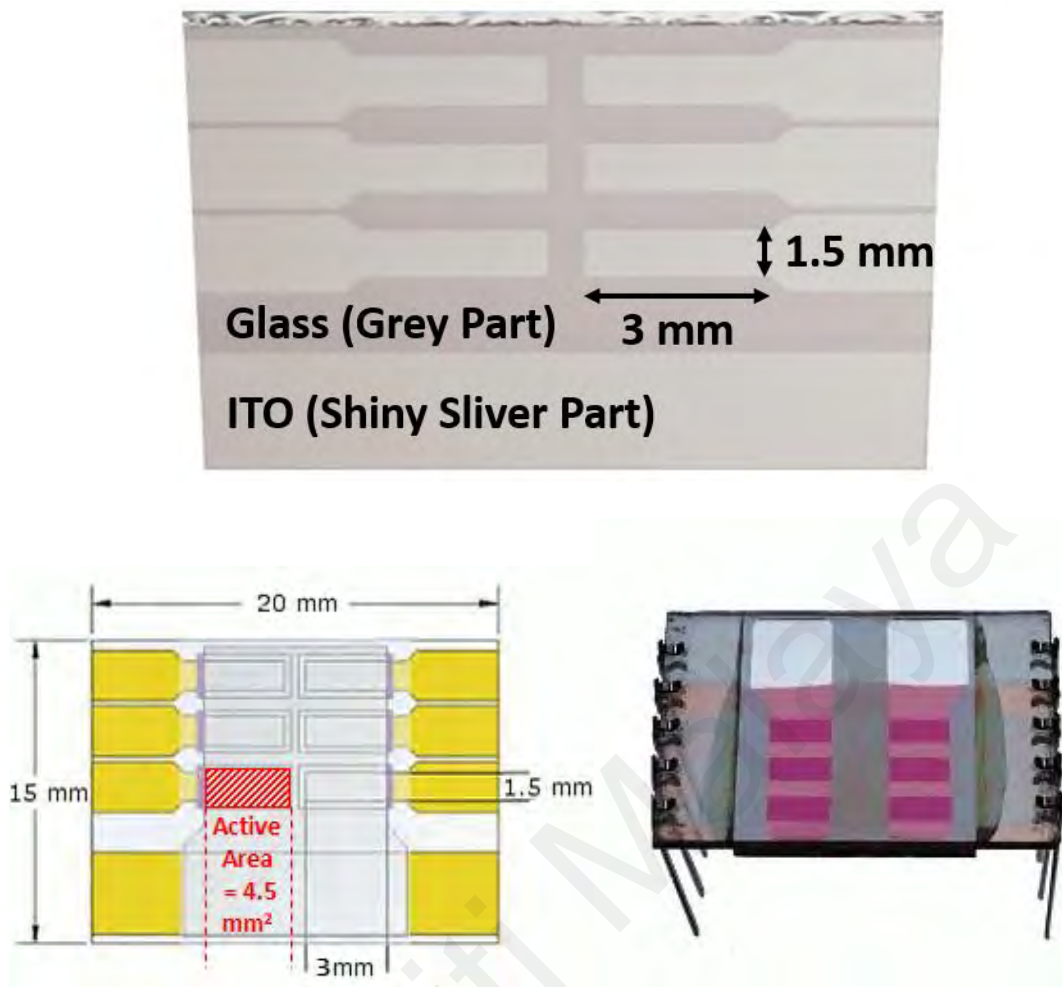


Figure 3.1: Schematic diagram of pre-patterned ITO substrates.

3.2.3 Thin Film Deposition

After the cleaning process, the aqueous solution of PEDOT:PSS was spun on top of the ITO coated surface at a spin rate of 3000 revolutions per minute (rpm) for 30 seconds. This process will form a 40-60 nm thin PEDOT:PSS buffer layer on the ITO substrates. This buffer layer improved the ITO substrates surface roughness and can lead to lower electrical resistance. The PEDOT:PSS coated ITO substrate was then annealed on hot plate at 120 °C for 10 minutes to remove residual water. This followed by the spin coating of P3HT:PC₆₁BM active layer onto the surface of PEDOT:PSS buffer layer. The P3HT:PC₆₁BM solution was spun at a spin rate of 3000 rpm for 30 seconds to create a

homogenous thin layer with a thickness of about 120-150 nm. Both P3HT:PC₆₁BM and PEDOT:PSS solutions were filtered respectively by using 0.20 μm and 0.45 μm nylon filters before use.

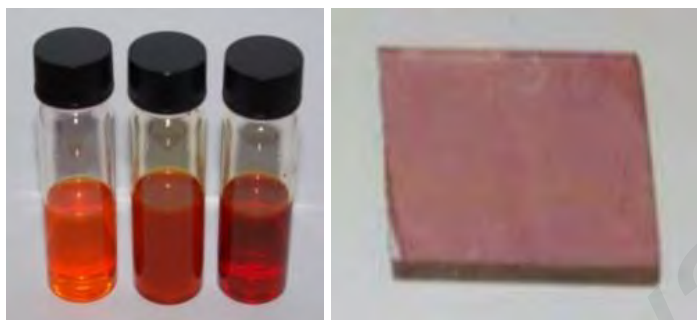


Figure 3.2: Selected samples of P3HT:PC₆₁BM in solution form and thin film.

3.2.4 Active Layer Treatment

In the production of organic solar cells, an additional step is introduced in which aqueous solutions of acetic acid (5 %, 10 %, 25 %, 50%, 75 % and 100 %) are spun onto the surface of P3HT:PC₆₁BM active layer at a spin rate of 3000 revolutions per minute (rpm) for 30 second. After this simple and easy process, the substrate is immediately transferred to the thermal evaporator chamber to coat the aluminum (Al) electrodes (cathodes).

3.2.5 Al Electrode (Cathode) Deposition

After the acid treatment, the device was transferred to a high vacuum (1×10^{-5} mbar) chamber in thermal evaporator in order to coat aluminium (Al) electrodes as cathodes through a shadow mask on top of the active layer. The average thickness of the coated Al electrodes were about 90-120 nm. The final device structure of ITO/PEDOT:PSS/P3HT:PC₆₁BM/Al were fabricated in this study. The device then

underwent post-deposition thermal annealing at 120 °C for 10 minutes on a hot plate. The active area of the device was 4.5 mm². Encapsulations were carried out on the devices as the final fabrication process to prevent device degradation while performing the electrical characteristics measurements in the ambient environment. All the device fabrication processes (except ITO substrates cleaning process) for example spin coating of active layer, annealing of the PEDOT:PSS layer, acetic acid treatment were prepared under nitrogen atmosphere condition inside a glovebox while Al electrodes deposition process was under high vacuum (1×10^{-5} mbar) condition.

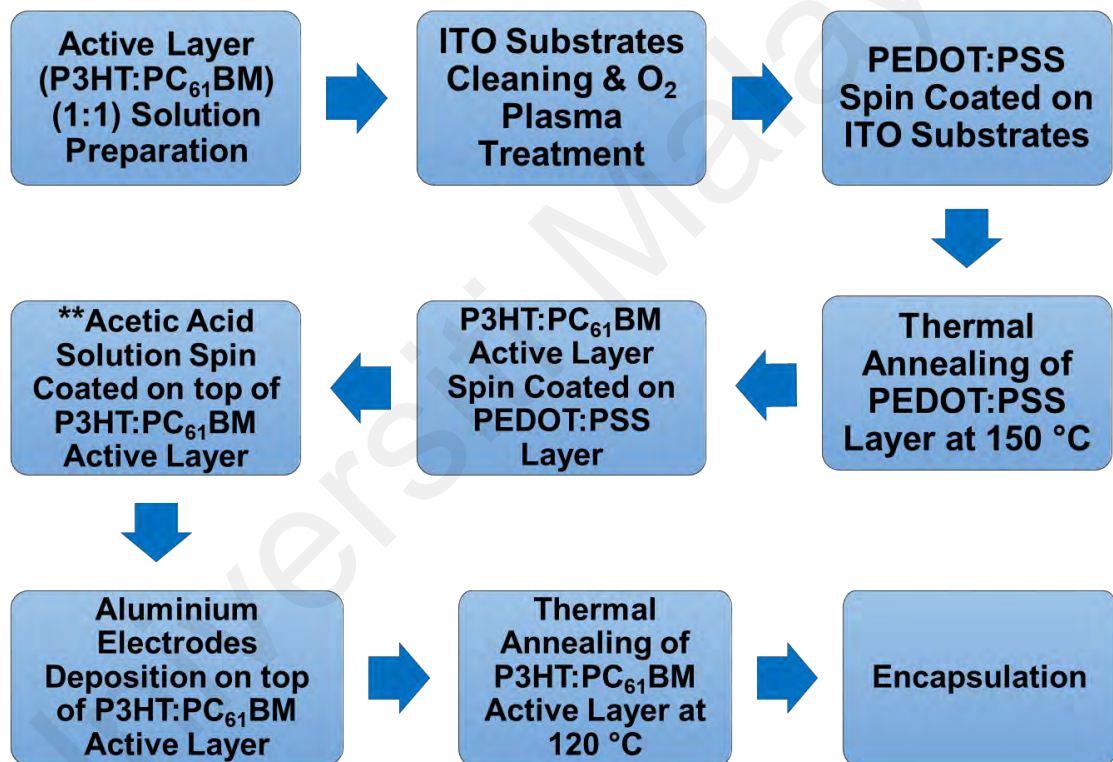


Figure 3.3: Flow chart of thin film deposition and treatment process.

The flow chart as shown in Figure 3.3 summarised the organic solar cells fabrication processes from chapter 3.2.1 until chapter 3.2.5.

3.3 Thin Films/Devices Characterisations

3.3.1 Ultraviolet-Visible (UV-Vis) Spectroscopy

The optical absorption spectra of untreated and acetic acid solution treated P3HT:PC₆₁BM thin films coated on glasses substrates were obtained by performing UV-Vis spectroscopy. The spectrophotometer model used in this project was the Perkin Elmer Lamda 950 UV-Vis-NIR spectrophotometer. A deuterium discharge tube provides the ultraviolet radiation from wavelength 300-350 nm while a tungsten-halogen lamp supplies visible to near-infrared radiation range from wavelength 350-1100 nm. The light from the light source converged first and then entered the monochromator. After that, the light dispersed by a grating in the monochromator and it passed through an exit slit which the output was monochromated. This light is divided into two light paths by a sector mirror. One light directed on the sample to be measured and the other beamed on the reference sample. The incident light that passed through the sample or reference sample is detected by the photomultiplier tube or lead (II) sulphide (PbS) photoconductive cell. The light beam detected by the photomultiplier tube or PbS photoconductive cell is converted into an electrical signal. This electrical signal was synchronously rectified and converted into a digital form and entered into a microcomputer. The signal processed by the microcomputer is then displayed on the output device (computer) as spectrum or digital data.

Baseline correction was performed at the beginning of the absorption measurement. Glass has its own absorption wavelength which considered as background signal. Therefore, a baseline correction must be performed to eliminate this background absorption spectrum. The absorbance measurements on thin film is carried out by placing a clean and clear glass substrate on the reference holder of the spectrophotometer while the organic thin film coated on the glass substrates (same properties as the glass substrate

in the reference holder) was placed in the sample holder. The absorption spectrum was scanned in the wavelength range of 300-800 nm in ambient air.

3.3.2 Field Emission Scanning Electron Microscopy (FESEM)

FESEM produces images by scanning a sample with a high energy beam of electrons instead of using light/electromagnetic waves. The electrons beam is generated by thermionic emission from an electron gun equipped with a tungsten filament cathode. This beam travels vertically through lenses and an electromagnetic fields that focuses the beam onto the sample. The electrons interact with atoms near the sample surface to generate a signal that contains information about the topography of the sample surface when the electron beam hits the sample surface. The types of signals generated include primary backscattering electrons (due to elastic scattering), secondary electrons (due to inelastic scattering), X-rays (electromagnetic radiation) and light. These signals are picked up by detectors in the microscope and converted into an image for display on the computer monitor.

The FESEM magnification can be controlled over a wide range from about 10 times to more than 50,000 times. That's about 250 times better than a normal optical microscope. In this study, the Leica S440 model was used to visualize FESEM images.

3.3.3 X-Ray Diffraction (XRD)

XRD measurements were carried out with a Siemens D5000 X-ray Diffractometer. The results obtained in this study were used for phase identification for the untreated and acetic acid treated P3HT:PC₆₁BM thin films. X-ray Diffraction (XRD) is a universal, non-destructive analytical technique that can provide detailed information on the structural,

chemical and physical properties of materials and thin films. This technique is based on observing the scattering intensity of monochromatic X-ray incident on a sample as a function of the incident angle, scattering angle and wavelength.

In X-ray diffractometer, an X-ray beam is generated through a cathode ray tube by heating a filament to create electrons and then these generated electrons are accelerated by applying a high voltage. These high velocity electrons are directed to bombard on a target material. The high speed/velocity electrons have sufficient energy to dislodge the inner shells electrons of the target material and therefore able to produce X-rays. The target material for example iron, copper, chromium, molybdenum, etc. determines the specific wavelength of the X-ray. The Siemens D5000 X-ray Diffractometer use copper as the target material therefore the X-ray for this equipment is $\text{CuK}\alpha_1$ radiation with a wavelength of 1.5418\AA . X-rays are filtered through a monochromator to produce monochromatic radiation. The monochromatic X-ray beam is then collimated to concentrate and directed at the sample which is placed on a platform at an angle. The incident ray interacts with the crystal lattice to create constructive interference according to Bragg's Law:

$$n\lambda = 2d \sin\theta \quad (3.1)$$

Bragg's Law relates the electromagnetic radiation wavelength, λ to the diffraction angle, 2θ and the interplanar spacing, d . Monochromatic X-rays are used to create diffraction because their wavelengths are usually of the same order of magnitude as the distances between the planes in the crystal lattice. The interference pattern is recorded and processed by an X-ray detector. All possible diffraction directions of the lattice can be acquired by scanning the sample through a range of 2θ angles.

3.3.4 Raman Spectroscopy

Raman scattering spectroscopy is widely used to identify rotational, low frequency and vibrational modes in the thin films. In other words, it is a characterisation tool for studying the physical state and chemical structural fingerprint of the materials. The sample is irradiated with a laser source which the laser wavelength is either in the near ultraviolet, visible or near infrared range. Electromagnetic radiation from the illuminated area was collected with a lens and sent through a monochromator. Laser photons interacted with the electrons in the bonds of the molecules on the thin film surface and scattered. The scattered sample photons are filtered through either an edge pass filter, a band pass filter or a notch filter while the remaining collected light is scattered onto a detector. During the Raman process, the interaction between photons and vibrations of molecules (phonons) caused in a shift in wavelength of the photons to a lower (red shift) or higher (blue shift) energy states. These shifts provide information about the vibration mode of the sample. When a incident photon gains energy from annihilation of a phonon it is known as anti-Stokes shift or upshift and when a photon losses its energy to create a phonon, it is known as Stokes shift or downshift.

Raman scattering measurements were carried out by a RENISHAW inVia Raman microscope equipped with a Leica microscope and a charge-coupled device (CCD) camera. A grating of 2400 lines mm^{-1} provided a spectral resolution of $\pm 1 \text{ cm}^{-1}$ was used for all the measurements in this research. An excitation source of with a wavelength of 514 nm from a Ar^+ laser with a laser power less than 0.5 mW was used. Measurements with 5 seconds of exposure time at 10 accumulations were taken. The laser spot was focused on the surface of the sample with a 50 times objective lens on a microscope. Raman spectra were collected at several points on the sample and recorded with a Peltier cooled CCD camera. The ratio of the intensity of D-Raman peak and G-Raman peak

(ID/IG) was obtained by taking the peak intensities after the baseline adjustments. Data were collected and analysed using Renishaw Wire and OriginLab software.

3.3.5 Thickness Measurement

The untreated and acetic acid treated P3HT:PC₆₁BM thin films were deposited on glass substrates and their thicknesses were measured by KLA Tencor P-6 Surface Profilometer. All thickness measurements were carried out under atmospheric condition. First, the sample is positioned at the centre of the disk holder inside the profilometer. The scan parameters were then set in the profilometer command software as shown in Table 3.2.

Table 3.2: Scan parameters of KLA Tencor P-6 Surface Profilometer.

Scan Type	Two Dimensional (2D)
X-Direction Scan Range	2000 μm
Scan Velocity	100 $\mu\text{m/s}$
Sampling Frequency	20 Hz
Multi Scan Average	1
Applied force	0.50 mg
Resolution/Range	0.1953 $\text{\AA}/327 \mu\text{m}$
Profile type	

Once the parameters are set, a command was given to manually load the sample to the profilometer through the profilometer command software. The profilometer probe then began to move downward until it touched the sample surface. Due to the soft nature of the organic thin film, a minimum scanning force of 0.5 mg is applied to the sample. After completing the scan, the data was saved and the probe was manually controlled to return to initial position.

3.3.6 J-V Characteristics Measurement

Current density-voltage (J-V) measurements were performed using a Keysight B2902A Precision Source/Measure Unit (SMU). Measurements of J-V characteristics took place in the ambient condition inside a custom made dark box. The dark box was designed to effectively block out the background light. For photovoltaic studies, the device was put under Air Mass 1.5 Global (AM 1.5 G) illumination with the calibrated light intensity of 100 mW/cm^2 supplied by Newport Xenon Arc Lamp. The OPVC was mounted on a custom made sample holder to measure the J-V characteristics. Tungsten needle probes were used to provide direct contacts to the cathode (ITO) and anode (Al) of the OPVC with SMU. The OPVC was connected to the Keysight B2902A Precision Source/Measure Unit via the Tungsten needle probes and custom made sample holder. The SMU was connected to a desktop via General Purpose Interface Bus (GPIB). The SMU worked as a current measure unit and voltage source simultaneously. It supplied the voltage to the device which is preset by the user and measured the photocurrent induced by the OPVC. Figure 3.4 shows the simplified schematic diagram of the electrical measurement on the photovoltaic device.

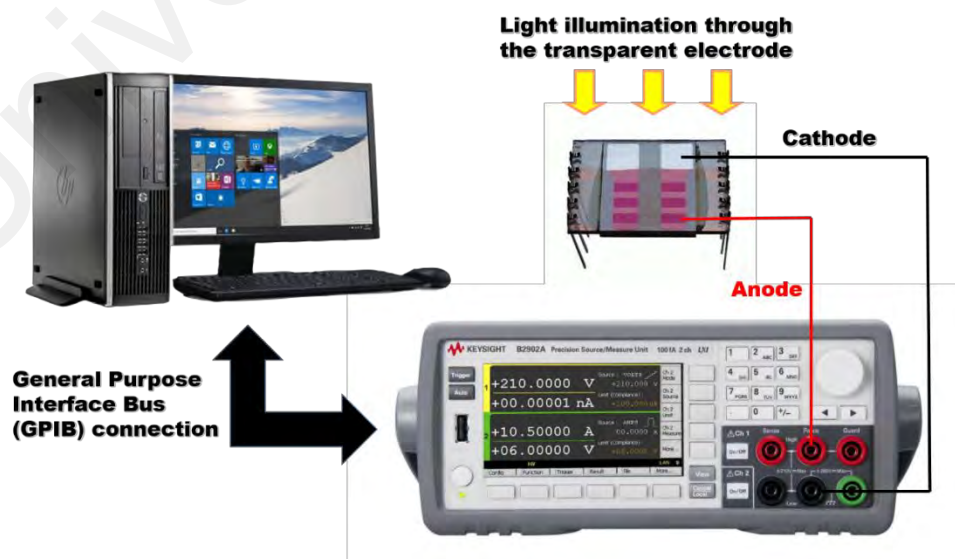


Figure 3.4: Schematic diagram of the electrical measurement on photovoltaic device.

CHAPTER 4: ACID ACETIC SOLUTION TREATMENT ON P3HT: PC₆₁BM

ORGANIC SOLAR CELLS

4.1 Overview

In this chapter, firstly the performance of the untreated and acetic acid solutions treated organic solar cells will be presented and compared. The electrical properties of the photovoltaic cells will be determined and presented based on the current-density (J-V) curves under light illumination condition. Short circuit current (J_{sc}), open circuit voltage (V_{oc}), fill factor (FF) and power conversion efficiency (PCE) will be determined and discussed in detail.

The process of photon energy conversion into electricity involved in four steps:

1. Light absorption and excitons formation
2. Excitons diffusion
3. Excitons dissociation
4. Transportation of charges to electrodes

The photoconversion mechanism of the organic photovoltaic cell is different from the conventional inorganic photovoltaic cell. Free electron hole pairs are generated immediately upon light absorption in inorganic photovoltaic cell while in organic photovoltaic cell, the light absorption causes the generation of excitons. It is not a free electron hole pair. An exciton or also called mobile excited state is a bound state of an electron and a hole which are attracted to each other by their electrostatic Coulomb attraction force. It is considered as an electrically neutral quasiparticle.

An exciton forms when a photon with energy, $h\nu$ equal or larger than the energy band gap, E_g of a semiconductor absorbed in the organic semiconductor. The difference in the energy levels of the Highest Occupied Molecular Orbital (HOMO) and Lowest Unoccupied Molecular Orbital (LUMO) is the energy band gap of the organic

semiconductors. The absorbed photon excites the electron from the HOMO to the LUMO of the organic semiconductor. As a result, this leaves behind a localized positively charged hole. The electron in the LUMO is then bounded by the Coulomb attraction force of this localized hole. This attraction provides a stabilizing energy balance. Therefore, the exciton has slightly less energy than the unbound electron and hole. The exciton can be dissociated to free electron hole pair by a sharp drop of potential at the donor-acceptor interface (or called heterojunction) of the photovoltaic cell. In order to generate the separated positive and negative charges, the excitons need to diffuse through the active layer to the heterojunction where they can dissociate. Since the excitons are electrically neutral, their motion is not influenced by any electric field and they diffuse by random hops. The excitons have short diffusion length (~10nm-20nm). It is important for the excitons to reach to the interface before they decay back to the ground state. Hence, the thickness of active layers in the device plays a key factor in the performance of the solar cell.

Once the excitons have separated, the separated charges need to be collected at the electrodes to contribute as the photocurrent. As the active layers of the device are sandwiched between two electrodes with different work function, the built-in potential in the active layers results in an electric field that assists the transport of the charges. By applying an external bias, the charge carriers can be collected with the efficiency depending on their mobility (Kippelen & Bredas, 2009). Electrons in the donor materials travel to the acceptor LUMO and then reach to the cathode. Holes in the acceptor on the other hand, firstly travel from HOMO of acceptor to the HOMO of donor and then collected at the anode.

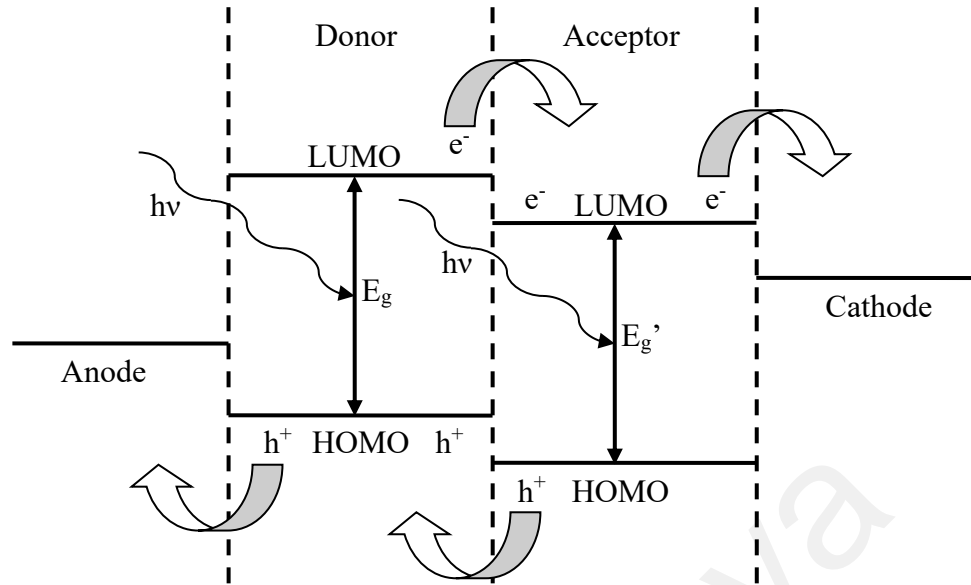


Figure 4.1: Photons with energy, $h\nu$ equal or larger than the band gaps, E_g (acceptor) or E_g' (donor) excited the electrons from the HOMO to the LUMO leaving holes behind in the HOMO. Electrons are collected at the anode and holes transported to the cathode.

Under illumination, an OPV solar cell can be represented by an equivalent circuit based on a single-diode model. The equivalent circuit of ideal solar cells is shown in Figure 4.2 (a). Under light illumination, the photo-generated current density, J_{ph} is simulated by a constant current source. The current flowing in the device can be controlled by the diode when a voltage is applied. In this circuit model, the shape of the J-V curve is determined only by the diode. It is easy to see that FF can approach to 100% but can never reach 100% even in an ideal solar cell because the J-V curve of the diode cannot be rectangular. From the equivalent circuit, the J-V curve of ideal solar cells can be expressed by:

$$J(V) = J_s \left[\exp\left(\frac{qV}{k_B T}\right) - 1 \right] - J_{ph} \quad (4.1)$$

where $J(V)$ is the recorded current density on the external load, J_s is the reverse saturation current density of the diode in the dark, q is the elementary charge, V is the applied voltage, k_B is the Boltzmann constant, T is the temperature and J_{ph} is the photo-generated current density (Qi & Wang, 2013).

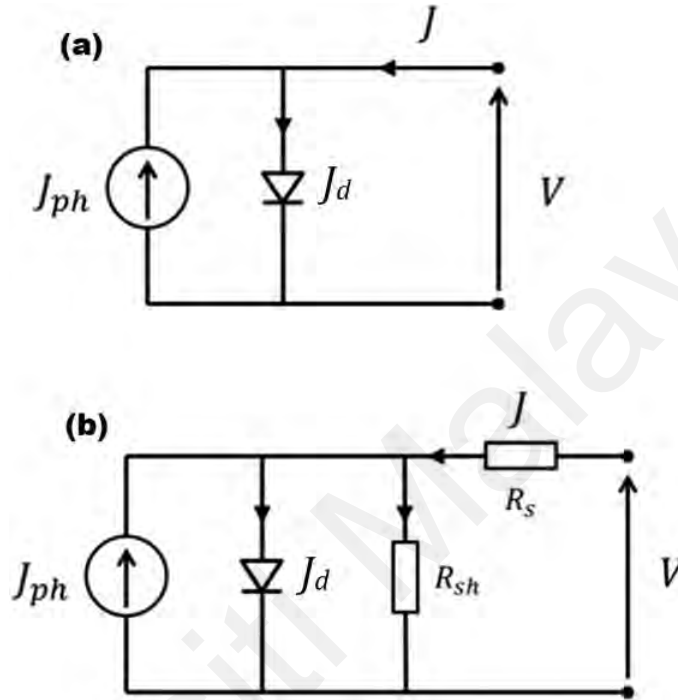


Figure 4.2: Equivalent circuit for (a) ideal and (b) practical solar cells, J_{ph} is the photoinduced current density, J_d is the current density of the diode, R_s and R_{sh} are the series and shunt resistance, respectively, J is the current flow in the external load and V is the applied voltage (image taken from (Qi & Wang, 2013).

The short circuit current density, J_{sc} is the current that flow through an area per second when the solar cell is illuminated and the voltage applied across the device is zero ($V = 0$) (i.e. the electrodes are short circuited). Therefore, the J_{sc} can be obtained at the interception of y-axis in the J-V graph. The largest power output, P_{max} of the OPVC is determined by the point where the product of voltage and current is maximized (V_{max} and J_{max}).

$$P_{max} = \frac{V_{max}}{J_{max}} \quad (4.2)$$

This can be done by plotting a power versus voltage (P-V) graph as shown in Figure 3.6 to search for the maximum power output, P_{max} at the maximum voltage, V_{max} . The power output of the OPVC firstly increases with the applied voltage until reaches a maximum point, then starts to decrease rapidly to zero around the value of V_{oc} . The maximum point in the P-V graph corresponds to the maximum power output, P_{max} and the maximum voltage, V_{max} of the device as shown in Figure 3.5. Division of P_{max} by the product of J_{sc} and V_{oc} yields the filling factor, FF as shown in Equation 4.3:

$$FF = \frac{P_{max}}{J_{sc} \times V_{oc}} \quad (4.3)$$

The fill factor of the solar cell is defined as the ratio of the actual maximum obtainable power ($V_{max} \times J_{max}$) to the theoretical power ($J_{sc} \times V_{oc}$) of the cell. An ideal solar cell has a FF equally to 1. As a simple view, the FF is a parameter allows the researchers inspect the quality of the manufactured cell compare to the ideal cell.

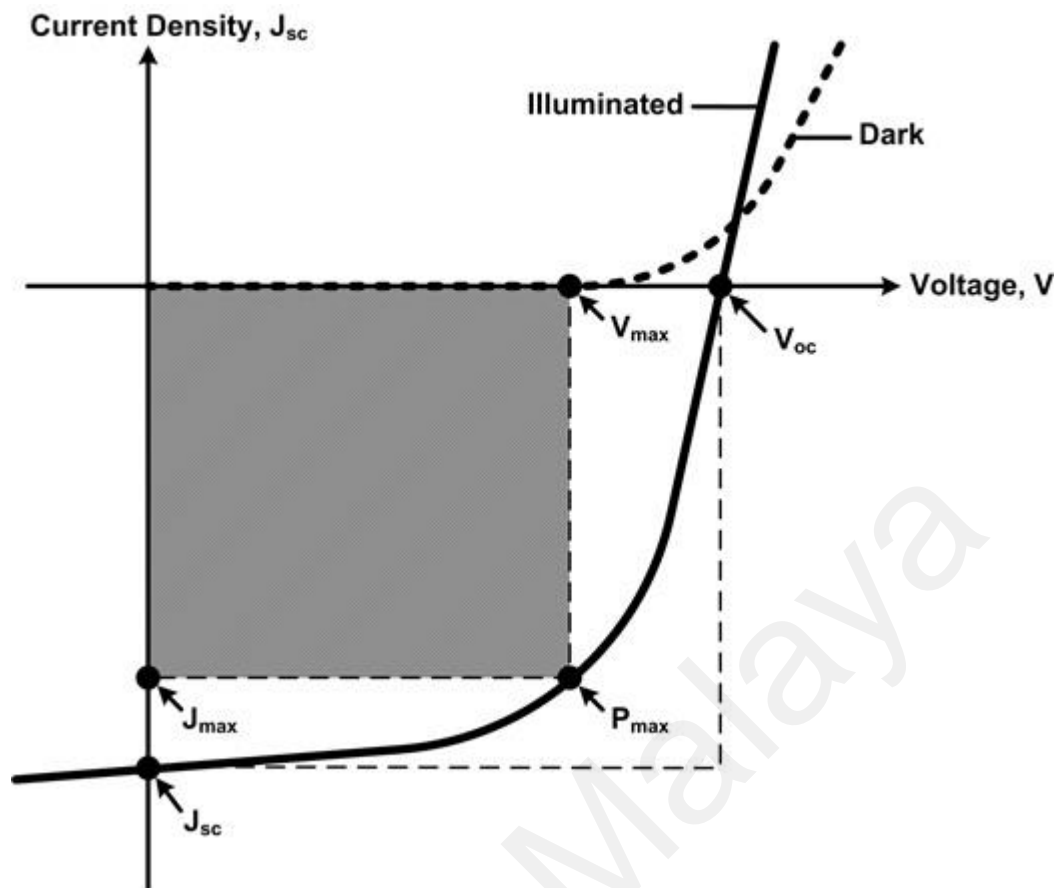


Figure 4.3: The current-voltage curve (J-V curve) of an organic solar cell under dark condition (dash line) and illuminated (full line).

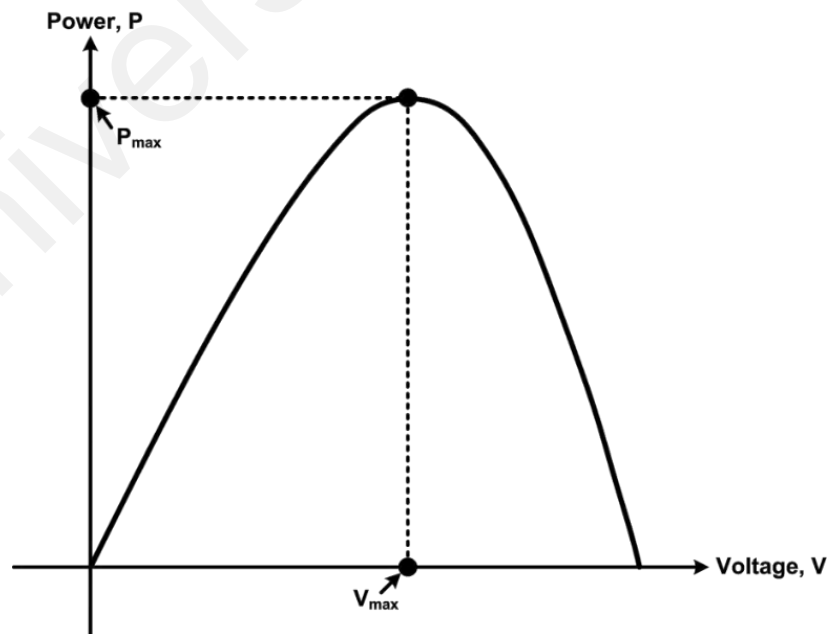


Figure 4.4: The power-voltage curve (P-V curve) of an organic solar cell under illuminated radiation.

The power conversion efficiency (PCE) is defined as:

$$PCE = \frac{P_{out}}{P_{in}} \times 100 \% = \frac{P_{max}}{P_{in}} \times 100 \% = \frac{J_{sc} \times V_{oc} \times FF}{P_{in}} \times 100 \% \quad (4.4)$$

To determine the PCE of an OPVC, the P_{max} needs to be compared with the power output of the incident light, P_{in} . PCE simply is a measurement the amount of power produced by a solar cell relative to the power available in the incident solar radiation, P_{in} (The ratio of power output to power input). For a standard measurement, a simulated air mass 1.5 (AM 1.5) illumination with intensity of 100 mW/cm^2 is utilised to determine the PCE of an OPVC. An AM 1.5 illumination defines as the solar radiation travelled through 1.5 times atmosphere thickness corresponds to a zenith angle of $z = 48.2^\circ$ relative to the normal of the Earth's sea level.

Next part of this chapter is the analysis of electrical properties of the untreated and acid treated devices being performed via the Schottky diode approach. The J-V curves in the dark condition will be fully utilised to find the crucial electrical properties such as turn on voltage, rectification ratio (RR), ideality factor (n), series resistance (R_s), shunt resistance (R_{sh}), zero bias barrier height (Φ_{bo}) of the devices. Those parameters may provide a better insight on the performance of the untreated and acid treated OSCs. The subsequent part of this chapter is the utilisation of two alternative methods: Cheung & Cheung and Norde's functions in examining and analysing the I-V curves in the dark condition. The electrical parameters determined from these two methods will compared with the parameters obtained from the Schottky diode approach. In addition, explanation of the performance enhancement of the acid treated organic solar cells will be discussed utilizing the Space Charge Limited Conduction (SCLC) analysis in the following section. After the electrical properties investigations, the experimental results obtained from the optical and morphological measurements including ultraviolet-visible (UV-Vis) spectroscopy, X-Ray Diffraction (XRD), Raman spectroscopy and Field Effect Scanning

Electron microscopy (FESEM) will be presented. The investigation on how the device degradation with time would affect the performance of the fabricated devices will be presented to show the durability of the untreated and acid treated organic solar cells. Finally, the versatility of acetic acid treatment on other organic semiconductor materials will be reported at the end of this chapter.

4.2 Fabrication of ITO/PEDOT:PSS/P3HT:PC₆₁BM/Al Devices

Organic solar cells with the structure of ITO/PEDOT:PSS/P3HT:PC₆₁BM/Al devices were fabricated according to the methods explained in chapter 3. The organic active layers of OSCs were spin coated with different percentage of diluted acetic acid, as tabulated in Table 4.1.

Table 4.1: Description of acetic acid treated active layer utilised in ITO/PEDOT:PSS/P3HT:PC₆₁BM/Al devices.

Device Notation	Description of P3HT:PC ₆₁ BM Active Layer
Untreated	Pristine active layer without acetic acid treatment
5 %	5 % diluted acetic acid spun on the surface of the active layer
10 %	10 % diluted acetic acid spun on the surface of the active layer
25 %	25 % diluted acetic acid spun on the surface the active layer
50%	50 % diluted acetic acid spun on the surface the active layer
75 %	75 % diluted acetic acid spun on the surface the active layer
100 %	Pure acetic acid (not diluted) spun on the surface the active layer

The untreated and treated P3HT:PC₆₁BM thin films were used as active layers in the solar devices. Figure 4.5 (a) shows the device structure of the

ITO/PEDOT:PSS/P3HT:PC₆₁BM/Al. An image of a typical device with metal connection legs is shown in Figure 4.5 (b). Each device consists of six pixels, thus six measurements can be obtained. Besides, the fabrication of all samples were repeated six times to ensure repeatability of the electrical performance.

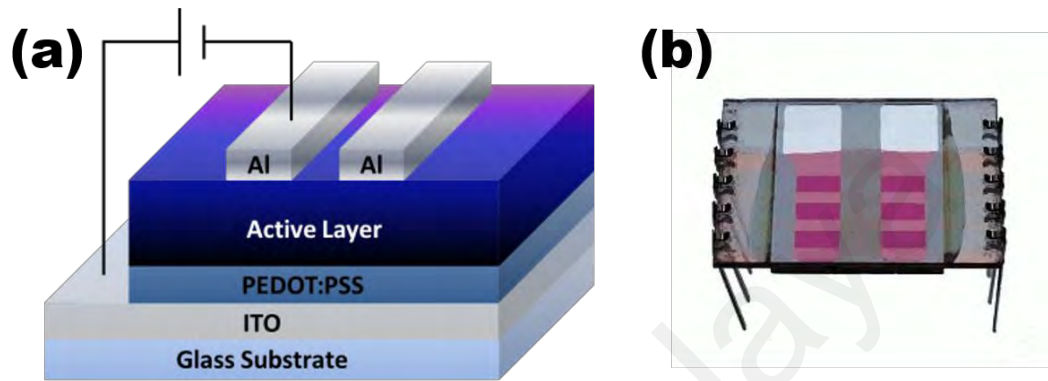


Figure 4.5: (a) Device structure of ITO/PEDOT:PSS/P3HT:PC₆₁BM/Al and (b) Diagram of the fabricated device with connection legs.

4.3 Current-density Curves of the Fabricated Devices under Light Illumination

The current density-voltage (J-V) characteristics of untreated and acetic acid treated ITO/PEDOT:PSS/P3HT:PC₆₁BM/Al organic solar cells under reverse and forward biases are depicted in Figure 4.6. Under AM 1.5 G 100 mW/cm² simulated solar illumination, the untreated bulk heterojunction organic solar cell exhibited typical photovoltaics effect with short circuit current, J_{sc} of 2.0 mA/cm² and open circuit voltage, V_{oc} of 0.58 V. The fill factor, FF and power conversion efficiency, PCE of the untreated device are determined as 46 % and 0.53 % respectively. Notably, all devices that gone through the acetic acid treatment show enhancement in the short circuit current output, J_{sc} and PCE. By utilising Equation 4.4, the PCE of the of 50 % acid concentration treated device can be determined and the calculation of PCE is shown in detail as below:

$$PCE = \frac{J_{sc} \times V_{oc} \times FF}{P_{in}} \times 100 \% \quad (4.4)$$

$$= \frac{11.0 \text{ mA/cm}^2 \times 0.58 \text{ V} \times 0.32}{100 \text{ mW/cm}^2} \times 100 \%$$

$$= 2.04 \%$$

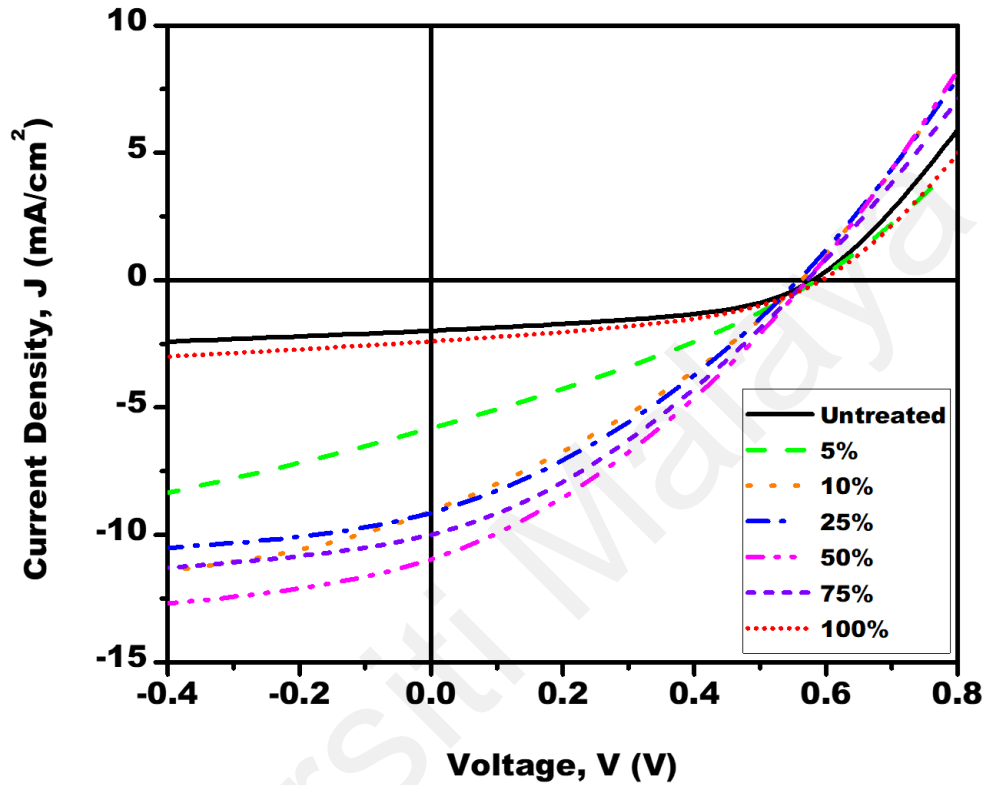


Figure 4.6: The J-V characteristics of the untreated and acetic acid treated ITO/PEDOT:PSS/P3HT:PC₆₁BM/Al organic solar cells.

Figure 4.7 shows the effect of acid treatment on the short-circuit current and power conversion efficiency. A rising peak trend of J_{sc} and PCE can be observed in this figure. The maximum J_{sc} and PCE of the devices both occurred at 50 % acid concentration treatment. The J_{sc} drastically increased to 5.8 mA/cm² in 5 % acid concentration treated device and further up to maximum of 11.0 mA/cm² in 50 % acid concentration treated device which is around 5.5 times higher compared to the J_{sc} produced by the untreated device ($J_{sc} = 2.0$ mA/cm²). Increase in the concentration of acetic acid after 50 % diluted acetic acid solution will cause the J_{sc} output of the devices start to fall back. The J_{sc} output

of 75 % acid concentration treated device achieved 10.0 mA/cm² and further down to 2.4 mA/cm² for the 100 % acid concentration treated device. In spite of that, the 100 % acid concentration treated device yet showed nearly 21 % enhancement in the J_{sc} output. As a result of the drastically increment in the J_{sc} output after the acetic acid solution treatment, the PCE of the organic solar cells rose from 0.53 % for the untreated device to maximum of 2.04 % for the 50 % acid concentration treated device. The PCE of the 75 % and 100 % acid concentration treated devices then subsided to 1.89 % and 0.60 % respectively. The maximum J_{sc} and PCE of the devices both occurred at 50 % acid concentration treatment. The acid acetic solution treatment on P3HT:PC₆₁BM organic solar cells is surprisingly effective method to enhance the performance of the organic solar cells despite of the simplicity and unsophisticated approach. Owing to this simplicity and unsophisticated approach, no advanced machinery or equipment and complicated chemical processes are required. The application of spin coating and injecting acid solution on the surface of organic solar cells enable this method can be applied on large scale production and therefore able to significantly reduce the cost of fabrication with great enhancement of organic solar cells efficiency. For this reason, this method could be a promising new method that can significantly enhance the current low efficiency problems in organic solar cells with minimum cost and effects. The table below (Table 4.2) is the summary of the performance for the untreated and acid solution treated organic solar cells.

Table 4.2: Photovoltaic properties of ITO/PEDOT:PSS/P3HT:PC₆₁BM/Al organic solar cells.

Acid Concentration (%)	Short Circuit Current Density, J_{sc} (mA/cm ²)	Open Circuit Voltage, V_{oc} (V)	Fill Factor, FF (%)	Power conversion Efficiency, PCE (%)
Untreated	2.0 ± 0.7	0.58 ± 0.01	46 ± 2	0.53 ± 0.20
5 %	5.8 ± 1.7	0.59 ± 0.02	30 ± 2	1.03 ± 0.37
10 %	9.1 ± 1.3	0.57 ± 0.01	30 ± 2	1.58 ± 0.30
25 %	9.2 ± 0.4	0.56 ± 0.01	33 ± 1	1.67 ± 0.13
50 %	11.0 ± 1.9	0.58 ± 0.02	32 ± 3	2.04 ± 0.57
75 %	10.0 ± 0.6	0.58 ± 0.01	33 ± 2	1.89 ± 0.24
100 %	2.4 ± 0.8	0.60 ± 0.03	42 ± 2	0.60 ± 0.23

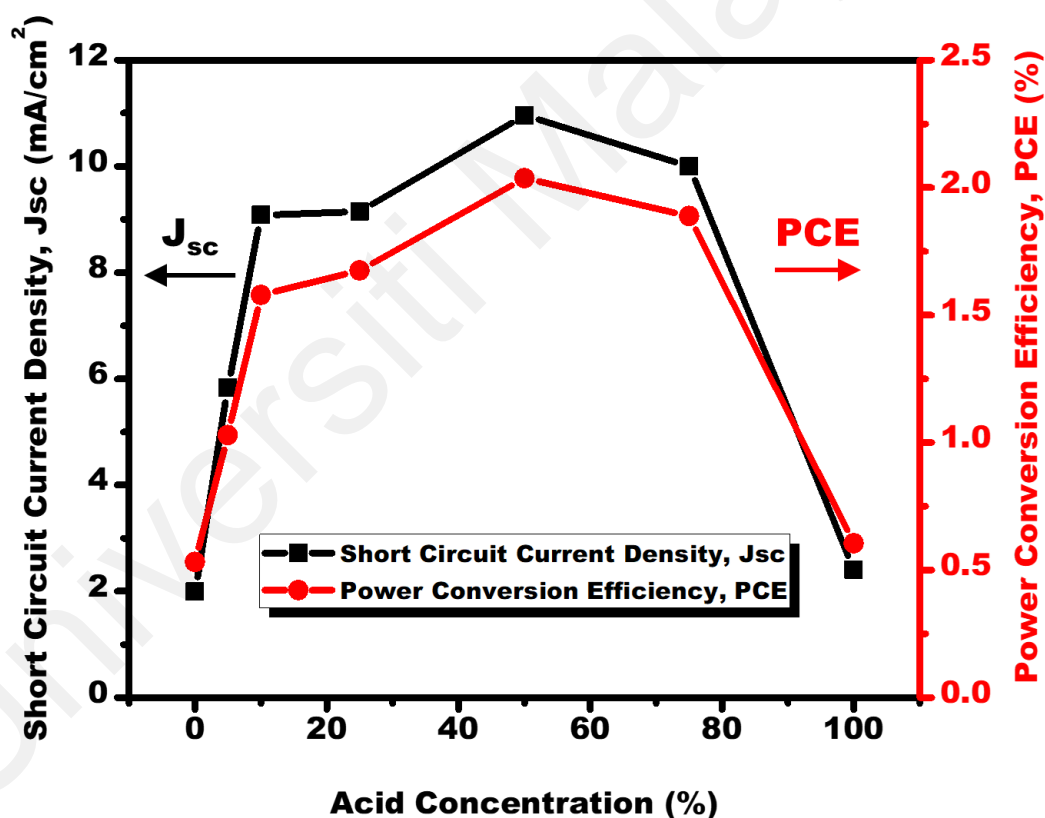


Figure 4.7: The J_{sc} output and PCE of the untreated and acetic acid treated ITO/PEDOT:PSS/P3HT:PC₆₁BM/Al organic solar cells.

Further investigation reveals that despite the drastic increase of J_{sc} output, the open circuit voltage, V_{oc} of the devices remain nearly constant in the range of 0.56 V to 0.60 V. Consequently, this leads to a decrement in the fill factor, FF of the acid treated devices.

The fill factor decreased to as low as 30 % for the 5 % and 10 % acid concentration treated devices. The fill factor of the 100 % acid concentration treated device is the only device that its fill factor is comparable to the fill factor of the untreated device as illustrated in Figure 4.8. The decrease of FF is suspected due to the substantial increase in J_{sc} output as well as the decrease in shunt resistance, R_{sh} but relatively small differences in series resistance, R_s in the acid treated devices compare to the untreated device. To estimate the R_s and R_{sh} of the devices, an approach has been adopted from Lim et al (Lim, Aziz, Muhammad, Supangat, & Sulaiman, 2016). Note that the R_{sh} and R_s determined here are from the I-V curves that illuminated under light condition. The R_s , can be determined from the junction resistance in forward bias where it decreased and reached a constant value (region where $J_{sc} \approx 0 \text{ mA/cm}^2$). In the reverse bias region, the maximum value of the junction resistance represents the R_{sh} of the device, (region where $V = 0 \text{ V}$). The R_{sh} determined for the untreated device is about $171.25 \text{ }\Omega\text{cm}^2$ but significantly decreased to around $31 \text{ }\Omega\text{cm}^2$ to $47 \text{ }\Omega\text{cm}^2$ after the acetic acid treatments except for the 100 % acid concentration treated device. For the 100 % acid concentration treated device, the R_{sh} is around $120.24 \text{ }\Omega\text{cm}^2$ which is slightly lower than the untreated device. However, the R_s of the acid solution treated devices slightly decreased after the acetic acid treatment compare to the untreated device except the 100 % acid concentration treated device. For the untreated device, the R_s is determined at $11.83 \text{ }\Omega\text{cm}^2$ then decreased to $10.72 \text{ }\Omega\text{cm}^2$ upon 5 % acid concentration treatment and further decreased to minimum $6.78 \text{ }\Omega\text{cm}^2$ for the 50 % acid concentration treatment. The R_s slightly increased to $7.75 \text{ }\Omega\text{cm}^2$ for the 75 % acid concentration treated device and exceed the value of the untreated device for the 100 % acid concentration treated device to $15.56 \text{ }\Omega\text{cm}^2$. Nevertheless, the overall performance of the devices enhanced after the acetic acid treatments. The significant decrease in R_{sh} and notable increase in J_{sc} clearly explained the causes of the decrease in FF of the treated devices as it can be seen that the rise of J_{sc} with V_{oc} remain almost

constant in Region III will make the slope of the J–V curve decreases correspondingly, leading to less “squareness” of J–V curve, therefore a lower FF. The summary of the series resistance, R_s and shunt resistance of, R_{sh} of the untreated and acid treated P3HT:PC₆₁BM organic solar cells are listed in Table 4.3.

Table 4.3: Summary of the series resistant, R_s and shunt resistant, R_{sh} of the untreated and acetic acid solution treated OSCs.

Acid Concentration (%)	Series Resistance, R_s (Ωcm^2)	Shunt Resistance, R_{sh} (Ωcm^2)
Untreated	11.83	171.25
5 %	10.72	31.41
10 %	7.26	39.59
25 %	8.08	42.20
50 %	6.78	45.90
75 %	7.75	46.62
100 %	15.66	120.24

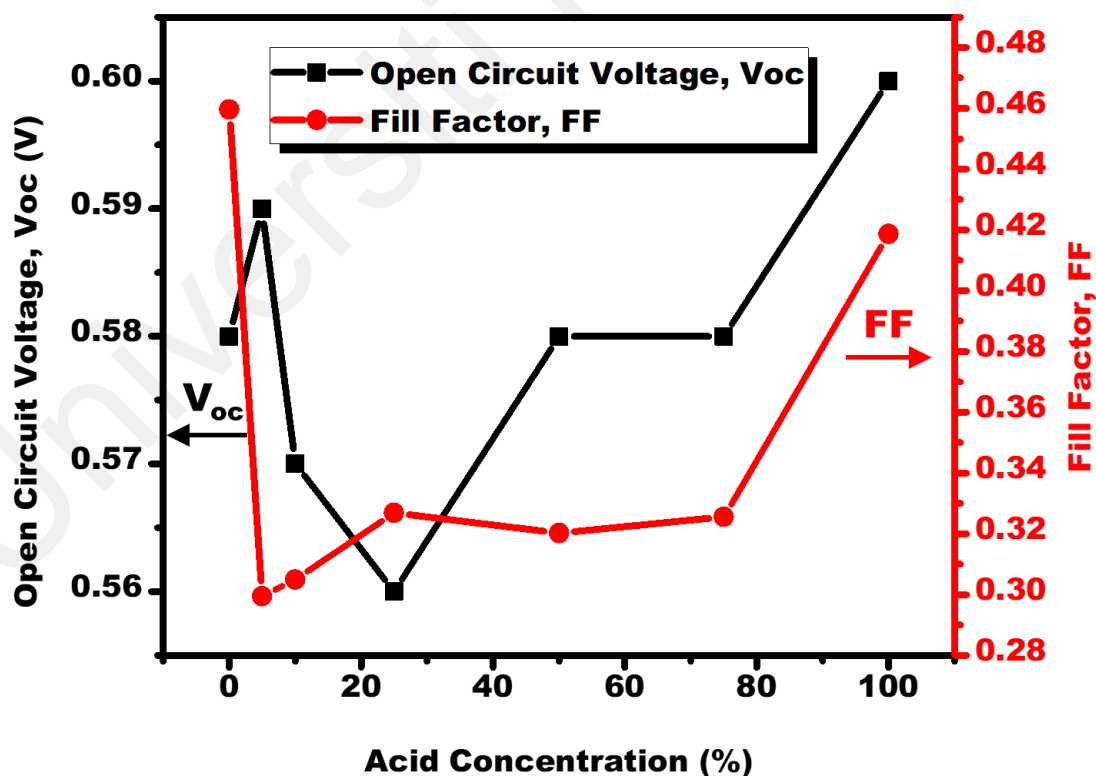


Figure 4.8: The plot of open circuit, V_{oc} and fill factor, FF versus acid concentration.

The cause of enhancement after the acetic acid treatment is remain unclear after viewing from the preliminary results from the performance of the organic solar cells. Therefore, in order to better understand the cause of enhancement, it is essential to investigate the electrical, optical and morphological properties of the devices through various of scientific measurements.

4.4 Investigation of Electrical Properties via Schottky Diode Method

To view solar cell as a light absorbing diode, photocurrent in the solar cell flows in the diode reverse bias direction. In the dark, the solar cell simply functions as a diode. In solar cells characterization of photovoltaic effect, much information can be obtained from the current-voltage (I-V) curves under the light illumination while the I-V curves in the dark condition always get neglected. Therefore, a method has been adapted to characterise the OSC device containing active layer of P3HT:PC₆₁BM using the Schottky diode method in order to derive more electrical properties from the I-V curves in the dark condition. It is important to gain a better insight of the electrical properties of the device including ideality factor (n), rectification ratio (RR), barrier height (Φ_{bo}), series resistance (R_s) and shunt resistance (R_{sh}) which will significantly influence the performance of the organic solar cells. By determining these electrical properties might help to explain the enhancement of the organic solar cells upon the acid solution treatment. All of these important electrical properties can be deduced from further analysis of current-voltage (I-V) curves of the device measured in dark condition at room temperature (300K). The charge conduction mechanism of the organic solar cells can be further investigated with the help of these electrical properties determined from the Schottky diode method.

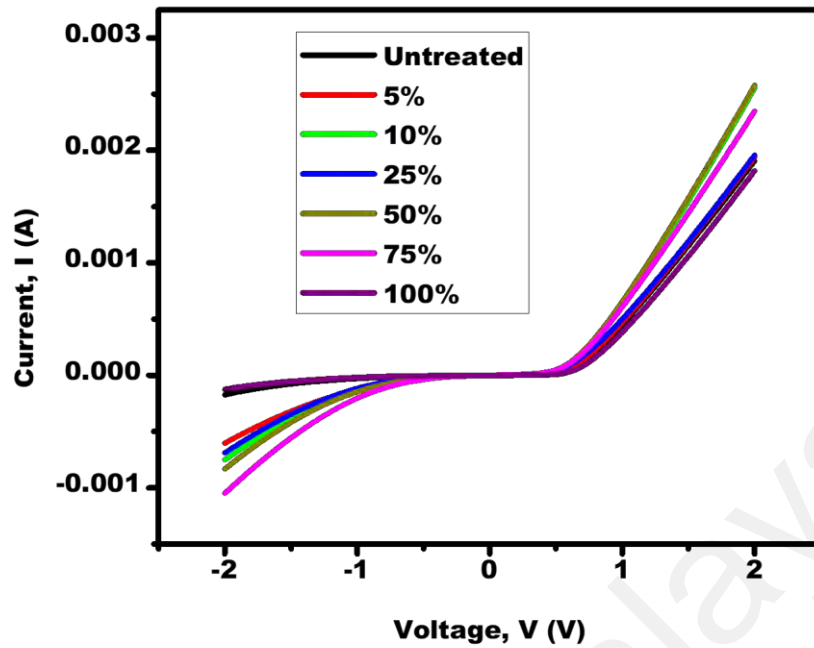


Figure 4.9: The current-voltage (I-V) curves of the devices measured in the dark condition at room temperature (300K).

The turn-on voltage and the rectification ratio, RR are determined by the I-V curves in the dark. The turn-on voltage is the threshold point at which the rectification initiates. Note that this turn on voltage is not equivalent to the open circuit voltage, V_{oc} . The V_{oc} is defined as the voltage across the output terminal when the solar cell is operated at open circuit i.e. $I = 0$ A. These two voltages are two different terms and cannot be used interchangeably. However, turn-on voltage is an important parameter that decides the rectification behavior of OSCs and affects the V_{oc} and thereby the efficiency of OSCs. The devices rectification ratio, RR can be extracted using the ratio of forward biased current to reverse biased current at ± 2 V from the I-V curves in dark condition as shown in Figure 4.9. The extrapolation of linear region at the forward biased current shows the turn-on voltage on the interception of x-axis as shown in Figure 4.10. The summary of the turn-on voltage and RR for the untreated and acid treated devices have been tabulated in Table 4.4.

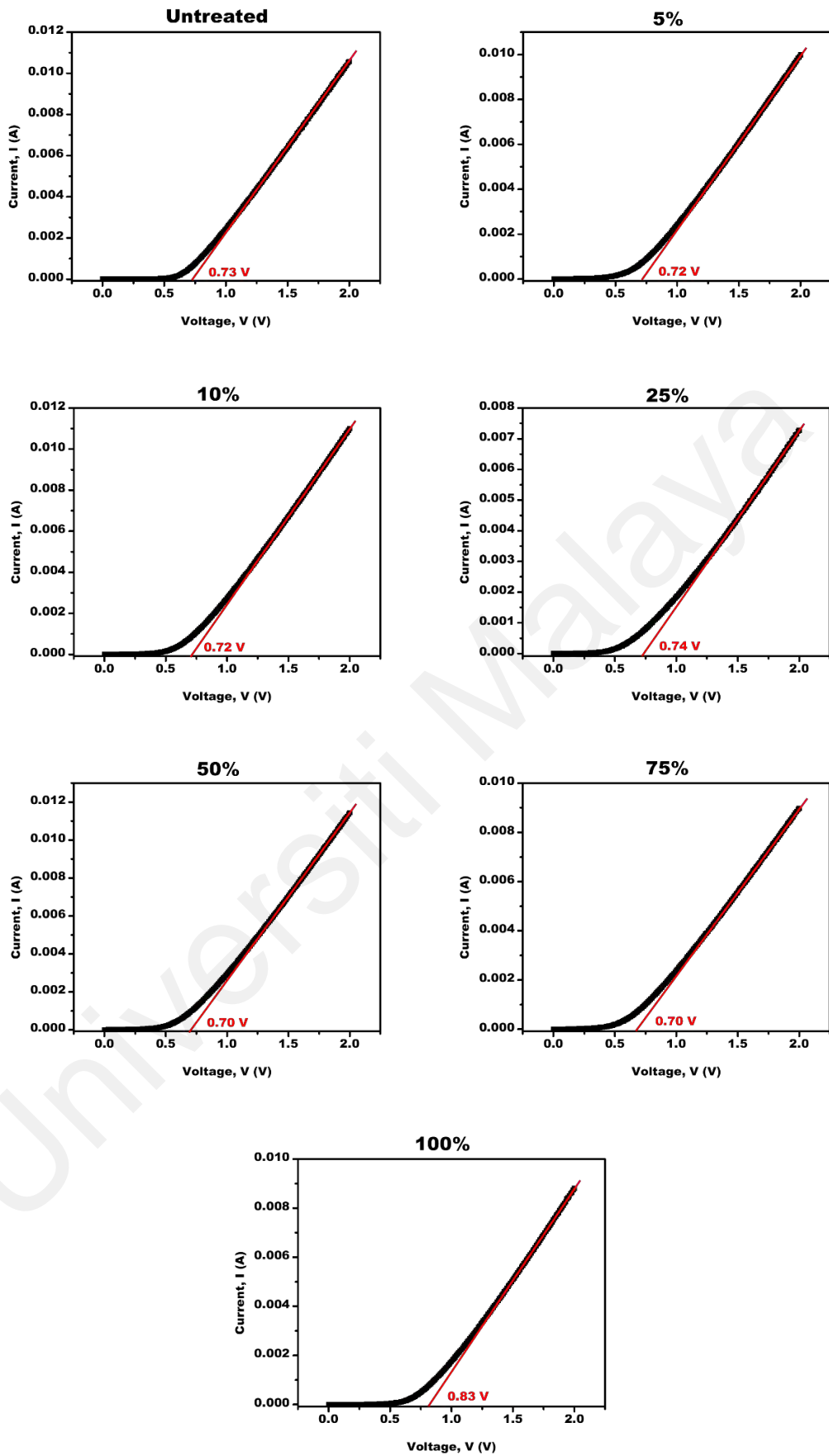


Figure 4.10: The turn-on voltage by extrapolating I-V curves of the OSC devices in the dark condition. The extrapolation lines in red indicates the turn-on voltage.

Table 4.4: The turn on voltage and rectification ratio of OSC.

	Turn-On Voltage	Rectification Ratio, RR
Untreated	0.73	12.39
4.5 5	4.6 0.72	4.7 3.21
10 %	0.72	2.87
25 %	0.75	2.68
50 %	0.70	2.90
75 %	0.70	2.06
100 %	0.83	14.59

From the summary of the results, almost all the devices have the same turn on voltage range between 0.70 V to 0.75 V except the device treated by 100 % acetic acid. The device that treated by 100 % acetic acid solution has the highest turn on voltage which is 0.83 V. The turn-on voltage of this device is 18.57 % higher compared to 0.70 V which are the lowest turn-on voltage for the devices with active layer being treated by 50 % and 75 % acetic acid. As the turn-on voltage indicates the barrier potential of the OSCs as above which the current conducts and below which conduction stops. At very low voltages, the OSCs has very high impedance therefore very small current flows through the device. The point where current starts to flow easily is beyond the "turn-on" voltage. Past this point the impedance of the device is very low thus the current significantly increases.

A natural logarithmic (\ln) forward and reverse bias I-V plot of the organic solar cells measured in the dark at room temperature (300K) is shown in Figure 4.11. It is believed that the asymmetric nature of the I-V curve and the rectification characteristics of the device are due to the difference in work function of the electrodes indicating the difference in the metal/polymer interface barrier. In addition, the impacts of series resistance (R_s), shunt resistance (R_{sh}) and the ideality factor (n) greater than unity (> 1) may have led to the non-linear I-V characteristics as observed in Figure 4.11. By considering these factors, the I-V characteristics of the organic solar cells can be

expressed by the thermionic emission theory. The I–V equation with respect to thermionic emission theory in the presence of the interfacial layer is provided by (Güllü, Aydoğan, & Türüt, 2008; Kılıçoğlu, 2008):

$$I = I_o \left[\exp \left(\frac{qV}{nkT} \right) - 1 \right] \quad (4.5)$$

where q , V , k and T are the electron charge, bias voltage, Boltzmann constant and temperature in kelvin (K), respectively. I_o is the saturation current derived from the ln I-V plot at zero bias, which can be expressed as below:

$$I_o = AA^*T^2 \exp \left(-\frac{q\Phi_{bo}}{kT} \right) \quad (4.6)$$

In Equation 4.6, A and A^* are the effective area of organic solar cells (0.045 cm^2) and Richardson constant of ITO contacts (Dey, Jana, Dhar, Das, & Ray, 2018; Güllü et al., 2008; Kılıçoğlu, 2008), respectively. The n in Equation 4.5 is the ideality factor which is considered as a measure of device's deviation from the ideal thermionic emission theory. Φ_{bo} is the zero bias barrier height. The value of zero bias barrier height, Φ_{bo} , of the organic solar cell is an essential parameter which can be determined from the following equation:

$$\Phi_{bo} = \frac{kT}{q} \ln \left(\frac{AA^*T^2}{I_o} \right) \quad (4.7)$$

There are a few methods to determine the ideality factor, n from the I-V curves. The most direct and the simplest method is determined from the slope of the Ohmic region of the dark I-V curve with the natural logarithmic scale as shown in Figure 4.11. The Ohmic region is defined from 0 V to 0.1 V range for this work as the current in this region showing the most linear (Ohmic) pattern. Figure 4.12 shows the linear fitted results for the untreated and acid solution treated devices in the Ohmic region in the dark. By taking the natural logarithm of both sides of Equation 4.5, it becomes:

$$\begin{aligned}
\ln I &= \ln \left[I_0 \exp \left(\frac{qV}{nkT} \right) \right] - \ln I_0 \\
&= \frac{qV}{nkT} + \ln I_0 - \ln I_0 \\
&= \frac{qV}{nkT}
\end{aligned} \tag{4.8}$$

Therefore, the slope of the natural logarithmic graph, m , in the Ohmic region (x- axis range 0 V to 0.1 V) is $\frac{q}{nkT}$. Finally, the ideality factor, n can be determined from the slope, m where

$$n = \frac{q}{mkT} \approx \frac{38.68}{m} \tag{4.9}$$

since q and k are constants and $T = 300$ K. The Richardson constant of ITO can be determined using the Equation 4.10 as shown below:

$$A^* = \frac{4\pi q m^* k^2}{h^3} \tag{4.10}$$

where q is the electron charge ($1.602176634 \times 10^{-19}$ C), m^* is the effective mass of ITO ($0.35 m_e$ where m_e is the electron rest mass = $9.109383701528 \times 10^{-31}$ kg), k is the Boltzmann constant (1.380649×10^{-23} J·K⁻¹), h is the Planck's constant ($6.62607015 \times 10^{-34}$ J·s). By utilising the Figure 4.11, the saturation current, I_0 can be obtained as abovementioned. By inserting all required values into Equation 4.7, the zero bias barrier height, Φ_{bo} of the devices can be determined. The summary of the electrical parameters calculated from the Schottky diode method is presented in Table 4.5.

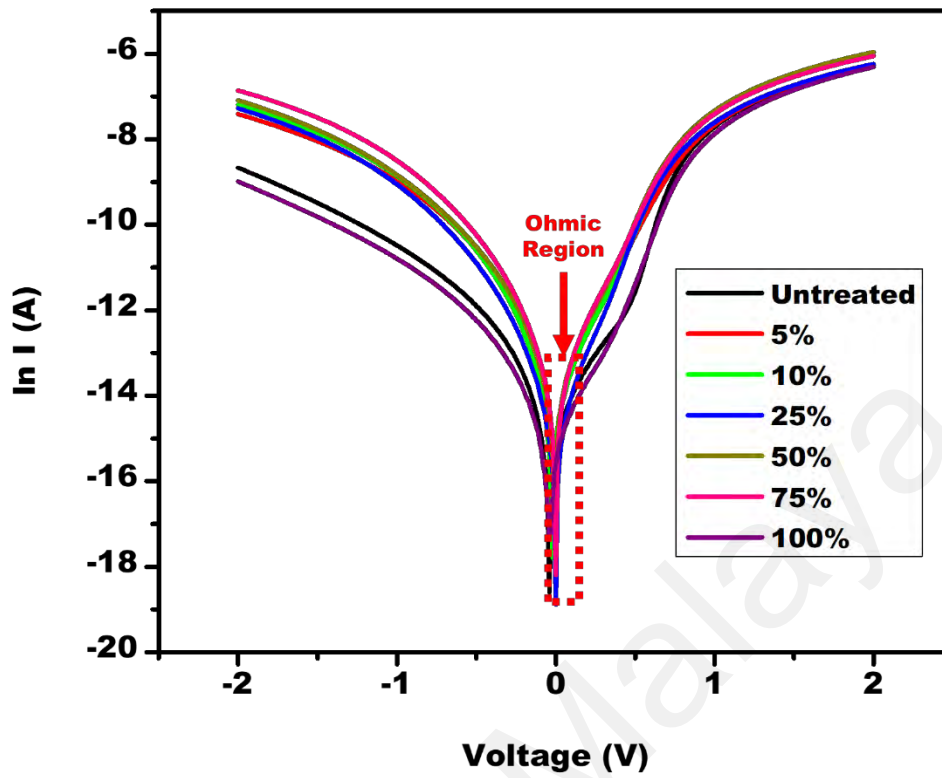


Figure 4.11: The Ohmic region of the dark I-V curve with the natural logarithmic (\ln) scale.

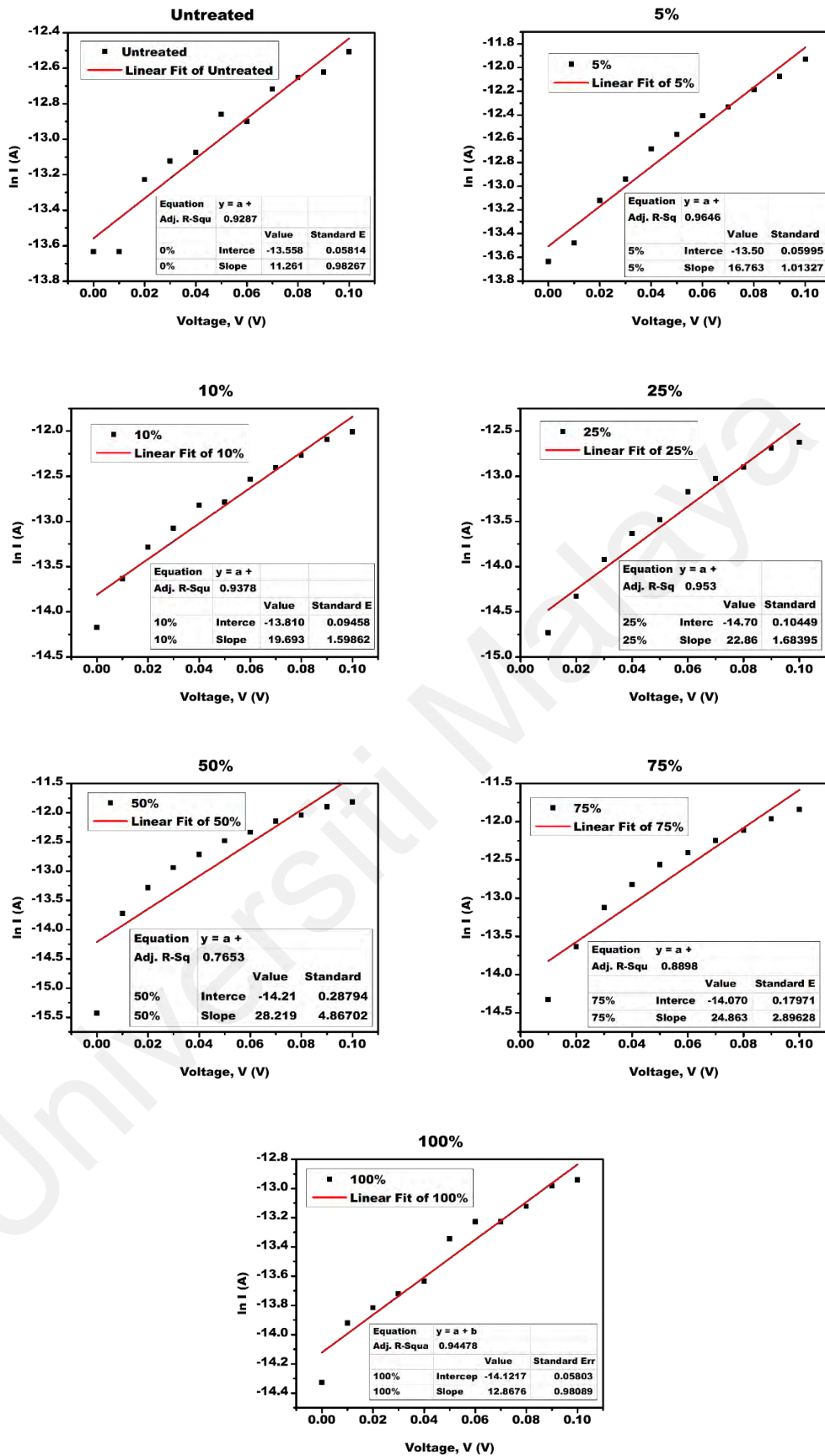


Figure 4.12: The linear fitted results for the untreated and acid solution treated devices in the Ohmic region in the dark condition.

Table 4.5: The electrical properties extracted from the Ohmic region of the dark I-V curve with the natural logarithmic scale.

	Slope, m	Ideality Factor, n	Saturation Current,	Barrier Height, Φ_{bo}
Untreated	11.26	3.43	0.22 μA	0.70 eV
5 %	16.76	2.31	0.26 μA	0.73 eV
10 %	19.69	1.96	0.28 μA	0.70 eV
25 %	22.86	1.69	0.01 μA	0.69 eV
50 %	28.22	1.37	0.10 μA	0.71 eV
75 %	24.86	1.56	0.13 μA	0.68 eV
100 %	12.87	3.01	0.17 μA	0.73 eV

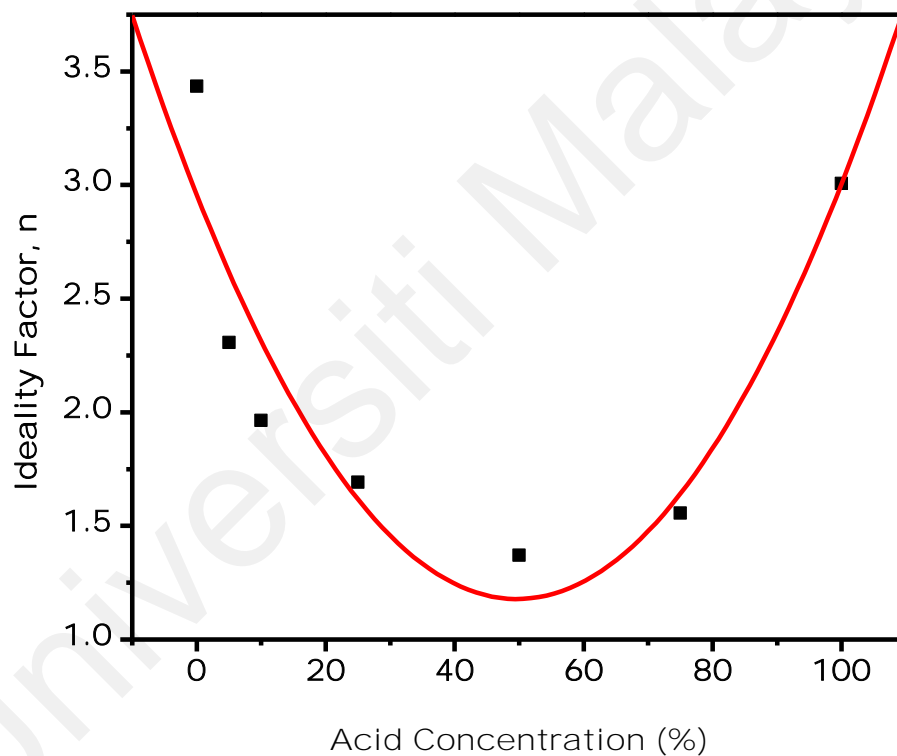


Figure 4.13: Ideality factor, n versus acetic acid concentration plot of the untreated and acetic acid solution treated devices.

As shown in the Figure 4.13, all the devices have the ideality factor greater than the unity ($n > 1$). However, the device that treated by 50 % acetic acid concentration exhibited the ideality factor close to the unity. The conversion of light to electricity on organic solar cells goes through 4 processes (Qi & Wang, 2013): (1) photons are being absorbed by the

active layer and excitons are being created; (2) excitons diffuse in the photoactive layer and reach the interface between acceptor and donor; (3) excitons dissociate to free electrons and holes at the acceptor/donor interface; (4) free electrons and holes are being transported and collected by the respective electrodes. The total efficiency of photons converted to charge carriers can be expressed by the product of the efficiency of these four processes $\eta = \eta_A \cdot \eta_{ED} \cdot \eta_{CT} \cdot \eta_{CC}$ where η_A is absorption efficiency, η_{ED} is exciton dissociation efficiency, η_{CT} is charge transfer efficiency and η_{CC} is carrier collection efficiency (Qi & Wang, 2013). In general, η_{CT} and η_{CC} approach unity in many organic semiconductors. Recombination of charge carriers often occurs in the process of exciton diffusion. Even after exciton dissociation, electrons and holes may also have high possibility to recombine. This recombination is characterised as bimolecular recombination. Hence, the possibility of recombination in OSCs is greater than that of conventional inorganic crystalline p-n junction solar cells. This indicates that the ideality factor, n for OSCs is usually higher than that of inorganic crystalline p-n junction solar cells (Qi & Wang, 2013). The OPV active layer is composed of an interwoven network of donor and acceptor atoms. A gemination pair is typically formed at the boundary between the donor and acceptor materials and remains in bounded state due to Coulombic attraction. In order for the electrons and holes in these gemination pairs to contribute to the current, they have to overcome this Coulombic attraction force that binds them at the donor-acceptor interface. However, even if the geminate pair undergoes dissociation, the charge carriers are not completely free. There remains the possibility that the free carriers will recombine with other electrons and vacant holes in the active layer of the semiconductor before reaching the electrodes (Gaspari & Quaranta, 2018). Geminate recombination occurs when a hole and electron that originate from the same photon recombine before separating into free charges. By definition, this includes the loss of excitons that relax to the ground state before they can diffuse to an interface as well as

geminate pairs that recombine at a D/A interface. There is another type of recombination known as non-geminate recombination. Trap-assisted recombination and bimolecular recombination are non-geminate recombinations. Trap-assisted recombination or monomolecular recombination is a first order process in which one electron and one hole recombine through a localized energetic trap (trap state). Though it involves two carriers, it is considered monomolecular recombination because it involves one carrier at a time; first one carrier is trapped and then the second oppositely charged carrier finds the trapped carrier and recombined. Historically, monomolecular recombination refers to either Shockley-Read-Hall recombination. The recombination rate is determined by the amount of sites that act as traps and by how fast the free carrier can find the trapped carrier. Impurities in the fullerene and polymer materials and incomplete phase separation (interfacial defects that function as traps) are likely to contribute to a trap-based recombination (Sarah R Cowan, Roy, & Heeger, 2010; Proctor, Kuik, & Nguyen, 2013). The recombination process caused by high trapping concentrations can limit the performance of the solar cell (Taibi, Belghachi, & Abid, 2016). Bimolecular recombination involves non-radiative recombination of a free electron and a free hole. It is considered as the most common observed non-geminate recombination in OPV devices. Bimolecular recombination is often assumed to be the dominant recombination mechanism in most efficient OPV systems. In a disordered semi-conductor with localized charge carriers, bimolecular recombination is limited by the rate at which oppositely charged carriers find one another. The faster charge carriers move, the faster they will find each other; consequently, the rate of bimolecular recombination in OPV is proportional to the charge carrier mobilities. The key distinction from geminate recombination is that the hole and electron in non-geminate recombination do not originate from the same photon (Sarah R Cowan et al., 2010; Gaspari & Quaranta, 2018; Proctor et al., 2013; Taibi et al., 2016).

The results show that the Φ_{bo} values of the OSC devices appear in the range of 0.68 eV to 0.73 eV as summarised in Table 4.4. To make the measurement more reliable, two alternative methods have been adopted to determine the Φ_{bo} and to be compared later. Next section describes the utilization of (i) Cheung and Cheung method and (ii) Norde's Function, to elucidate the electrical parameters of the OSC devices in the dark.

4.5 Alternative Methods to Determine Electric Properties from Dark I-V Curves

Two alternatives approaches have been adopted to obtain ideality factor n , series resistance, R_s and zero bias barrier height, Φ_{bo} , of the organic solar cells. These two approaches are Cheung and Cheung method and Norde's Functions. There is no single method is more accurate than the other, but one approach may possess advantages compare to the other method and can be use as complement methods to provide detail insight on the electrical properties of the organic solar cells.

4.5.1 Cheung & Cheung Method

From Equation 4.5, derivation of the equation with respect to V given the ideality factor, n of the organic solar cells as below:

$$\frac{dV}{d(\ln I)} = IR_s + n \left(\frac{kT}{q} \right) \quad (4.11)$$

A plot of $\frac{dV}{d(\ln I)}$ vs I will give R_s as the slope and $n \left(\frac{kT}{q} \right)$ as the y-axis intercept. Therefore n can be easily determined by substituting the constants into $n \left(\frac{kT}{q} \right)$. To evaluate Φ_{bo} , Cheung and Cheung (Cheung & Cheung, 1986) have defined a function $H(I)$:

$$H(I) = V - n \left(\frac{kT}{q} \right) \ln \left(\frac{I}{AA * T^2} \right) \quad (4.12)$$

where $H(I)$ can be written as follows:

$$H(I) = n\Phi_{bo} + IR_s \quad (4.13)$$

From Equation 4.13, the series resistance, R_s can be obtained from the slope of the linear region of the $H(I)$ vs I graph while the barrier height, Φ_{bo} can be extracted from the y-interception of the graph by utilising the n determined from Equation 4.11 as shown in Figure 4.17. For the value of $V > 3kT/q$, the ideality factor can be determined from the linear region of the I-V curve by using Equation 4.12. Figure 4.14 shows the linear fitting of the $\frac{dV}{d(\ln I)}$ vs I graph in the linear region for the untreated and acetic acid solutions treated devices.

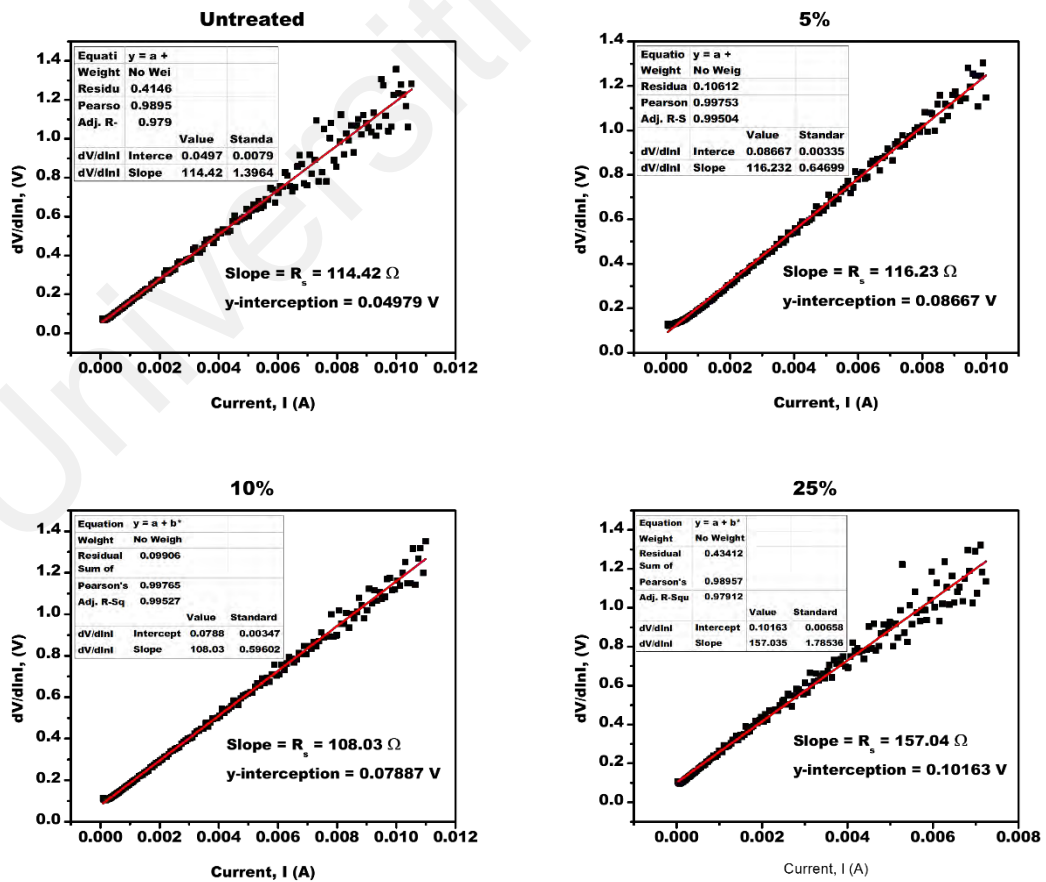


Figure 4.14, continued.

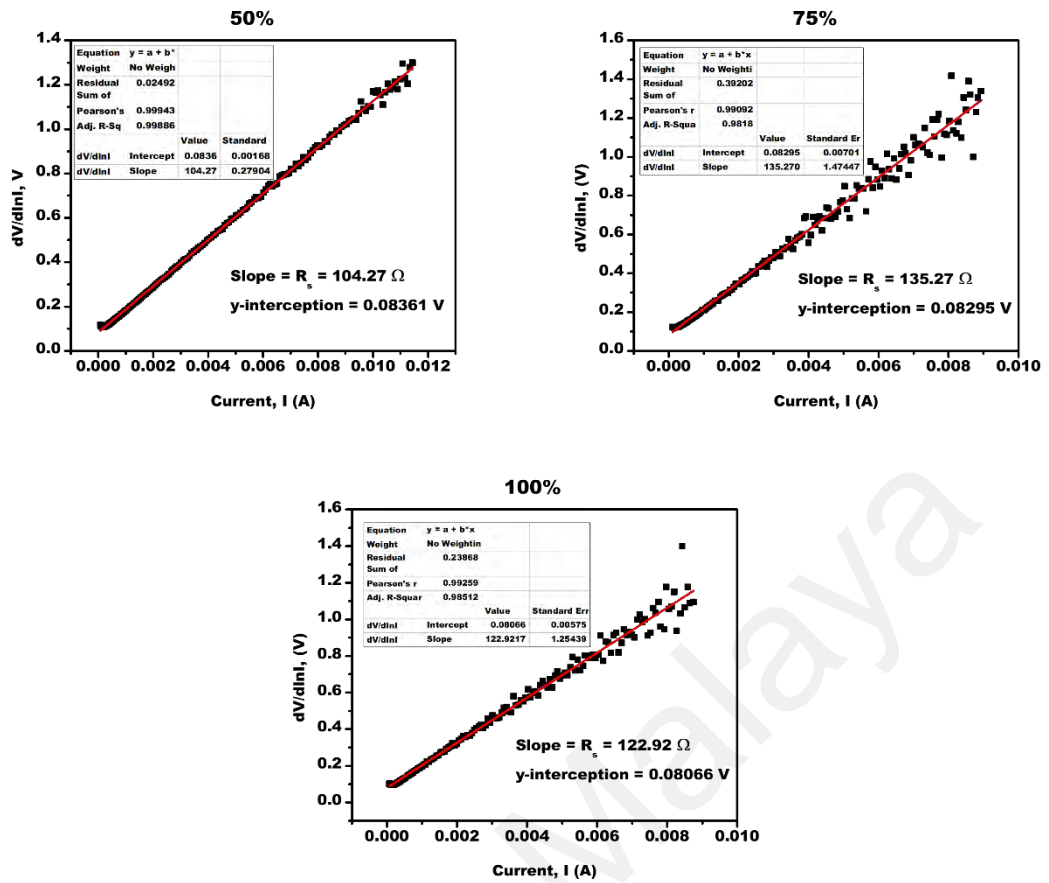


Figure 4.14: The linear fitting of $\frac{dV}{d(\ln I)}$ vs I graphs in the linear region for the untreated and acetic acid solutions treated devices.

Table 4.6: Ideality factor, n , series resistant, R_s and shunt resistant, R_{sh} determined from the $\frac{dV}{d(\ln I)}$ vs I graphs based on the Cheung and Cheng method, for the untreated and acetic acid solutions treated devices.

	Ideality Factor, n	Series Resistance, R_s (Ω)	Shunt Resistance, R_{sh} (Ω)
Untreated	1.93	114.43	5.15
5 %	3.35	116.23	5.23
10 %	3.05	108.03	4.86
25 %	3.93	157.04	7.07
50 %	3.23	104.27	4.69
75 %	3.21	135.27	6.09
100 %	3.12	122.92	5.53

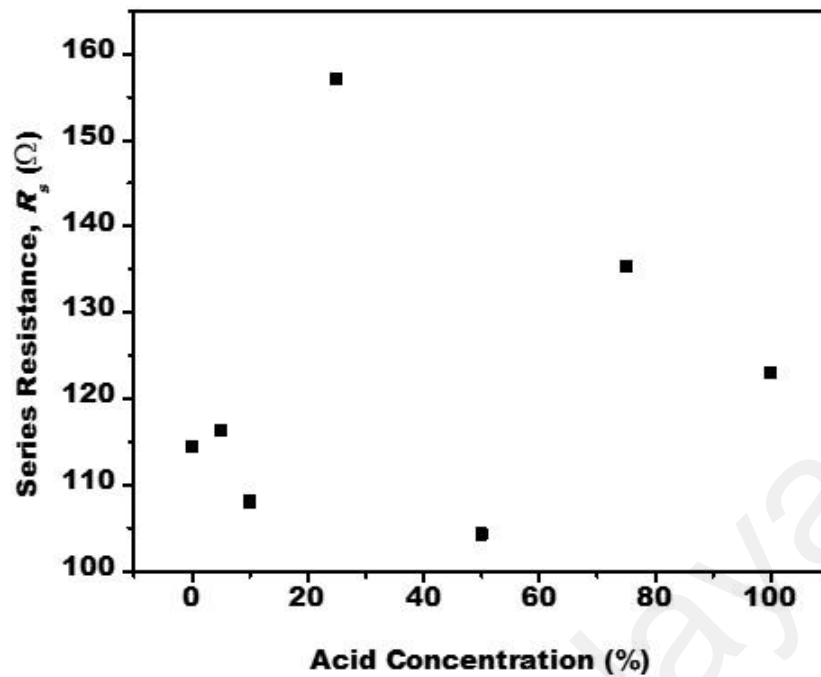


Figure 4.15: Series resistance, R_s versus acetic acid concentration plot for the untreated and acetic acid solutions treated devices extracted from linear fitting of $\frac{dV}{d(\ln I)}$ vs I plots.

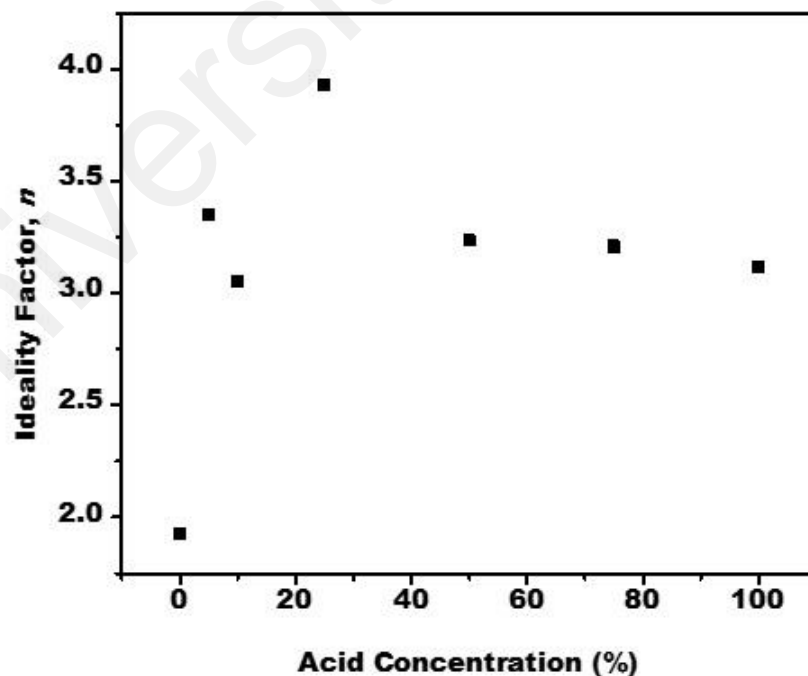


Figure 4.16: Ideality factor, n versus acetic acid concentration plot for the untreated and acetic acid solutions treated devices extracted from linear fitting of $\frac{dV}{d(\ln I)}$ vs I plots.

The determined ideality factor values calculated using Cheung and Cheung method (see Table 4.6), are higher than that calculated from ln I–V characteristics of the Schottky approach (see Table 4.5) except for the untreated device. It is apparent that the ideality factor increase after the acetic acid treatments. The discrepancies found in the n values can be ascribed to the fact that the semilogarithmic I–V characteristics depend on the interfacial properties and series resistance, R_s whereas $\frac{dV}{d(\ln I)}$ versus I plot is only governed by the series resistance, R_s (Kırsoy, Ahmetoglu, Asimov, & Kucur, 2015). The series resistances, R_s determined from while $\frac{dV}{d(\ln I)}$ versus I plot are comparable to values determined from Table 4.3. The different is that Table 4.3 results are obtained from I-V curves under light illumination while this method is utilising I-V curves in dark condition. The comparable results indicating this method is suitable to use as an alternative method to study the electrical properties of the OSCs. The values of ideality factors of the OSC devices in this research are in agreement to the previously reported of the same active layer of P3HT:PCBM (Altan, Özer, & Ezgin, 2020; Kadem, Hassan, & Cranton, 2016; Özge Tüzün Özmen, 2014; Ö Tüzün Özmen & Yağlıoğlu, 2014).

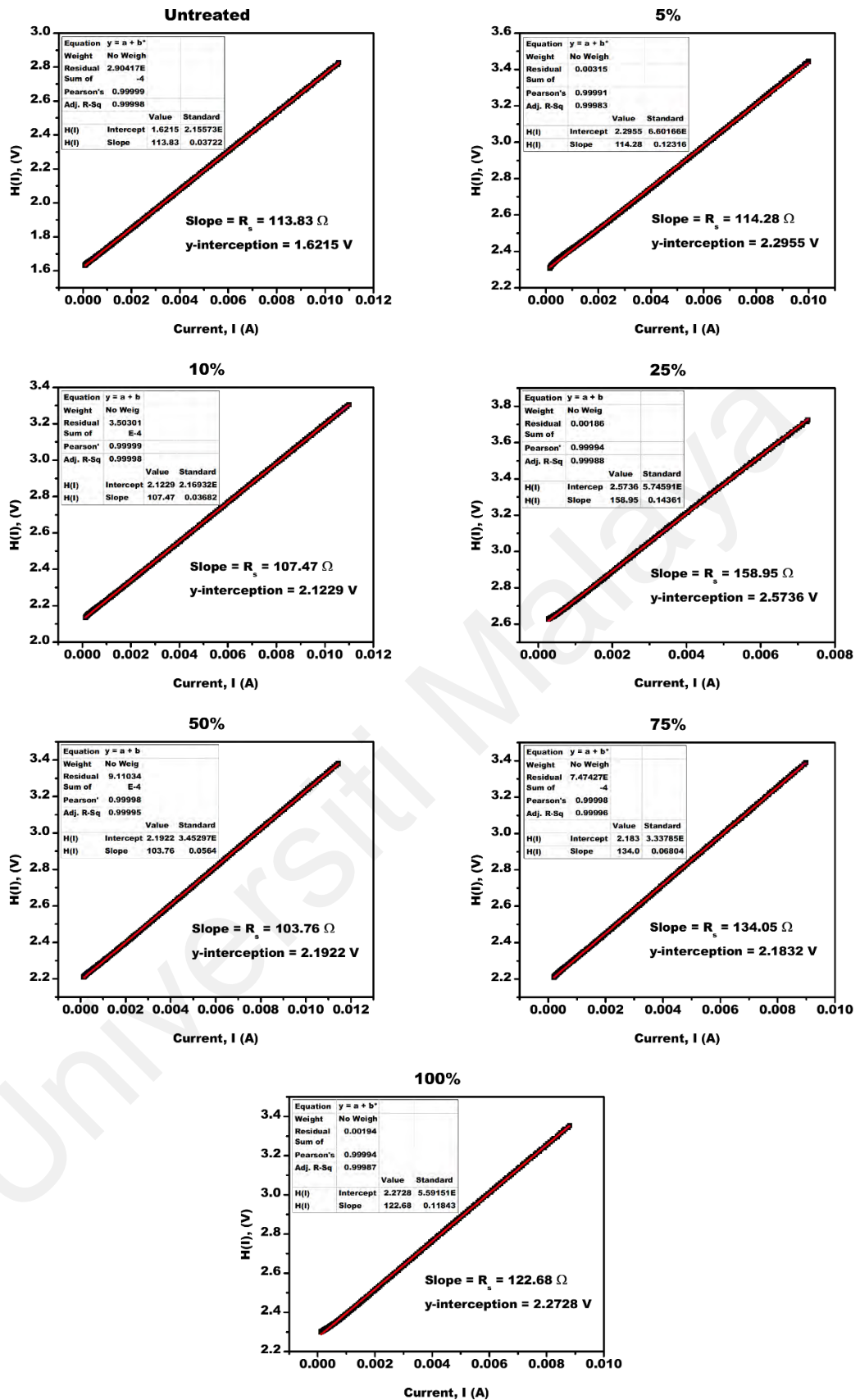


Figure 4.17: The linear fitting of $H(I)$ vs I graphs in the linear region for the untreated and acetic acid solutions treated devices.

Table 4.7: Series resistance, R_s , shunt resistance, R_{sh} and barrier height, Φ_{bo} determined from linear fitting of $H(I)$ vs I graphs based on the Cheung and Cheung method.

	Series Resistance, R_s (Ω)	Shunt Resistance, R_{sh} (Ω)	Barrier Height, Φ_{bo} (eV)
Untreated	113.84	5.12	0.84
5 %	114.28	5.14	0.68
10 %	107.48	4.84	0.70
25 %	158.95	7.15	0.65
50 %	103.77	4.67	0.68
75 %	134.06	6.03	0.68
100 %	122.68	5.52	0.73

Furthermore, the R_s and Φ_{bo} can be further examined using the $H(I)$ function. From the $H(I)$ versus I plots as shown in Figure 4.17 and by substituting the n determined from Equation 4.12 into Equation 4.13, the R_s of the devices (as tabulated in Table 4.7) are found to be similar to the results in Table 4.6 and the Φ_{bo} of the devices are around 0.65 eV to 0.84 eV. The R_s determined from $H(I)$ versus I plots do not show any useful trend as shown in Figure 4.18. However, the Φ_{bo} of the devices obtained from this method are comparable to the values calculated from the Ohmic region slope of the dark I-V curve on the natural logarithmic (ln) scale and Equation 4.7. The Φ_{bo} of the devices shows a dropping trend as soon as the OSCs gone through the acetic acid treatments as shown in Figure 4.19. This suggesting that the acetic acid effectively reducing the barrier height and improve the charge transfer mechanism in the devices. Noted that the Φ_{bo} determined using the $H(I)$ versus I plots as shown in Table 4.7 is comparable to the values determined in Table 4.5 which showing $H(I)$ function method is highly reliable and suitable to use an alternative tool to investigate electrical properties of the OSCs. Furthermore the obtained barrier height in this study found to be in agreement with those reported (Kadem, Fakher Alfahed, Al-Asadi, & Badran, 2020; Kadem et al., 2016; Ö Tüzün Özmen & Yağlıoğlu,

2014). Some of the previous study also showed the barrier height can be reduced upon post thermal annealing, embedment of gold nanoparticles or fabricate the device with appropriated mass ratio of P3HT:PCBM (Aloui, Adhikari, Nunzi, Bouazizi, & Khirouni, 2015; C.-E. Cheng, Pei, Hsu, Chang, & Shih-Sen Chien, 2014; Khan, Bhargav, Kaur, Dhawan, & Chand, 2010; Özge Tüzün Özmen, 2014).

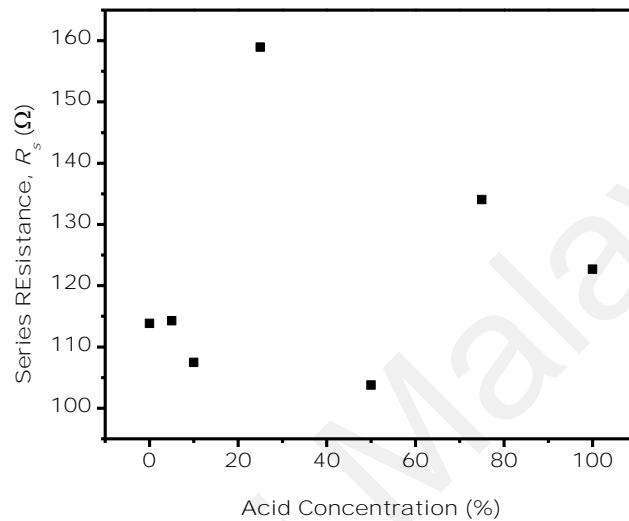


Figure 4.18: Series resistance, R_s versus acetic acid concentration plot for the untreated and acetic acid solutions treated devices extracted from linear fitting of $H(I)$ vs I plots.

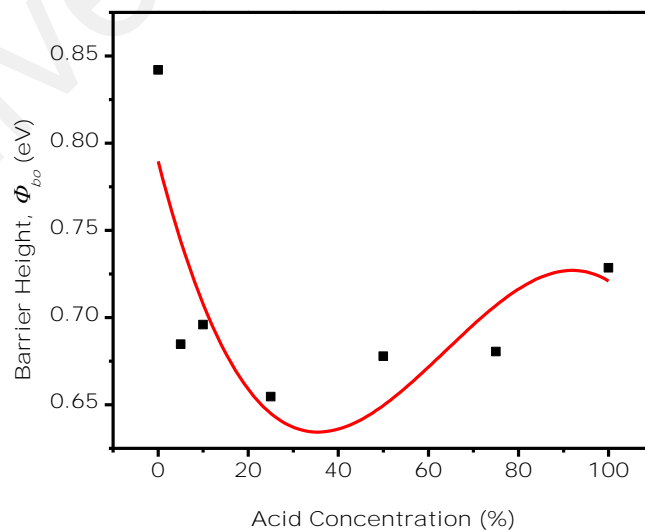


Figure 4.19: Barrier height, Φ_{bo} versus acetic acid concentration plot for the untreated and acetic acid solutions treated devices extracted from linear fitting of $H(I)$ vs I plots.

4.5.2 Norde's Function

Norde's function is another approach used to obtain the series resistance, R_s and the barrier height, Φ_{bo} of the organic solar cells. The Norde's function can be inscribed as below (Aziz, Ahmad, Abdullah, Sulaiman, & Sayyad, 2015; Norde, 1979):

$$F(V) = \frac{V}{\gamma} - \left(\frac{kT}{q}\right) \ln\left(\frac{I}{AA^*T^2}\right) \quad (4.14)$$

where γ is a dimensionless arbitrary integer greater than the value of ideality factor, n , acquired from the I-V characteristics. According to the previously obtained results in chapter 4.5.1 (Cheung & Cheung method), the value of γ is chosen as 4. The Norde's function plotted against V ($F(V)$ vs V graph) using Equation 4.14 is displayed in Figure 4.20. The barrier height, Φ_{bo} can be determined from the following equation:

$$\Phi_{bo} = F(V_o) + \frac{V_o}{\gamma} - \left(\frac{kT}{q}\right) \quad (4.15)$$

where $F(V_o)$ is the minimum point of $F(V)$ versus V plot. V_o is the corresponding voltage of $F(V_o)$. Additionally, the value of R_s can be determined using the following relation:

$$R_s = \frac{kT(\gamma-n)}{qI_o} \quad (4.16)$$

where I_o is the corresponding current at the minimum point of the $F(V_o)$. From Norde's method, the determined series resistance, R_s and the barrier height, Φ_{bo} of the organic solar cells can be compared with the values acquired from the Cheung and Cheung's functions.

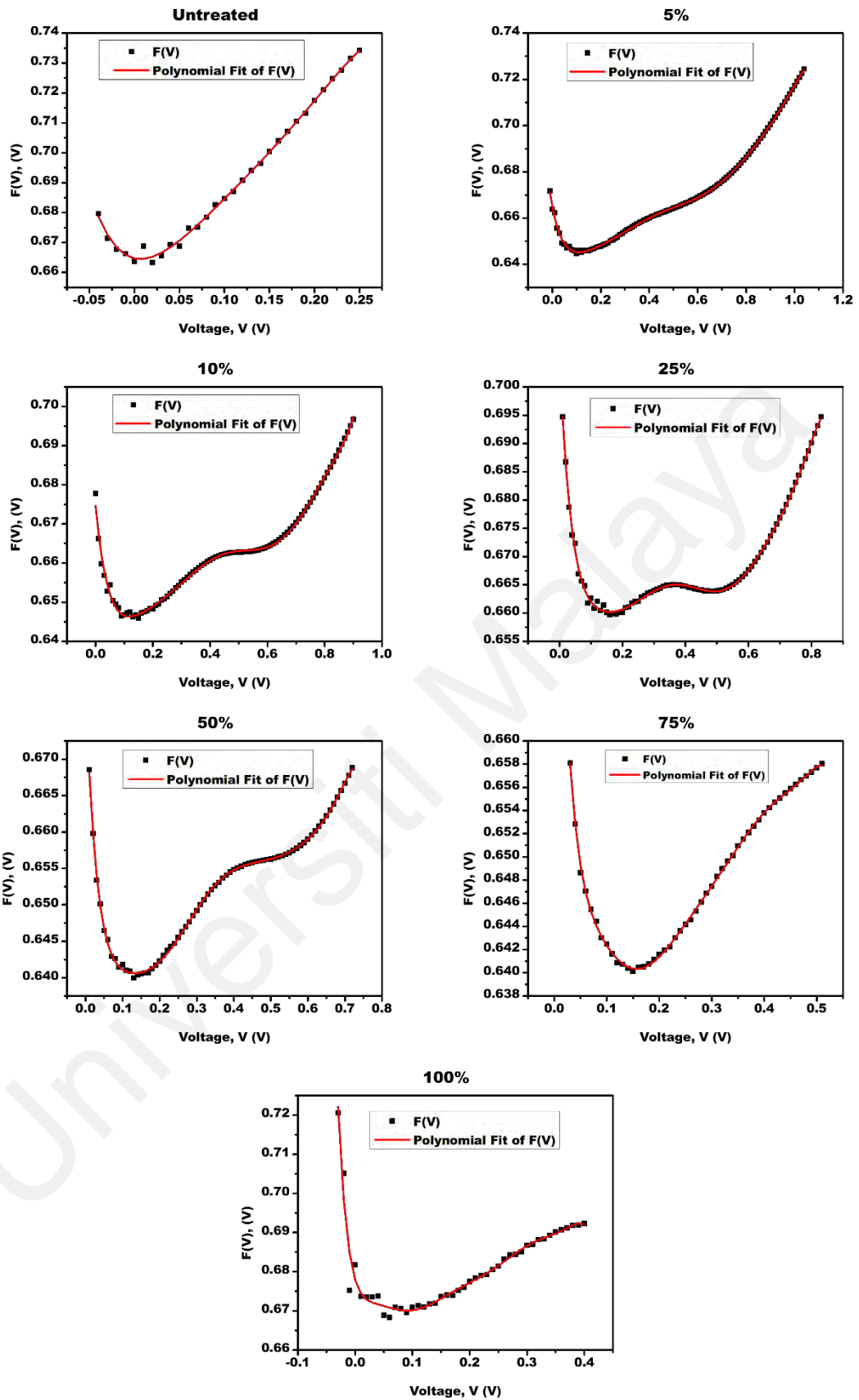


Figure 4.20: The polynomial fitting of $F(V)$ vs V graphs in the linear region based on the Norde's function, for the untreated and acetic acid solutions treated devices.

Table 4.8: The electrical properties for the untreated and acetic acid solutions treated devices extracted from polynomial fitting of F(V) vs V graphs.

	F(V _o) (V)	V _o (V)	Φ_{bo} (eV)	I _o (A)	R _s (Ω)	R _s (Ωcm^2)
Untreated	0.6646	0.01	0.644	1.2×10^{-6}	1592	72
5 %	0.6452	0.11	0.647	6.9×10^{-6}	2426	109
10 %	0.6463	0.12	0.650	7.2×10^{-6}	3409	153
25 %	0.6602	0.16	0.675	6.6×10^{-6}	269	12
50 %	0.6406	0.13	0.647	10.6×10^{-6}	1868	84
75 %	0.6403	0.16	0.417	13.9×10^{-6}	1472	66
100 %	0.6700	0.09	0.667	2.3×10^{-6}	9892	445

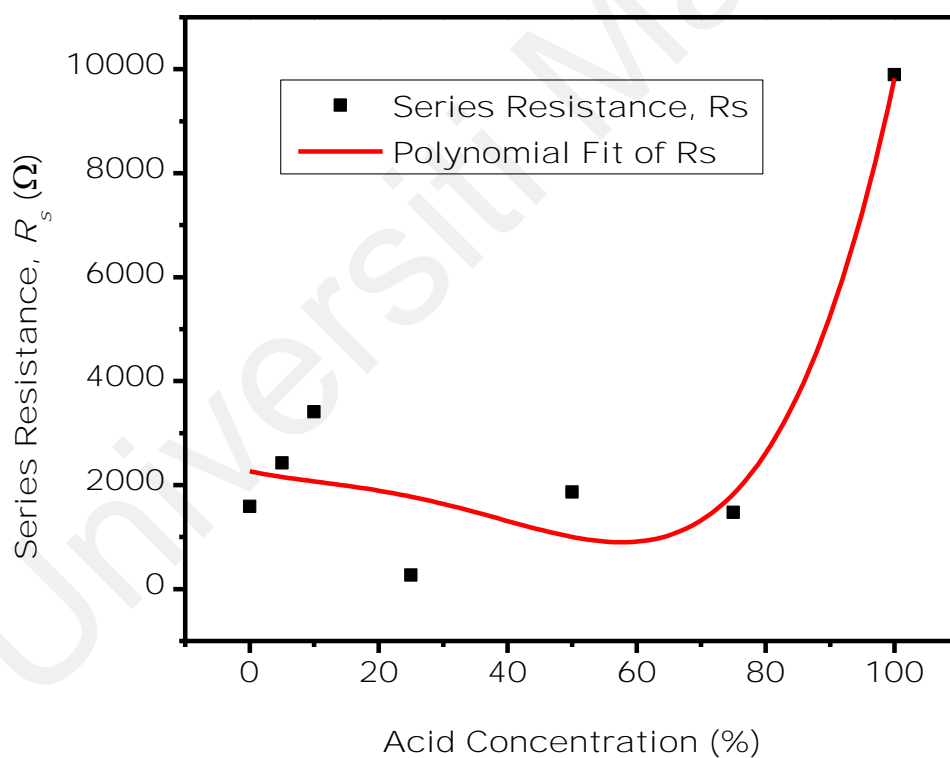


Figure 4.21: Series resistance, R_s versus acetic acid concentration plot for the untreated and acetic acid solutions treated devices determined from Norde's function.

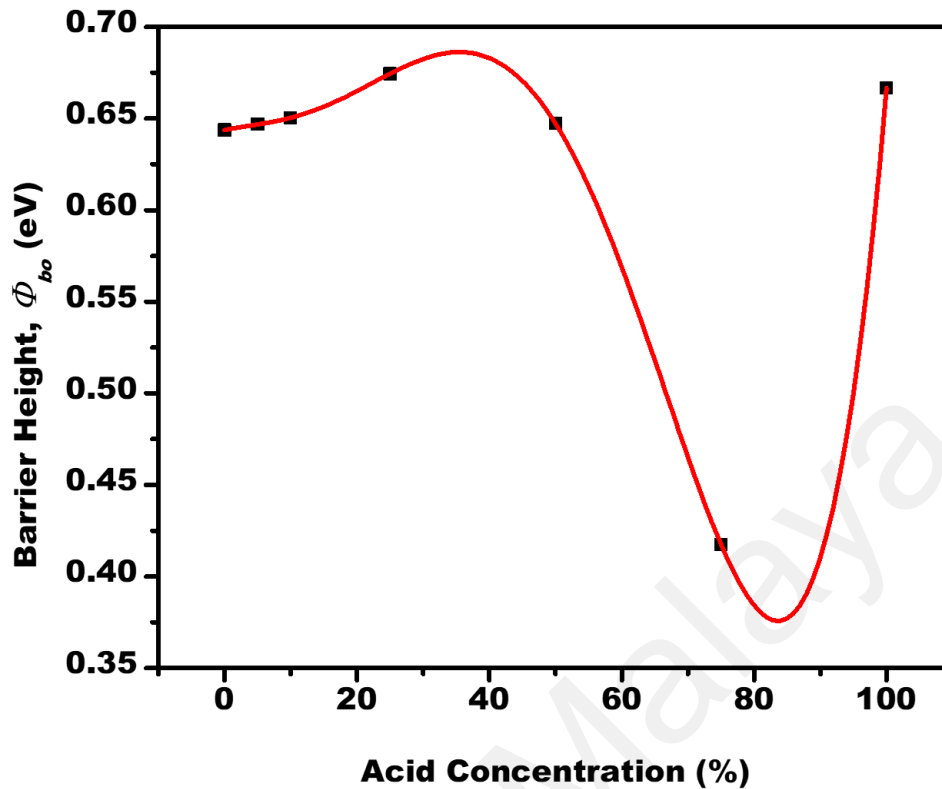


Figure 4.22: Barrier height, Φ_{bo} versus acetic acid concentration plot for the untreated and acetic acid solutions treated devices determined from Norde's function.

The series resistance, R_s determine from Norde's function (as tabulated in Table 4.8) is greater than the series resistance determined from Cheung and Cheung's method (as tabulated in Table 4.7) and I-V curves under light illumination (as tabulated in Table 4.3). However, the R_s are showing a dropping trend after the acid solution treatments as shown in the Figure 4.21. The barrier height, Φ_{bo} determined by Norde's function (as tabulated in Table 4.8) are comparable to the results acquired from Cheung and Cheung's functions (as tabulated in Table 4.7) and I-V curves in the dark condition (as tabulated in Table 4.5). Figure 4.22 shows the barrier height, Φ_{bo} versus acetic acid concentration plot for the untreated and acetic acid solutions treated devices determined from Norde's function. The fitting (red line) shows the Φ_{bo} will be the minimum for 85 % acetic acid solution.

Both the Cheung & Cheung method and Norde's function show that the Φ_{bo} of the OPVCs have been reduced after the acetic acid solution treatment. This indicates that the acetic acid solution treatment can be an important process on the refining interfacial condition including the surface morphology of blending films which results in the reduction of barrier height at the interface of Al/P3HT:PC₆₁BM. It is supported by the FESEM observations in that the surface morphology of blending films is smoothed and most impurities have been removed after the acetic acid treatments which will be showed in chapter 4.10. The analysis in J-V characteristics show that the improved J_{sc} is attributed to lowered barrier height at the interface of Al/P3HT:PC₆₁BM. Reduction in barrier height facilitates hole transport and decreases the contact resistance. A possible explanation for this improvement is owing to the decreased series resistance (R_s). The values of the R_s extracted from the J-V curves. R_s can reflect the ohmic loss in the OPVC which includes the resistance of the organic photoactive layer/electrode contacts, the photoactive layer, the electrodes and the parasitic probe resistance. Low barrier height allows efficient charge collection and thus increases J_{sc} of the solar cells. Such electrical improvements may due to the reduction in interfacial trap states as well as enhancement in interfacial dipole-moment for given solar cells (Moiz, Alahmadi, & Karimov, 2020).

4.6 Space Charge Limited Conduction (SCLC) Explanation

Space charge limited conduction (SCLC) theory was developed by Mott Gurney (Mott & Gurney, 1948; X. Zhang & Pantelides, 2012) in 1940 for a trap-free insulator with single carrier injection. It was later adapted by Rose and Lampert for localized trapping states in the gap of an insulator (Lampert, 1956) and was used for the first time in organic crystals system by Helfrich and Mark in 1962 (Mark & Helfrich, 1962). Thenceforth, this

method is accepted for measurements in various kind of organic amorphous and crystalline semiconductors.

Figure 4.23 shows the semi-logarithmic J-V graph of ITO/PEDOT:PSS/P3HT:PC₆₁BM/Al OSC devices under influence of light illumination. The reverse bias region shows an upward shifting of current density between untreated and acid treated devices indicating enhancements of current density output after the acetic acid treatments. However, the forward bias region has no substantially difference in the semi-logarithmic J-V plot under light illumination. Noteworthy that the semi-logarithmic J-V graph of OSCs under dark condition is telling another story. The forward bias region shows a noticeable shape inconsistency between the untreated and acid treated OSCs (as indicated in the red dotted circle in Figure 4.24). Figure 4.25 is the enlarged image of the red dotted circle region in Figure 4.24 to display the curves shifting clearer.

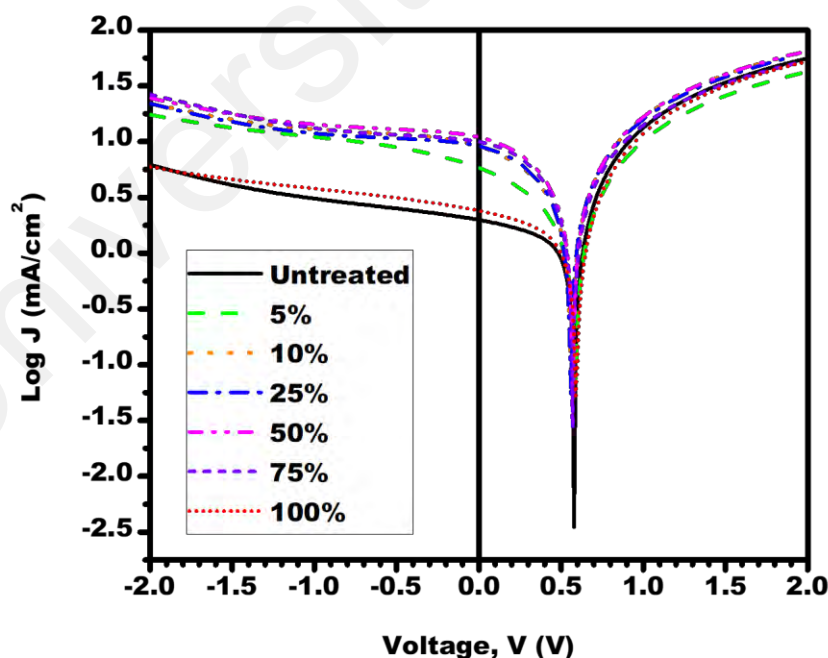


Figure 4.23: Log J versus V plot for the untreated and acetic acid solutions treated devices under light illumination.

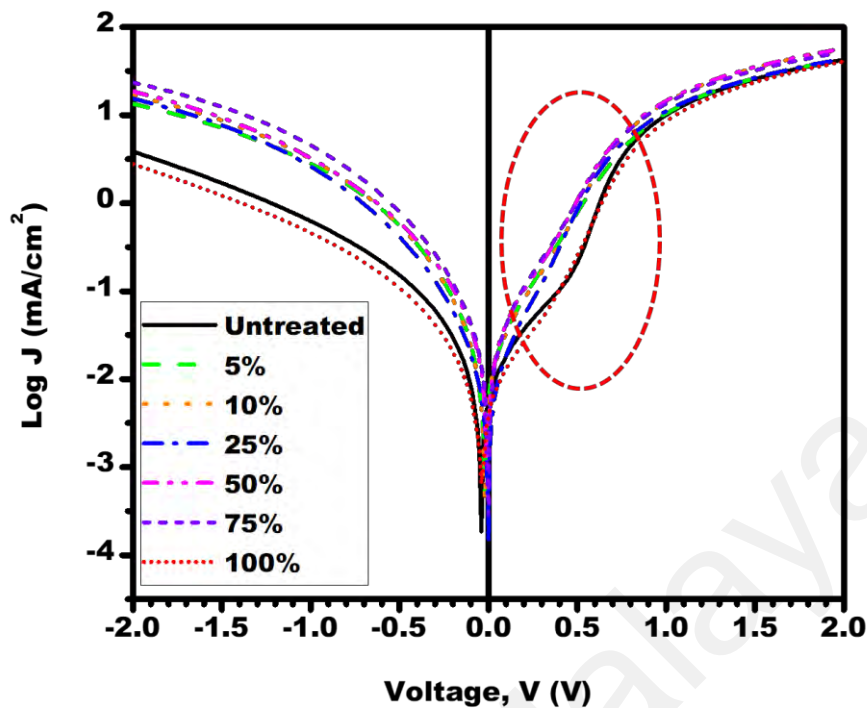


Figure 4.24: Log J versus V plot for the untreated and acetic acid solutions treated devices under dark condition. Red circle indicates differences which showed in Figure 4.25 as enlarged plot.

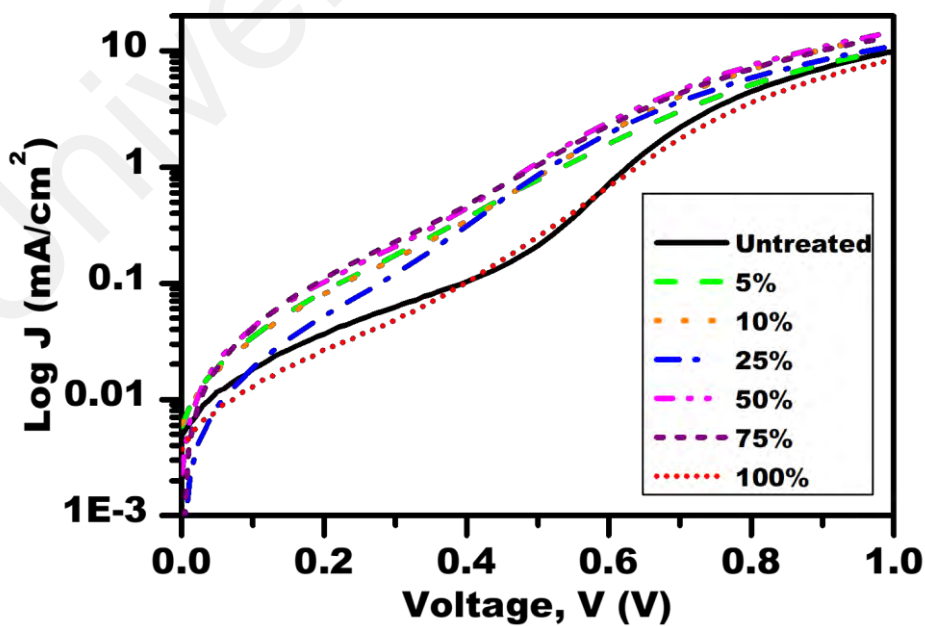


Figure 4.25: Enlarged plot on the red circle area of Figure 4.20 (Log J versus V plot for the untreated and acetic acid solutions treated devices under dark condition).

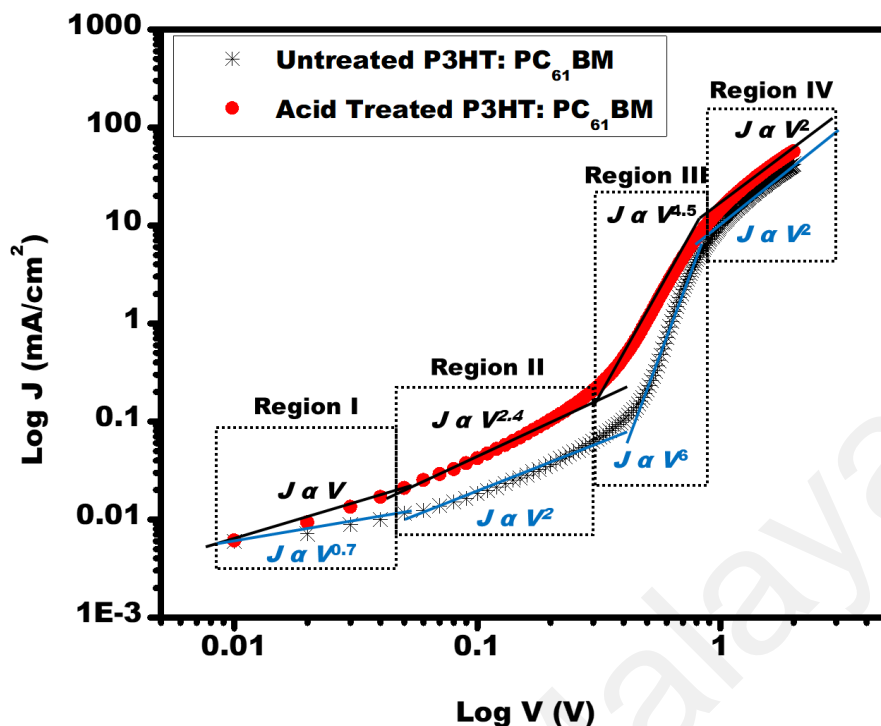


Figure 4.26: Log J versus log V plot of OSCs with pristine and acetic acid solutions treated P3HT:PC₆₁BM active layers in dark condition.

In SCLC measurement, an organic material of thickness L is placed between two electrode contacts and a current curve is recorded with the applied voltage. As can be seen in Figure 4.26, four regions can be distinguished in which the current density, J is plotted against the applied voltage, V . In small electric field (low V), the charge transport is considered to be Ohmic and the current density increased linearly with the applied voltage ($J \propto V$). Hence it is called Ohmic regime. In higher electric field, the current density (region II) becomes space-charge limited which the current density showed quadratic dependence to the applied voltage, $J \propto V^2$ (Mihailetchi, Wildeman, & Blom, 2005; Nikitenko, Heil, & Seggern, 2003; Ostroverkhova, 2018). In the first region of the SCLC regime (region I), a portion of the injected carriers is trapped and the steady-state space charged limited current is decreased by a factor θ . Using a simplified explanation, the current represents the ratio between the number/concentration of free (n_f) and total

(n_{tot}) charge carriers in the material (Ostroverkhova, 2018). However, θ can have more complex dependencies on the device geometry, applied voltage, energy and spatial distribution of traps, etc. As the voltage increases, the Fermi level moves towards the valence band of the semiconductor for the p-type conduction case or towards the conduction band for the n-type conduction case and traps are filled gradually, resulting a rise in the free charge carriers density/concentration (region II). At the trap-filling limit voltage (V_{TFL}), all traps are filled ($\theta = 1$) causing the current increases drastically (region III). After this point, the system is in the trap-free SCLC region (region IV). The transition point to region IV is determined by the traps density and the current can sometimes be increased by orders of magnitude for material with a high traps density. The V_{TFL} value contains important information about the traps concentration, N_t because these two quantities are related by a very simple expression:

$$N_t \cong \frac{\epsilon_0 \epsilon_t V_{\text{TFL}}}{e L^2} \quad (4.17)$$

Where ϵ_0 is the permittivity of the free space and ϵ_t is the dielectric constant of the semiconductor. Note the N_t represents the volume concentration of traps which is an intrinsic property of the organic semiconductor while N_t from Equation 4.17 quantifies the surface trap densities at the organic semiconductor/dielectric interface. The mobility estimated from the trap-free SCLC regime represents the intrinsic mobility of the material (Ostroverkhova, 2018).

The current in an organic solid is determined by the intrinsic properties of the material as well as the carrier concentration gradients which are strongly dependent on the trap density of states. Several assumptions are made in developing the SCLC theory:

- Unipolar, 1-dimensional current flow: The charge carriers are injected from the contact placed at position $x = 0$ and collected at the contact placed at $x = L$. the

case of hole-transport will be discussed here but the electron-transport model is similar.

- The contacts are Ohmic: they represent an infinite source of charge carriers. Ohmic contacts yield an Ohmic regime at low applied voltage. Deviations from a slope of 1 in the double logarithmic plot of J versus V at low voltages are a clear indication that the contacts are not Ohmic.
- All traps are homogeneously distributed in space and correspond to one discrete energy level.
- The density of free charge carriers (n_f) follows Boltzmann statistics (Equation 4.18) and the density of the trapped (localised) carriers (n_t) follows the Fermi-Dirac statistics (Equation 4.19). The free and trapped charge carriers are in equilibrium under SCLC flow, in the dark and the photo-effects are not considered.

$$n_f = N_V e^{-\frac{E_F(x)}{kT}} \quad (4.18)$$

$$n_t = \frac{h(E)}{1 + e^{\frac{E_i - E_F}{kT}}} \quad (4.19)$$

Here N_V represents the effective density of states in the valence band, E_F is the Fermi level, E_i is the trap energy, $h(E)$ describes the energetic distribution of localised states and k is the Boltzmann's constant.

If there are discrete trapping energies separated by an energy barrier greater than kT or if the trap energies follow a more complex distribution, the current-voltage curve will deviate from the $J \propto V^2$ to $J \propto V^n$ dependency where $n > 2$. Compared to single trap case described in SCLC, the drastic increase of current as a function of voltage for the case of traps distributed in energy derived from the differences in the shift of Fermi level where the Fermi level is proportional to the space charge which in turn is proportional to the

applied voltage. For this reason, the shape of the I-V curve can offer important information about the of trap states density in the band gap of an organic semiconductor.

Figure 4.26 is the double-logarithmic of the J-V response of the pristine and acid treated devices in dark condition which further shows distinct differences in the slopes of the OSCs' J-V curves, respectively. One can notice from Figure 4.26 that current density change in the low voltage range (region I) is linear ($J \propto V$) for the acid-treated device (Ohmic regime). This observation has been discussed earlier in Schottky diode approach.

Region II, where the slope of the curve is approximately 2, can be expressed as trap-filling space charge limited current (TFSCLC) which carrier charges are injected into active layer (Lou, Wang, Naka, & Okada, 2012; Ostroverkhova, 2018; Rehman, Yang, Yang, Karimov, & Choi, 2017; Schauer, 2005). In this region, the injection of charge into the device is taken place by tunneling and the active layer bulk is able to use up all the injected charges in the conduction of current, until it reached a point where the active layer bulk became saturated and injected charges built up near the injected electrode. In region III, the rate of increasing current density following a power law relation (Lou et al., 2012; Rehman et al., 2017; Schauer, 2005). This is because all possible traps are filled and current approaches the trap-free space charge limit (Ostroverkhova, 2018; Wilken, Sandberg, Scheunemann, & Österbacka, 2020). It should be pointed out that the space charge limited current (SCLC) region is predominantly observed for the pristine devices since the traps are filled rapidly and the current density raised up by several orders of magnitude with the power values in the value of 6 ($J \propto V^6$) compared to the acetic acid treated device where the current density raised up with the power values in the value of 4.5 ($J \propto V^{4.5}$). These high power values in the bulk heterojunction system of organic solar cells are commonly observed. Other researchers also reported higher values in the range of 4.85 to 44 (Lou et al., 2012; Rehman et al., 2016; Rehman et al., 2017; Schauer, 2005).

From the double-logarithmic of J-V response in dark condition (Figure 4.26), the trap-filling limit voltage (V_{TFL}) is estimated and tabulated in Table 4.9. As can be observed that V_{TFL} decreased after the acetic acid treatment except for pure acetic acid concentration. The V_{TFL} becomes the lowest at 50 % acetic acid concentration. From Equation 4.17, the concentration of traps, N_t can be estimated for the untreated and acetic acid treated devices and tabulated in Table 4.9. It is apparent that the N_t follows the same trend as V_{TFL} which is the minimum at 50 % acetic acid concentration. This result can well explain higher current produced in the acetic acid treated OSCs which the concentration of traps in the acetic acid treated devices become lower compare to the untreated device. The acetic acid treated devices have lower V_{TFL} indicating the traps can be filled faster and causing the slope of the double-logarithmic of the J-V curves to be lower. Fast filling of traps is the resultant of lower traps concentration in the acetic acid treated devices (except 100 % acetic acid). Hence, it is concluded that acetic acid treated P3HT:PC₆₁BM based devices present larger exciton dissociation and could be attributed to lower trap densities compared to those of the pristine devices. However, these electrical parameters are not conclusive on the description of higher photocurrent generation for sample being treated by acetic acid. Hence the optical measurements of UV-Vis spectroscopy and analysis are required and will be discussed in next section.

Table 4.9: The trap-filling limit voltage, V_{TFL} and concentration of traps, N_t of the untreated and acetic acid solutions treated devices extracted from double-logarithmic of the J-V.

	Trap-Filling Limit Voltage, V_{TFL} (V)	Concentration of Traps, N_t ($\times 10^{22} \text{ cm}^{-3}$)
Untreated	0.82 ± 0.02	1.10 ± 0.03
5 %	0.76 ± 0.02	1.02 ± 0.03
10 %	0.75 ± 0.02	1.01 ± 0.03
25 %	0.75 ± 0.02	1.01 ± 0.03
50 %	0.73 ± 0.02	0.98 ± 0.03
75 %	0.73 ± 0.02	0.99 ± 0.03
100 %	0.82 ± 0.02	1.11 ± 0.03

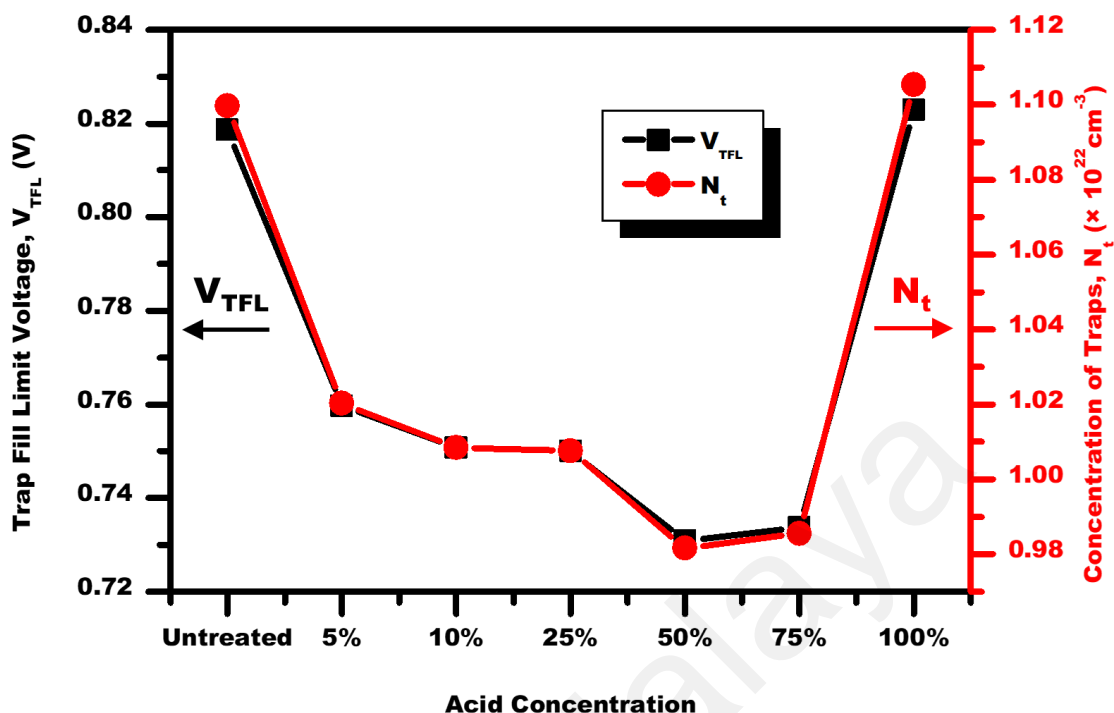


Figure 4.27: The trap-filling limit voltage, V_{TFL} and concentration of traps, N_t of the untreated and acetic acid solutions treated devices plot against acid concentration.

4.7 Ultraviolet - Visible (UV-Vis) Absorption Measurements

Attempts have been made to ascertain the cause of the enhancement of the organic solar cells after gone through the acetic acid treatments through optical measurements. In this section, experimental results of UV-Vis spectroscopy are reported. The active layer of P3HT:PC₆₁BM organic thin films deposited prepared via spin-coating method on the glass substrates were used in this study. Besides, the pristine films of P3HT polymer and PC₆₁BM fullerene derivative were also prepared and characterized.

Figure 4.28 shows the normalized UV-Vis spectrum of the untreated and acid treated P3HT:PC₆₁BM organic thin films. Illustrative spectra of pristine P3HT and PC₆₁BM are also included in this figure, to show the intrinsic absorption of the films before the mixing. It is obvious that the absorbance of the blended P3HT:PC₆₁BM organic thin films are the

superposition of the absorbance of the pristine P3HT and PC₆₁BM thin films. In the spectra, P3HT dominated the absorption between 400 nm and 650 nm while PC₆₁BM dominated the absorption below 400 nm.

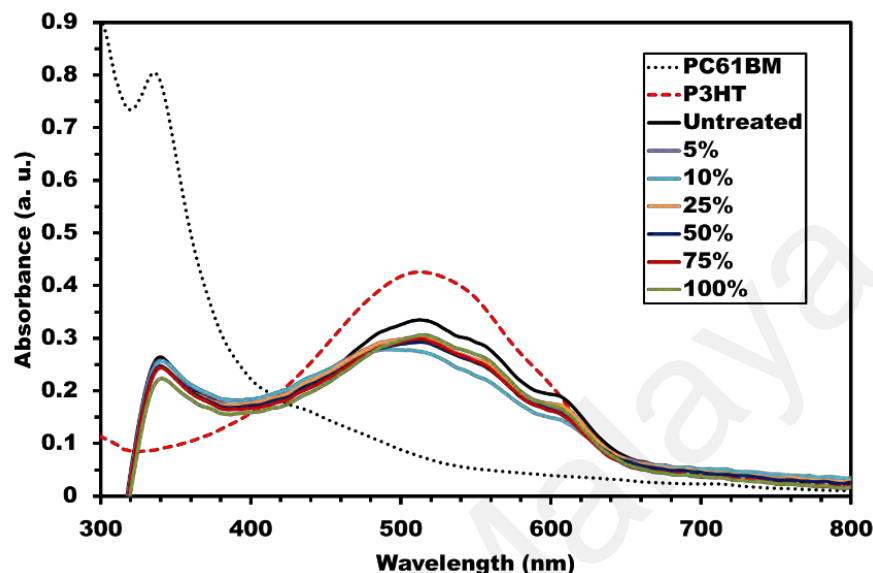


Figure 4.28: UV-Vis spectrum of the untreated and acid treated P3HT:PC₆₁BM organic thin films. The pristine films of P3HT and PC₆₁BM are also displayed.

The sharp absorption peak located around the wavelength of 300 nm to 400 nm is assigned to the B (Soret) Band of PC₆₁BM and P3HT while the Q bands lie in the visible region (400nm to 650nm). The spectra consist of two main absorption bands at 330 and 515 nm which tie in with the π - π^* transition in P3HT and PCBM-bis-PCBM, respectively. Noticeably, the inclusion of PC₆₁BM into P3HT has led to a quenched photo-absorption, suggesting the occurrence of intermolecular interaction between the P3HT polymer host and PC₆₁BM, while lowering the interaction among the P3HT chains (Shrotriya, Ouyang, Tseng, Li, & Yang, 2005). However, the overall absorption spectra for the untreated and treated thin films exhibit similar pattern without any shift in wavelength indicates that the acid treatment process does not alter the molecular packing of the P3HT and PC₆₁BM in the bulk heterojunction system. This finding is further examined via Raman spectroscopy in next section.

4.8 Raman Spectroscopy Measurements

Figure 4.29 and Table 4.10 present resonant Raman spectroscopy characterizations of untreated and acid treated P3HT:PC₆₁BM organic thin films. One can clearly observe that there is no Raman shift in the measurements indicates that the acid treatment does not cause any structural alteration of chemical structure in the molecules. This Raman finding support the results obtained in the UV-Vis spectra.

Two most intense and sharp peaks located at 1450 cm⁻¹ and 1380 cm⁻¹ are attributed to the C=C symmetric stretching mode and the C-C in-plane skeleton mode of the P3HT thiophene ring respectively. The peak at 727 cm⁻¹ is assigned to the vibrational frequency of the antisymmetric C-S-C in-plane ring skeleton mode of the P3HT. The peak at 1002 cm⁻¹ is due to C-C stretching mode. The 1092 cm⁻¹ peak can be assigned to C-H bending mode. The vibrations at 1208 cm⁻¹ originate from the combination of C-C stretching mode and C-H stretching mode. The 1514 cm⁻¹ peak is due to C=C antisymmetric stretching mode. The peaks at 2823 cm⁻¹ and 2901 cm⁻¹ are caused by the C-H symmetric stretching and C-H antisymmetric stretching respectively (Shao et al., 2014).

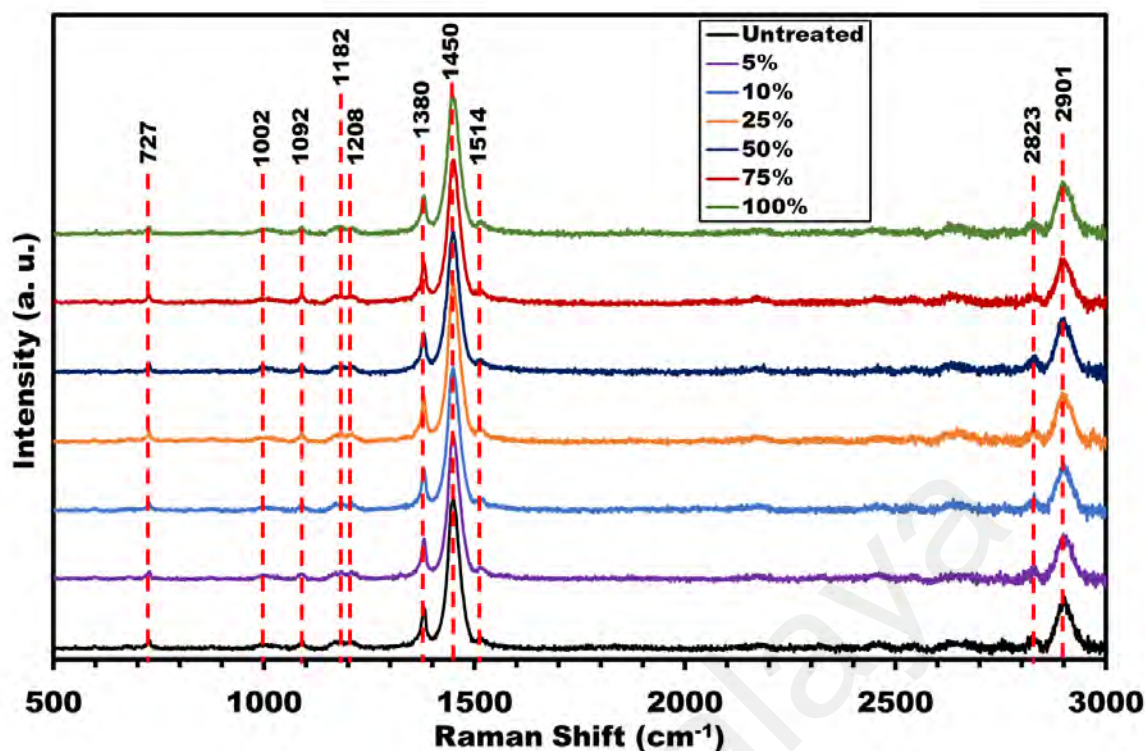


Figure 4.29: Raman spectroscopy measurements of untreated and acid treated P3HT:PC₆₁BM organic thin films.

Table 4.10: Summary of Raman spectroscopy measurements of untreated and acid treated P3HT:PC₆₁BM organic thin films.

Wavenumber (cm ⁻¹)	P3HT:PC ₆₁ BM
2901	C-H antisymmetric stretching
2823	C-H symmetric stretching
1514	Inter-ring C=C symmetric stretch
1450	Thiophene symmetric C=C stretching vibrations
1380	Thiophene C-C intra-ring/skeletal stretch mode
1208	Inter-ring C-C stretch mode
1182	C-H bending mode & C-C inter-ring stretch mode
1092	C-H bending mode
1002	C-C stretching mode
727	C-S-C deformation mode

4.9 X-Ray Diffraction (XRD) Measurements

The X-ray diffraction spectra of the P3HT:PC₆₁BM organic thin films obviously show the presence of a crystalline phase. There is only one single peak was observed in the

measurement range between 3° and 30° as shown in Figure 4.30. The crystalline peak located at around $2\theta = 5.2^\circ$. The corresponding lattice constant, d can be determined using Bragg's law:

$$2d \sin \theta = n\lambda \quad (4.20)$$

where $\lambda = 0.154$ nm is the wavelength of the incident X-ray beam; 2θ is the angle between the incident X-ray beam and the scattered X-ray wavevectors, and n is the interference order.

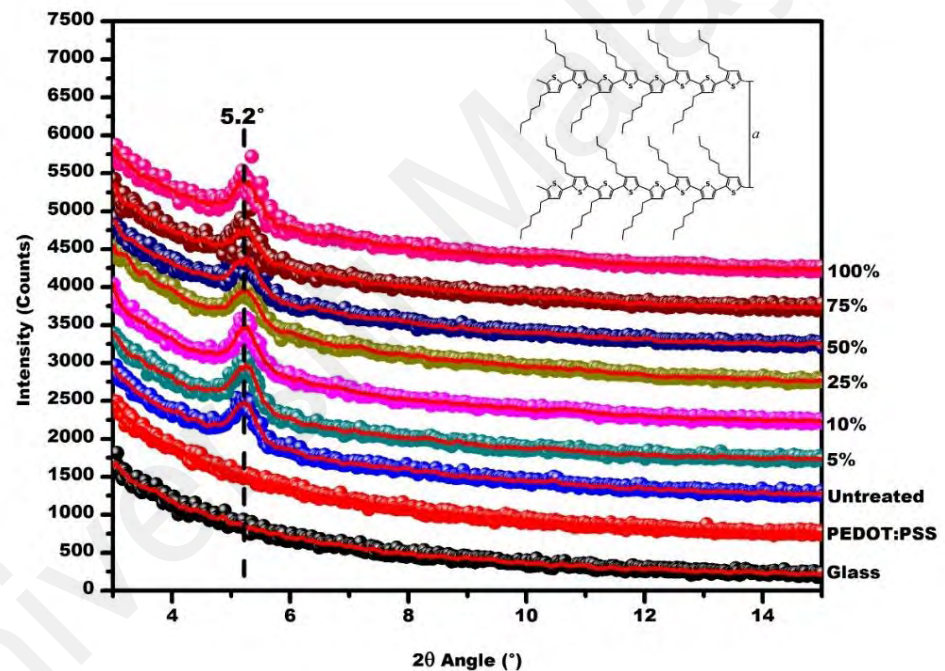


Figure 4.30: The X-ray diffraction (XRD) spectra of the untreated and acetic acid treated P3HT:PC₆₁BM organic thin films.

The interplanar distance, d determine from the Equation 4.20 is 1.70 nm. By comparing with the literature data (Aasmundtveit et al., 2000; Erb et al., 2005), it can be concluded that the detected peak is contributed by P3HT crystallites in the blend films with a -axis orientation (main chain parallel and side chain perpendicular to the substrate as shown in Figure 4.31).

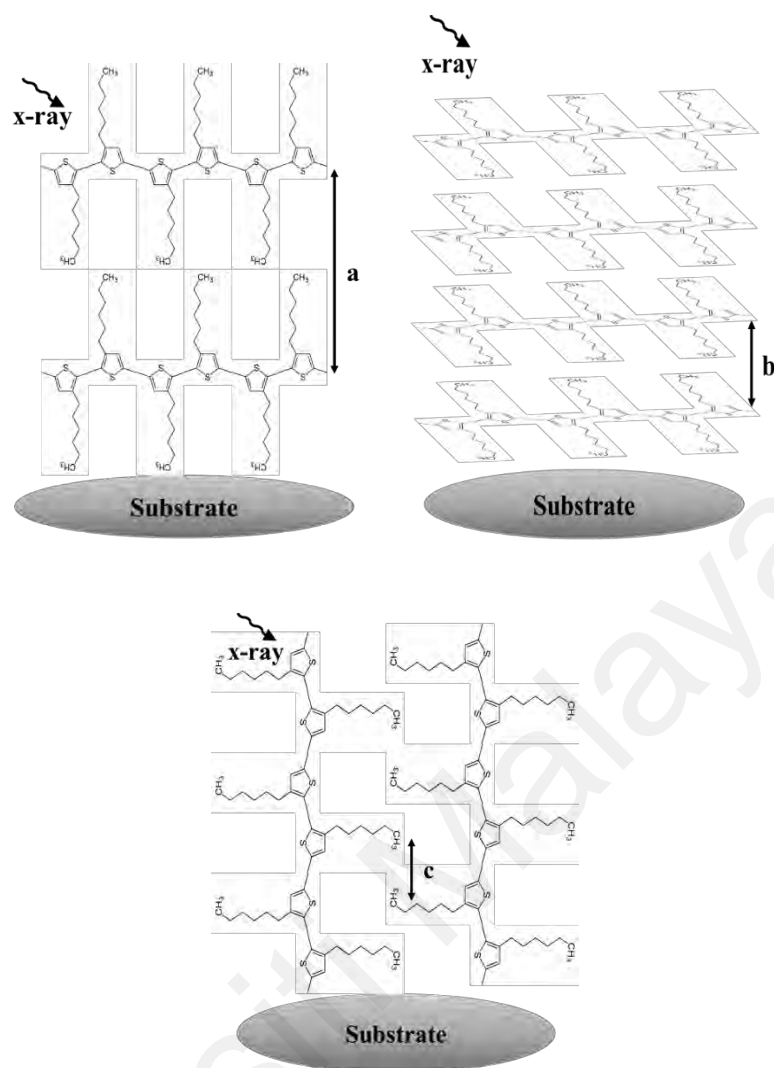


Figure 4.31: P3HT crystallites in the blend films with a-axis orientation where main chain parallel and side chain perpendicular to the substrate.

There is no polymer crystallites with *b*-axis or *c*-axis orientation can be detected since there is only a single peak is observed at $2\theta = 5.2^\circ$. There is no higher order of XRD peak found in the XRD spectra. This could be attributed to a lower ordering in the P3HT which may be caused by PC₆₁BM. As a consequence, the structure crystallinity in the blend is dominated by amorphous environment. It could be attributed to the aggregation of the PC₆₁BM which leads to increased disorder in the blend and decreases the P3HT crystallinity. The mean size of the P3HT crystallites can be evaluated using the Scherrer's relation:

$$L \sim \frac{0.9\lambda}{\Delta_{2\theta} \cos \theta} \quad (4.21)$$

Diffraction peak caused by PC₆₁BM crystallites was not detected in this XRD characterisation. It is believed that the formation of PC₆₁BM crystallites cannot occurred due to the disturbance of side chain of P3HT and P3HT crystallites (Erb et al., 2005). However, the peaks do not alter in any of the films after the acetic acid treatments. It shows that the treatment does not affect the molecular packing structure of P3HT:PC₆₁BM. This result commensurate the UV-Vis and Raman results in the previous sections.

4.10 Field Effect Scanning Electron Microscopy (FESEM) Measurements

The microscopic measurements were performed to visualize the effect of acid treatment on the surface morphology of the P3HT:PC₆₁BM active films. The Field Effect Scanning Electron Microscopy (FESEM) images of P3HT:PC₆₁BM organic thin films are displayed in Figure 4.32. The first two FESEM images reveal that the surface of the untreated and 5 % acetic acid treated active layer contains some particles-like features. Such particles could be associated with the impurities even after the polymer:fullerene derivative solution being filtered using a 0.20 µm nylon filter prior to the spin-coating process. Low photocurrent generation in the pristine sample as well as 5 % acid treated device (see Table 4.2), can be assigned to the formation of impurities in the active layer.

Commonly, the presence of impurities associate with higher resistance and barrier height in OSCs. Even a very small amount of impurities for example one part per one thousand in polymer bulk heterojunction solar cells, can change the electronic properties of the device such as reducing the J_{sc}, the V_{oc} and the FF of the device therefore leading to decrease in PCE (Sarah R. Cowan, Leong, Banerji, Dennler, & Heeger, 2011).

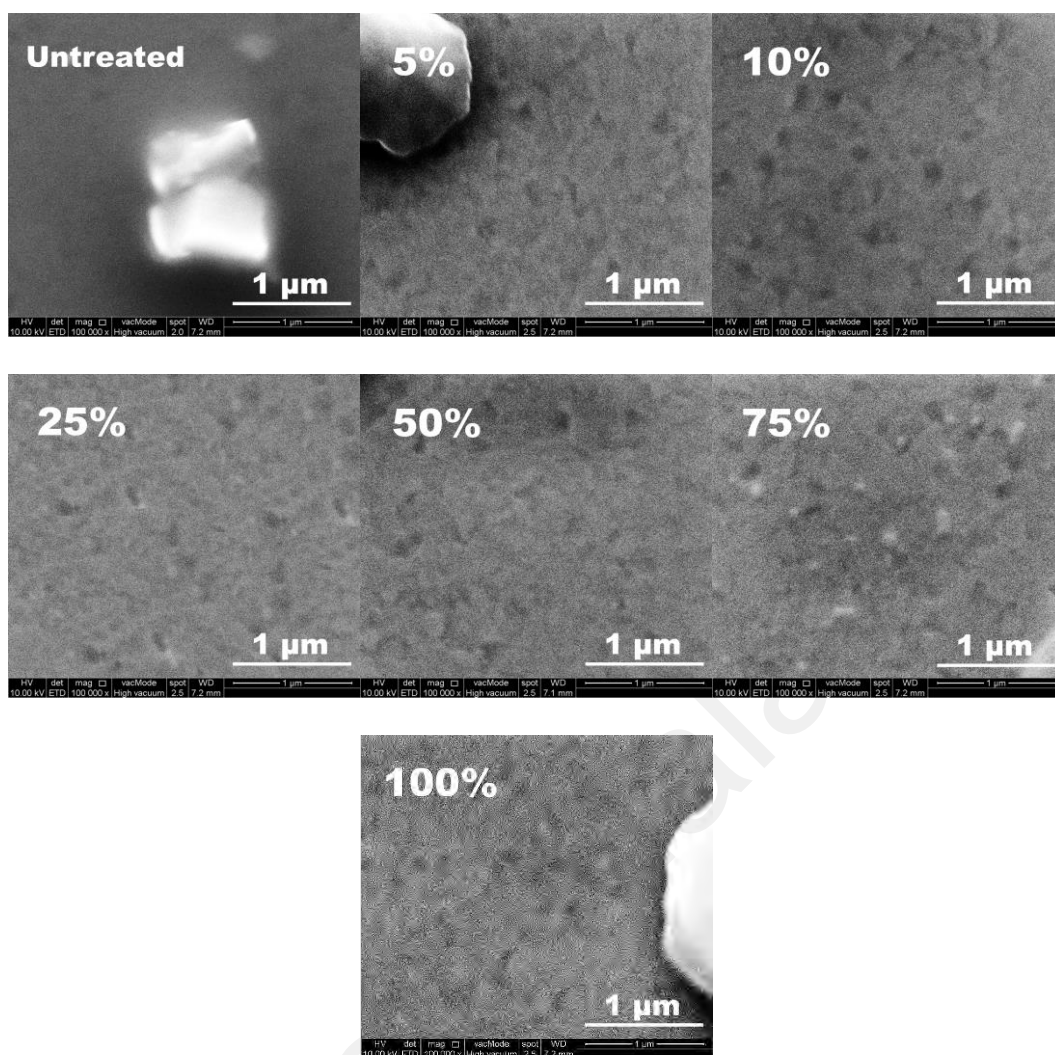


Figure 4.32: Field Effect Scanning Electron Microscopy (FESEM) images on the surface of untreated and acid treated P3HT:PC₆₁BM organic thin films. The bar-scale is 1 μm.

On the other hand, the impurity particles have been completely removed after the samples being treated with 10 %, 25 % and 50 % of acetic acid. From these images, it can be speculated that the etching effect of the acetic acid might not only created some cavities but at the same time the acetic acid might have dissolved the particles/impurities therefore purification on the active layer surface might have taken place. This speculation can be supported by the decrease of series resistance and barrier height of acetic acid solution treated devices.as have shown in the previous results.

Results in chapter 4.3, have shown that 50 % acetic acid solution is the optimum acid concentration to treat the OSC with highest J_{sc} and lowest R_s . The possible explanation is that the 50 % acetic acid solution consist of equally half of acetic acid molecules and half of water molecules. This combination created an effective and efficient working condition for the solution to remove the impurities where the function of acetic acid molecules is to dissolve the impurities while the water molecules were able to carry away the dissolved impurities from the device when spun away from the surface. More research works need to be done to prove this speculation in the future in order to get better insight of the purification mechanism of acetic acid molecules and water molecules remove the impurities.

From FESEM images in Figure 4.32, visible nanosize cavities on the surface of the active layer can be seen after the active layers being treated with acetic acid solutions of 10 % to 75 %. These cavities might have caused by the etching process of the acetic acid on the active layer and then increased the effective areas of the OSCs and slightly enhanced the performance. However, the enhancement caused by factor might insignificant.

4.11 Investigation of Degradation Process of the Fabricated Devices

This study was conducted for devices upon ageing process for a short period of time, which was 11 days. The reason for the short period was that the solar simulator (light source) was not in working order and needed to be sent to the manufacturer in the United State for repair in a very long period of time (more than a year). Hence, such issue has hampered the effort to pursue durability study in longer period.

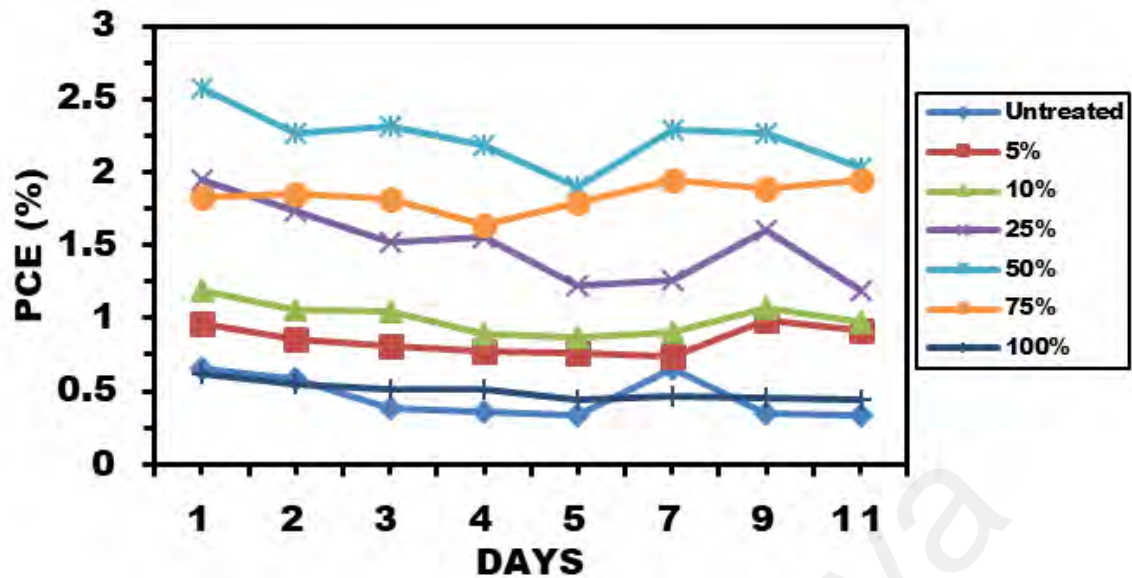


Figure 4.33: The performance of untreated and acid treated P3HT:PC₆₁BM organic solar cells for eleven days.

The performance of the untreated and acid treated P3HT:PC₆₁BM organic solar cells generally show slowly decreasing trends over the eleven days as shown in Figure 4.33. Even though the organic solar cells has been encapsulated, all devices degraded due to the degradation of the hole transport layer (PEDOT:PSS) as well as the active polymer:fullerene derivative layer on the device. Photodegradation of the organic-electrode interfaces which is trigger by the solar radiation and moisture adsorption by the hygroscopic PEDOT:PSS layer are associated with the degradation of hole transport layer (Ecker et al., 2011; Kawano et al., 2006; Voroshazi, Verreet, Aernouts, & Heremans, 2011). This degradation of PEDOT:PSS layer increases the resistance of the PEDOT:PSS/blend layer interface and in turn impaired the performance of the OSCs. There are studies showing that the effect of moisture/humidity on the PEDOT:PSS is to increase the resistance of the PEDOT:PSS/active layer interface, but not interfere with the charge mobility of the active layer. (Kawano et al., 2006). This PEDOT:PSS layer degradation appears to be spatially inhomogeneous which is related to the formation of insulating areas leading to decrease of device current and consequently the decrease

efficiency of the device. Studies show that the active layer itself is not inherently unstable or its degradation is caused by heat (Reese et al., 2008; Voroshazi et al., 2011).

Degradation can also be associated with oxidation of the electrode to a polymeric active layer. The decomposition of the cathode is mainly due to the oxidation of the metal. (Grossiord, Kroon, Andriessen, & Blom, 2012; Krebs, 2008; Nikiforov, Strzalka, & Darling, 2013). It is well known that water and oxygen can diffuse through the boundaries and pores of the metal and deform the inner surface of the electrode. The metal electrode reacts chemically with O_2 and H_2O . The latter leads to mechanical degradation and ultimately to the formation of cavities or isolation areas (leading to reduced charge transfer of the electrode/active layer interface) which can be associated with mechanical disintegration and ultimately delamination of electrode/active layer interface with longer exposure times (in the order of months) and/or mechanical stresses are considered. In both cases, the contact area of the metal/active layer interface decreases due to wear, which can be evidenced by a decrease in FF due to an increase in R_s . The degradation mechanisms usually degrades the quality of the interface between the electrode and the active layer (which corresponds to a loss in effective area) thus leading to a reduction of the charge transfer and extraction.

Choosing the appropriate electrode is able to reduce interfacial degradation, storing the active layer in dark and inert environment do not cause notable degradation and placing the active layer under constant illumination resulted only limited reduction in device performance. The studies reported that the importance of searching a moisture insensitive alternative to the PEDOT:PSS layer in OSCs. The development of such an alternative would significantly reduce the need for a water barrier layer for the encapsulation of OSCs and thus enable the production of stable OSCs on inexpensive and flexible substrates.

4.12 Versatility of Acetic Acid Treatment on Other Materials

A solution processable small organic material, namely 2, 2'-Bithiophene end-capped dihexyloxy phenylene pentamer (BHBT₂) was utilised for versatility study of acetic acid treatment. This small organic semiconductor was locally synthesized in the lab, by a postdoctoral researcher, via Williamson etherification, bromination and Suzuki coupling. The chemical structure of BHBT₂ (see inset in Figure 4.34) was confirmed by the characterization of Fourier Transform Infrared (FTIR) spectroscopy and Nuclear Magnetic Resonance (NMR) spectroscopy (Lim, Teh, et al., 2016).

Figure 4.34 shows the normalized absorption spectra of PC₆₁BM, BHBT₂ and BHBT₂:PC₆₁BM (ratio 1:1) blended thin films with their respective molecular structures. The BHBT₂ thin film exhibits UV absorption ranging from 315-360 nm with maximum absorption at 335 nm and a shoulder peak at 350 nm. The thin film also exhibit strong absorption in the visible wavelength (one characteristic that is favourable in OSCs) ranged within 360-500 nm where an absorption maximum at 430 nm and two shoulder peaks corresponded at 400 nm and 460 nm can be observed. The peak at 335 nm is associated to the π - π^* transition between thiophene and the peak at 430 nm is associated to bithiophene groups with 2, 5-bis(dihexyloxy)benzene moiety in the π -conjugated backbone (Lim, Teh, et al., 2016).

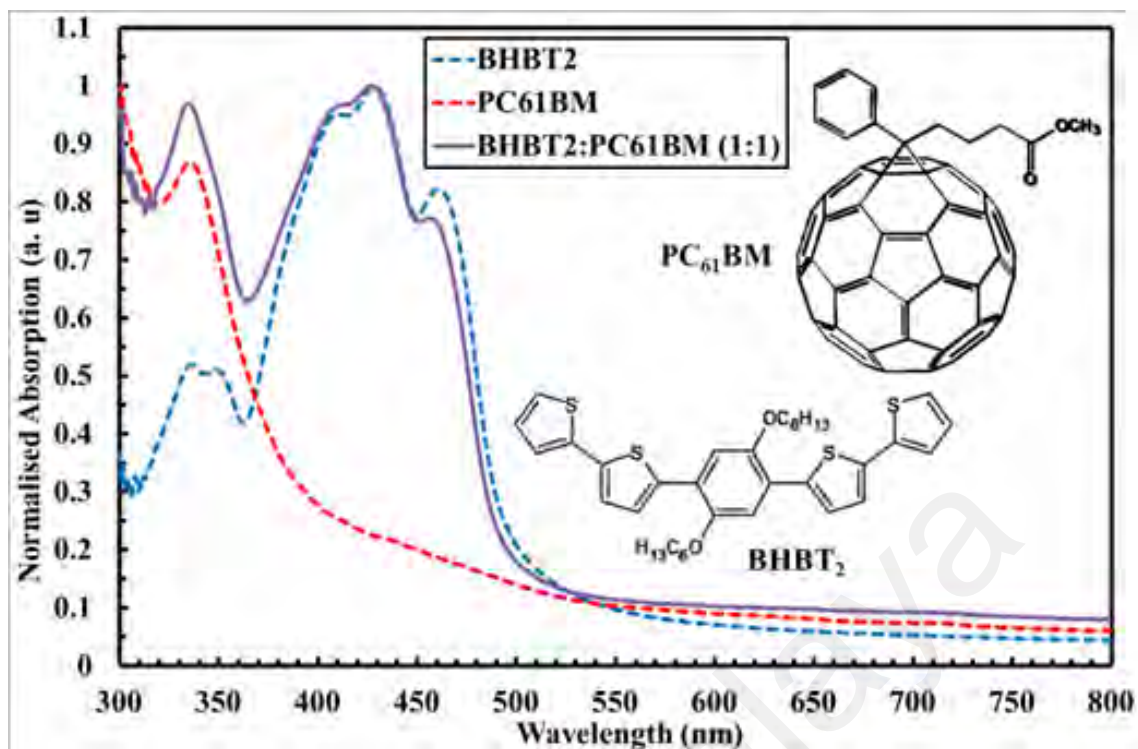


Figure 4.34: Normalized absorption spectra of PC₆₁BM, BHBT₂ and BHBT₂:PC₆₁BM thin films. (Inset) PC₆₁BM and BHBT₂ molecular structure.

The fabrication of bulk heterojunction ITO/PEDOT:PSS/BHBT₂:PC₆₁BM/Al organic solar cells was performed and the active layer was treated with acetic acid solution. The device structure is shown in Figure 4.35. The findings in the UV-Vis absorption spectroscopy shows that BHBT₂ thin film has superb absorption in UV wavelength (high energy region). The blended BHBT₂:PC₆₁BM thin film also displays indistinguishable absorption pattern as the BHBT₂ thin film implying that mixing of PC₆₁BM with BHBT₂ did not change the chemical structures of the PC₆₁BM and BHBT₂ in the bulk heterojunction thin film. PC₆₁BM which have strong absorption in the UV region wavelength range (300-350 nm) is able to help in compensating the weak absorption of BHBT₂ in this region. Therefore, the blended BHBT₂:PC₆₁BM thin film can contribute to photogeneration of the charge carriers in the complementary absorption spectrum from 300-500 nm making it a prominence materials as light harvesting devices. Furthermore,

PC₆₁BM can be easily handled with solution process and it is believed that its high mobility property can improve the performance of the fabricated OSCs.

The BHBT₂:PC₆₁BM photoactive layer is sandwiched between an aluminium (Al) cathode and a transparent indium tin oxide (ITO) anode. The device has the same structure as for the bulk heterojunction ITO/PEDOT:PSS/P3HT:PC₆₁BM/Al. The charges injection from the electrodes becomes the main source of dark current under reverse bias. Therefore, a thin layer of PEDOT:PSS layer is sandwiched between the ITO electrode and the photoactive layer to act as an electron blocking layer to reduce the dark current by minimising the charge carriers injection during reverse bias.

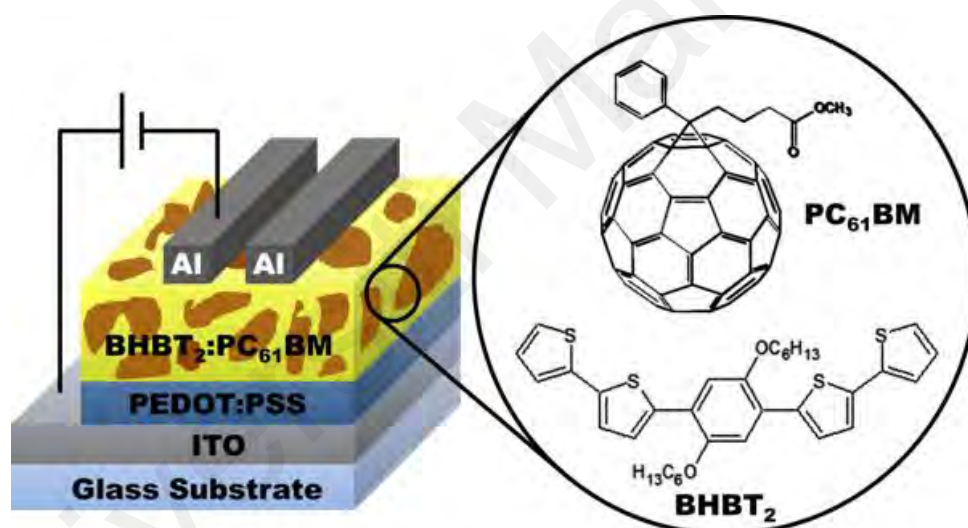


Figure 4.35: The diagram of device construction of ITO/PEDOT:PSS/BHBT₂:PC₆₁BM/Al organic solar cell and active layer consists of blended BHBT₂:PC₆₁BM.

Figure 4.36 illustrates the current-voltage (J-V) characteristics of untreated and acetic acid solution treated ITO/PEDOT:PSS/BHBT₂:PC₆₁BM/Al organic solar cells under 100 mW/cm² simulated sunlight by using AM 1.5 G solar illumination and dark condition with forward and reverse biases. The device is found to exhibit decent photovoltaic effect. The device shows a short-circuit current density, J_{sc} of 3.64 mA/cm² and open-circuit

voltage, V_{oc} of 0.64V for the untreated sample. Nonetheless, the achieved fill factor (FF) is merely 0.29 where it manages to bring about a photovoltaic conversion efficiency (PCE) of 0.68 %. The short-circuit current density, J_{sc} increased to 5.51 mA/cm² and open-circuit voltage, V_{oc} remains relatively unchanged with the value of 0.63V. Fill factor slightly dropped to 0.28 as the J_{sc} increased while the V_{oc} remain the same. Notably, the acetic acid solution treatment able to enhance the performance of this OSC almost 50 %. The findings indicate that acetic acid treatment on the active layer of organic solar cells not only applied to the P3HT:PC₆₁BM polymer:fullerene derivative system, but also can be utilised in small organic molecules. Hence the versatility of this acetic acid solution treatment, has been confirmed.

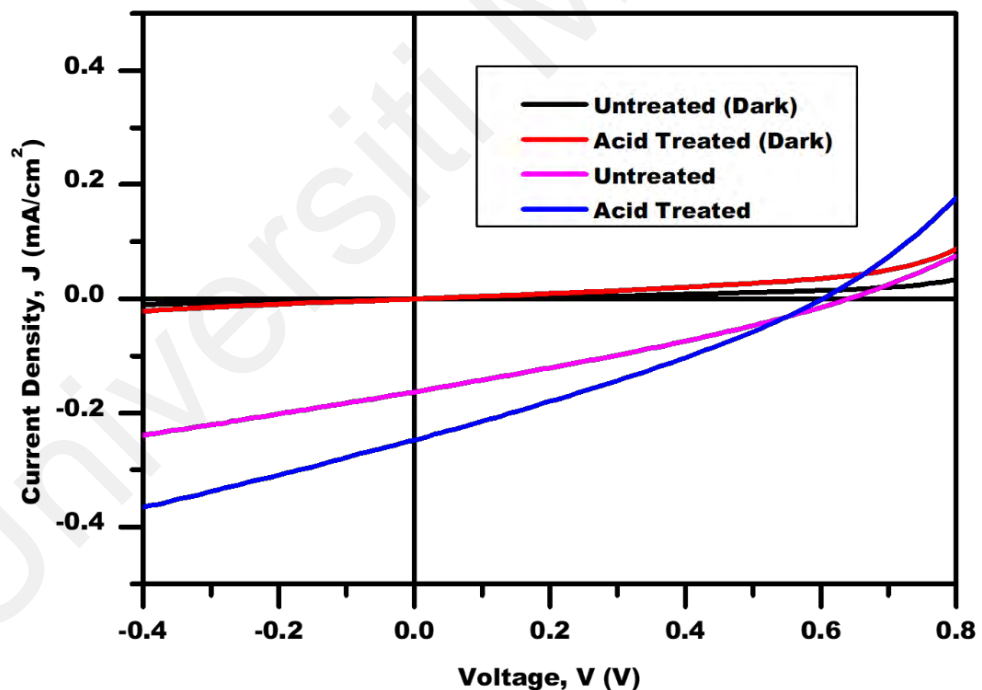


Figure 4.36: The J-V characteristics of the untreated and acetic acid treated ITO/PEDOT:PSS/BHBT₂:PC₆₁BM/Al organic solar cells.

Table 4.11: The summary of the performance for the untreated and acid solution treated ITO/PEDOT:PSS/BHBT₂:PC₆₁BM/Al organic solar cells.

BHBT ₂ : PC ₆₁ BM	Short Circuit Current Density, J _{sc} (mA/cm ²)	Open Circuit Voltage, V _{oc} (V)	Fill Factor, FF	Power conversion Efficiency, PCE (%)
Untreated	3.64	0.64	0.29	0.68
Acid Treated	5.51	0.63	0.28	0.97

Apparently, the enhancement is due to the drastic increase of J_{sc} of the treated device. Table 4.11 tabulates the performances of the untreated and acid treated BHBT₂:PC₆₁BM organic solar cells. The acetic acid solution treatment can be utilised and successfully enhanced the performance of this small molecule organic semiconductor solar cells. However, much more researches should be performed on other organic semiconductor systems so that a better conclusion can be made for the versatility of the acetic acid solution treatment on other organic semiconductor solar cells.

CHAPTER 5: CONCLUSION

5.1 Conclusion

The bulk heterojunction OSCs with the structure of ITO/PEDOT:PSS/P3HT:PC₆₁BM/Al (ratio of 1:1) were successfully fabricated. The pristine OSC that has gone through post-annealing process at 120 °C for 10 minutes exhibited photovoltaics effect with the performance of 0.53 % efficiency under AM 1.5 G 100 mW/cm² simulated solar illumination. This device was served as the control device. Diluted acetic acid solution with the concentration of 5 %, 10 %, 25 %, 50 %, 75 % and 100 % were used as the treatment mediums on the surface of photoactive layers of P3HT:PC₆₁BM. The treatment is effective, efficient, simple and inexpensive. No sophisticated or complex equipment/techniques are required for this acid solution treatment. The acid solution treatments were performed immediately once the P3HT:PC₆₁BM photoactive layer was spin coated. The same spin coating technique as P3HT:PC₆₁BM photoactive layer was used for the acid solution treatments. All the acid treated OSCs showed tremendous improvements on the performance efficiency. As high as 2.04 % of PCE has been observed in the OSC that gone through the 50 % acetic acid concentration treatment. Compared to the control device, this enhancement is more than three folds. Therefore, this new, uncomplicated and cost effective treatment process is a great potential candidate for the enhancement tool/technique for OSCs.

The optical, morphological, electrical characterisations such as UV-Vis spectroscopy, Raman spectroscopy, XRD, FESEM, I-V characterisations, etc. have been performed on the untreated and acid treated P3HT:PC₆₁BM thin films or OSCs to uncover the cause of the enhancement. Unfortunately, optical and morphological measurements do not reveal much useful information about the enhancement of the acetic acid solution treatment. It is the electrical measurements that give much insights of the charge transfer mechanism in the photoactive layer of P3HT:PC₆₁BM. The I-V curves of the OSCs disclosed a lot of

useful information on the electrical properties of the devices. The experimental results from the I-V characteristics under light illumination reveal that the J_{sc} increased drastically while R_s and R_{sh} decreased after the OSCs were treated with acetic acid solutions. The increment of J_{sc} and decrement of R_s make the enhancement of performance possible. However, the decrease in R_{sh} caused the FF to be dropped and this affected the performance of the OSCs to some extent. Further analysis of I-V curves under dark condition using Schottky diode model proves to be favourable as this method would be able to provide electrical properties such as ideality factor, R_s and Φ_{bo} that are essential to the behavior of the charge carriers/the charge transfer mechanism of the OSCs. Two new methods have been adopted to characterise the electrical properties of the OSCs: Cheung and Cheung's functions and Norde's function. These two methods are suitable to affirm the electrical properties determined from the I-V curves under light illumination and Schottky diode method. Through these methods, it is found that the acetic acid solutions are able to lower the barrier height of the OSCs hence the charge carriers' conduction is favourable. Consequently, the J_{sc} of the acid treated devices increased and the R_s decreased as well as gave rise to the performance enhancements of the OSCs.

The investigations of SCLC through semi-logarithmic J-V and double logarithmic graphs revealed distinct differences in the slopes of the OSCs' J-V curves under dark condition. The difference is due to the acid-treated P3HT:PC₆₁BM based devices present lower trap densities and better exciton dissociation compared to those of the untreated device. The V_{TFL} is decreased after the acetic acid treatment except for pure acetic acid concentration. The V_{TFL} becomes the lowest at 50 % acetic acid concentration. The concentration of traps, N_t can be estimated for the untreated and acetic acid treated devices by utilising V_{TFL} . The estimated N_t follows the same trend as V_{TFL} which is the minimum at 50 % acetic acid concentration. The acetic acid treated devices have lower V_{TFL} indicating the traps can be filled faster and causing the slope of the double-logarithmic of

the J-V curves to be lower. Fast filling of traps is the resultant of lower traps concentration in the acetic acid treated devices. This well explain the higher current that produced in the acetic acid treated OSC which has been observed in the J-V curve in chapter 4.3.

The FESEM images have showed that the etching effect of acetic acid has created cavities on the surface of the active layers causing the effective area to be increased. However, the performance enhancement caused by this factor is thought to be insignificant. The removal of particles/impurities from the surface of active layers by the dissolving ability of the acetic acid is speculated as the main reason of the performance enhancement of the OSCs. The concentration of 50 % acetic acid solution is the optimum solution concentration for this acetic acid treatment due an effective and efficient working condition has been created for the solution to dissolve the impurities (done by acetic acid molecules) and carried away the dissolved impurities from the device (done by water molecules) when spun away from the surface. More research works need to be done to prove this speculation in the future in order to get better insight of the purification mechanism of acetic acid molecules and water molecules remove the impurities.

The durability results show that even though the devices have been encapsulated, the performance degraded significantly within short period of time (11 days). Photodegradation of the organic-electrode interfaces which is trigger by the solar radiation and water adsorption by the hygroscopic PEDOT: PSS layer are thought to be the main causes of the degradation of performance of OSCs. The degradation of hole transport layer increases the resistance of the PEDOT:PSS/blend layer interface and impaired the performance of the OSCs. Further studies of searching appropriate alternative electrode which is humidity insensitive is able to reduce interfacial degradation which in turn would significantly facilitate the fabrication of stable OSCs on lower cost.

The application of acetic acid treatment on a solution processable small organic material, namely 2, 2'-Bithiophene end-capped dihexyloxy phenylene pentamer (BHBT₂) in the fabrication of bulk heterojunction ITO/PEDOT:PSS/BHBT₂:PC₆₁BM/Al organic solar cells was proved to be successful. However, much more researches should be performed on other organic semiconductor systems so that a better conclusion can be made for the versatility of the acetic acid solution treatment on other organic semiconductor solar cells.

The results of this research studies have shown that the acetic acid treatment is a potential revolutionary treatment method to increase the performance of the OSCs.

5.2 Future Works

In spite of the fact that the employment of the acetic acid solution treatment on the bulk heterojunction OSCs with the structure of ITO/PEDOT:PSS/P3HT:PC₆₁BM/Al has successfully enhanced the performance but more works need to carry out to investigate the mechanism in detail, stabilise this technique to a more stabilised development and further enhance the performance of the OSCs. Below are some suggestions that should be considered as future works:

1. Further investigation/analysis should be performed on the acid treated P3HT:PC₆₁BM thin films including (a) time resolved photoluminescence to investigate the charge carrier life-time; (b) XPS to find the charge binding energy and compare to the calculated values.
2. Durability of the acid treated OSCs with longer period (more than 3 months) should be studied to obtain a better view on the aging process of the devices with time.

3. The acid treatment approach may be utilised in other organic solar cell system, particularly newly synthesized materials.

Universiti Malaya

REFERENCES

- Aasmundtveit, K. E., Samuelsen, E. J., Guldstein, M., Steinsland, C., Flornes, O., Fagermo, C., . . . Ferrer, S. (2000). Structural anisotropy of poly (alkylthiophene) films. *Macromolecules*, 33(8), 3120-3127.
- Adams, W. G., & Day, R. E. (1877). IX. The action of light on selenium. *Philosophical Transactions of the Royal Society of London*, 167, 313-349.
- Aloui, W., Adhikari, T., Nunzi, J.-M., Bouazizi, A., & Khirouni, K. (2015). Effect of thermal annealing on the electrical properties of P3HT:PC70BM nanocomposites. *Materials Science in Semiconductor Processing*, 39, 575-581.
- Altan, H., Özer, M., & Ezgin, H. (2020). Investigation of electrical parameters of Au/P3HT:PCBM/n-6H-SiC/Ag Schottky barrier diode with different current conduction models. *Superlattices and Microstructures*, 146, 106658.
- Aziz, F., Ahmad, Z., Abdullah, S. M., Sulaiman, K., & Sayyad, M. H. (2015). Photovoltaic effect in single-junction organic solar cell fabricated using vanadyl phthalocyanine soluble derivative. *Pigment & Resin Technology*, 44(1), 26-32.
- Campoy-Quiles, M., Ferenczi, T., Agostinelli, T., Etchegoin, P. G., Kim, Y., Anthopoulos, T. D., . . . Nelson, J. (2008). Morphology evolution via self-organization and lateral and vertical diffusion in polymer:fullerene solar cell blends. *Nature Materials*, 7(2), 158-164.
- Chen, D., Nakahara, A., Wei, D., Nordlund, D., & Russell, T. P. (2011). P3HT/PCBM bulk heterojunction organic photovoltaics: correlating efficiency and morphology. *Nano Letters*, 11(2), 561-567.
- Cheng, C.-E., Pei, Z., Hsu, C.-C., Chang, C.-S., & Shih-Sen Chien, F. (2014). Hole transit in P3HT:PCBM solar cells with embedded gold nanoparticles. *Solar Energy Materials and Solar Cells*, 121, 80-84.
- Cheng, Y.-T., Ho, J.-J., Wang, C.-K., Lee, W., Lu, C.-C., Yau, B.-S., . . . Wang, K. L. (2010). Improvement of organic solar cells by flexible substrate and ITO surface treatments. *Applied Surface Science*, 256(24), 7606-7611.
- Cheung, S. K., & Cheung, N. W. (1986). Extraction of Schottky diode parameters from forward current - voltage characteristics. *Applied Physics Letters*, 49(2), 85-87.
- Chi, D., Qu, S., Wang, Z., & Wang, J. (2014). High efficiency P3HT:PCBM solar cells with an inserted PCBM layer. *Journal of Materials Chemistry C*, 2(22), 4383-4387.
- Cowan, S. R., Leong, W. L., Banerji, N., Dennler, G., & Heeger, A. J. (2011). Identifying a threshold impurity level for organic solar cells: Enhanced first-order recombination via well-defined PC84BM traps in organic bulk heterojunction solar cells. *Advanced Functional Materials*, 21(16), 3083-3092.

- Cowan, S. R., Roy, A., & Heeger, A. J. (2010). Recombination in polymer-fullerene bulk heterojunction solar cells. *Physical Review B*, 82(24), 245207.
- Dang, M. T., Hirsch, L., & Wantz, G. (2011). P3HT:PCBM, best seller in polymer photovoltaic research. *Advanced Materials*, 23(31), 3597-3602.
- Devižis, A., Hertel, D., Meerholz, K., Gulbinas, V., & Moser, J. E. (2014). Time-independent, high electron mobility in thin PC61BM films: Relevance to organic photovoltaics. *Organic Electronics*, 15(12), 3729-3734.
- Dey, A., Jana, R., Dhar, J., Das, P., & Ray, P. P. (2018). Gaussian distribution of inhomogeneous barrier height of Al/ZnS/ITO Schottky barrier diodes. *Materials Today: Proceedings*, 5(3, Part 3), 9958-9964.
- Dittmer, J. J., Lazzaroni, R., Leclère, P., Moretti, P., Granström, M., Petritsch, K., . . . Holmes, A. B. (2000). Crystal network formation in organic solar cells. *Solar Energy Materials and Solar Cells*, 61(1), 53-61.
- Ecker, B., Nolasco, J. C., Pallarés, J., Marsal, L. F., Posdorfer, J., Parisi, J., & von Hauff, E. (2011). Degradation effects related to the hole transport layer in organic solar cells. *Advanced Functional Materials*, 21(14), 2705-2711.
- Erb, T., Zhokhavets, U., Gobsch, G., Raleva, S., Stühn, B., Schilinsky, P., . . . Brabec, C. J. (2005). Correlation between structural and optical properties of composite polymer/fullerene films for organic solar cells. *Advanced Functional Materials*, 15(7), 1193-1196.
- Friedel, B., Keivanidis, P. E., Brenner, T. J. K., Abrusci, A., McNeill, C. R., Friend, R. H., & Greenham, N. C. (2009). Effects of layer thickness and annealing of PEDOT:PSS layers in organic photodetectors. *Macromolecules*, 42(17), 6741-6747.
- Gaspari, F., & Quaranta, S. (2018). 2.5 PV Materials. In I. Dincer (Ed.), *Comprehensive Energy Systems* (pp. 117-149). Oxford: Elsevier.
- González, D. M., Körstgens, V., Yao, Y., Song, L., Santoro, G., Roth, S. V., & Müller-Buschbaum, P. (2015). Improved power conversion efficiency of P3HT:PCBM organic solar cells by strong spin-orbit coupling-induced delayed fluorescence. *Advanced Energy Materials*, 5(8), 1401770.
- Green, M. A. (2002). Photovoltaic principles. *Physica E: Low-dimensional Systems and Nanostructures*, 14(1-2), 11-17.
- Grossiord, N., Kroon, J. M., Andriessen, R., & Blom, P. W. M. (2012). Degradation mechanisms in organic photovoltaic devices. *Organic Electronics*, 13(3), 432-456.
- Güllü, Ö., Aydoğan, Ş., & Türüt, A. (2008). Fabrication and electrical characteristics of Schottky diode based on organic material. *Microelectronic Engineering*, 85(7), 1647-1651.

- Guo, T.-F., Wen, T.-C., L'Vovich Pakhomov, G., Chin, X.-G., Liou, S.-H., Yeh, P.-H., & Yang, C.-H. (2008). Effects of film treatment on the performance of poly(3-hexylthiophene)/soluble fullerene-based organic solar cells. *Thin Solid Films*, 516(10), 3138-3142.
- Halls, J. J. M., Walsh, C. A., Greenham, N. C., Marseglia, E. A., Friend, R. H., Moratti, S. C., & Holmes, A. B. (1995). Efficient photodiodes from interpenetrating polymer networks. *Nature*, 376(6540), 498-500.
- Hashimoto, Y., & Hamagaki, M. (2006). Effect of oxygen plasma treatment of indium tin oxide for organic solar cell. *Electrical Engineering in Japan*, 154(4), 1-7.
- He, D., Du, X., Zhang, W., Xiao, Z., & Ding, L. (2013). Improving the stability of P3HT/PC61BM solar cells by a thermal crosslinker. *Journal of Materials Chemistry A*, 1(14), 4589-4594.
- Hiramoto, M., Fujiwara, H., & Yokoyama, M. (1991). Three - layered organic solar cell with a photoactive interlayer of codeposited pigments. *Applied Physics Letters*, 58(10), 1062-1064.
- Hu, T., Zhang, F., Xu, Z., Zhao, S., Yue, X., & Yuan, G. (2009). Effect of UV–ozone treatment on ITO and post-annealing on the performance of organic solar cells. *Synthetic Metals*, 159(7), 754-756.
- Hu, Z., Zhang, J., & Zhu, Y. (2014). Effects of solvent-treated PEDOT:PSS on organic photovoltaic devices. *Renewable Energy*, 62, 100-105.
- Jang, H., Kim, M. S., Jang, W., Son, H., Wang, D. H., & Kim, F. S. (2020). Highly conductive PEDOT:PSS electrode obtained via post-treatment with alcoholic solvent for ITO-free organic solar cells. *Journal of Industrial and Engineering Chemistry*, 86, 205-210.
- Kadem, B., Fakher Alfahed, R. K., Al-Asadi, A. S., & Badran, H. A. (2020). Morphological, structural, optical, and photovoltaic cell of copolymer P3HT:ICBA and P3HT:PCBM. *Optik*, 204, 164153.
- Kadem, B., Hassan, A., & Cranton, W. (2016). Efficient P3HT:PCBM bulk heterojunction organic solar cells; effect of post deposition thermal treatment. *Journal of Materials Science: Materials in Electronics*, 27(7), 7038-7048.
- Kawano, K., Pacios, R., Poplavskyy, D., Nelson, J., Bradley, D. D. C., & Durrant, J. R. (2006). Degradation of organic solar cells due to air exposure. *Solar Energy Materials and Solar Cells*, 90(20), 3520-3530.
- Kearns, D., & Calvin, M. (1958). Photovoltaic effect and photoconductivity in laminated organic systems. *The Journal of Chemical Physics*, 29(4), 950-951.
- Khan, M. T., Bhargav, R., Kaur, A., Dhawan, S. K., & Chand, S. (2010). Effect of cadmium sulphide quantum dot processing and post thermal annealing on P3HT/PCBM photovoltaic device. *Thin Solid Films*, 519(3), 1007-1011.

- Kılıçoğlu, T. (2008). Effect of an organic compound (Methyl Red) interfacial layer on the calculation of characteristic parameters of an Al/Methyl Red/p-Si sandwich Schottky barrier diode. *Thin Solid Films*, 516(6), 967-970.
- Kim, Y., Ballantyne, A. M., Nelson, J., & Bradley, D. D. C. (2009). Effects of thickness and thermal annealing of the PEDOT:PSS layer on the performance of polymer solar cells. *Organic Electronics*, 10(1), 205-209.
- Kim, Y., Choulis, S. A., Nelson, J., Bradley, D. D. C., Cook, S., & Durrant, J. R. (2005). Device annealing effect in organic solar cells with blends of regioregular poly(3-hexylthiophene) and soluble fullerene. *Applied Physics Letters*, 86(6), 063502.
- Kim, Y., Cook, S., Tuladhar, S. M., Choulis, S. A., Nelson, J., Durrant, J. R., . . . Ree, M. (2006). A strong regioregularity effect in self-organizing conjugated polymer films and high-efficiency polythiophene:fullerene solar cells. *Nature Materials*, 5, 197-203.
- Kippelen, B., & Bredas, J.-L. (2009). Organic photovoltaics. *Energy & Environmental Science*, 2(3), 251-261.
- Kırsoy, A., Ahmetoglu, M., Asimov, A., & Kucur, B. (2015). The electrical properties of Au/P3HT/n-GaAs Schottky barrier diode. *Acta Physica Polonica A*, 128(2B), B-170.
- Krebs, F. C. (2008). Air stable polymer photovoltaics based on a process free from vacuum steps and fullerenes. *Solar Energy Materials and Solar Cells*, 92(7), 715-726.
- Kumari, T., Lee, S. M., Kang, S.-H., Chen, S., & Yang, C. (2017). Ternary solar cells with a mixed face-on and edge-on orientation enable an unprecedented efficiency of 12.1%. *Energy & Environmental Science*, 10(1), 258-265.
- Lampert, M. A. (1956). Simplified theory of space-charge-limited currents in an insulator with traps. *Physical Review*, 103(6), 1648-1656.
- Laquai, F., Andrienko, D., Mauer, R., & Blom, P. W. (2015). Charge carrier transport and photogeneration in P3HT: PCBM photovoltaic blends. *Macromolecular rapid communications*, 36(11), 1001-1025.
- Lim, L. W., Aziz, F., Muhammad, F. F., Supangat, A., & Sulaiman, K. (2016). Electrical properties of Al/PTB7-Th/n-Si metal-polymer-semiconductor Schottky barrier diode. *Synthetic Metals*, 221, 169-175.
- Lim, L. W., Teh, C. H., Daik, R., Sarih, N. M., Mat Teridi, M. A., Muhammad, F. F., & Sulaiman, K. (2016). Synthesis and characterization of 2,2'-bithiophene end-capped dihexyloxy phenylene pentamer and its application in a solution-processed organic ultraviolet photodetector. *RSC Advances*, 6(66), 61848-61859.
- Liu, Q., Jiang, Y., Jin, K., Qin, J., Xu, J., Li, W., . . . Ding, L. (2020). 18% Efficiency organic solar cells. *Science Bulletin*, 65(4), 272-275.

- Liu, T., Yang, T., Ma, R., Zhan, L., Luo, Z., Zhang, G., . . . Yan, H. (2021). 16% efficiency all-polymer organic solar cells enabled by a finely tuned morphology via the design of ternary blend. *Joule*, 5(4), 914-930.
- Liu, X., Wen, W., & Bazan, G. C. (2012). Post - deposition treatment of an arylated - carbazole conjugated polymer for solar cell fabrication. *Advanced Materials*, 24(33), 4505-4510.
- Lou, Y., Wang, Z., Naka, S., & Okada, H. (2012). Charge transport characteristics in P3HT:PCBM organic blends under illumination: Influence of metal work functions. *Chemical Physics Letters*, 529, 64-68.
- Luo, J., Billep, D., Waechtler, T., Otto, T., Toader, M., Gordan, O., . . . Gessner, T. (2013). Enhancement of the thermoelectric properties of PEDOT:PSS thin films by post-treatment. *Journal of Materials Chemistry A*, 1(26), 7576-7583.
- Ma, W., Yang, C., Gong, X., Lee, K., & Heeger, A. J. (2005). Thermally stable, efficient polymer solar cells with nanoscale control of the interpenetrating network morphology. *Advanced Functional Materials*, 15(10), 1617-1622.
- Mark, P., & Helfrich, W. (1962). Space - charge - limited currents in organic crystals. *Journal of Applied Physics*, 33(1), 205-215.
- Mauer, R., Kastler, M., & Laquai, F. (2010). The impact of polymer regioregularity on charge transport and efficiency of P3HT:PCBM photovoltaic devices. *Advanced Functional Materials*, 20(13), 2085-2092.
- Meng, L., Zhang, Y., Wan, X., Li, C., Zhang, X., Wang, Y., . . . Chen, Y. (2018). Organic and solution-processed tandem solar cells with 17.3% efficiency. *Science*, 361(6407), 1094-1098.
- Mihailetchi, V. D., Wildeman, J., & Blom, P. W. M. (2005). Space-charge limited photocurrent. *Physical Review Letters*, 94(12), 126602.
- Moiz, S. A., Alahmadi, A. N. M., & Karimov, K. S. (2020). Improved organic solar cell by incorporating silver nanoparticles embedded polyaniline as buffer layer. *Solid-State Electronics*, 163, 107658.
- Moore, W., & Silver, M. (1960). Generation of free carriers in photoconducting anthracene. I. *The Journal of Chemical Physics*, 33(6), 1671-1676.
- Mott, N. F., & Gurney, R. W. (1948). *Electronic processes in ionic crystals*, by N.F. Mott and R.W. Gurney. by N.F. Mott and R.W. Gurney. Oxford: Clarendon Press.
- Nikiforov, M. P., Strzalka, J., & Darling, S. B. (2013). Delineation of the effects of water and oxygen on the degradation of organic photovoltaic devices. *Solar Energy Materials and Solar Cells*, 110, 36-42.
- Nikitenko, V. R., Heil, H., & Seggern, H. v. (2003). Space-charge limited current in regioregular poly-3-hexyl-thiophene. *Journal of Applied Physics*, 94(4), 2480-2485.

- Norde, H. (1979). A modified forward I - V plot for Schottky diodes with high series resistance. *Journal of Applied Physics*, 50(7), 5052-5053.
- O'Regan, B., & Grätzel, M. (1991). A low-cost, high-efficiency solar cell based on dye-sensitized colloidal TiO₂ films. *Nature*, 353(6346), 737-740.
- Oseni, S. O., Kaviyarasu, K., Maaza, M., Sharma, G., Pellicane, G., & Mola, G. T. (2018). ZnO:CNT assisted charge transport in PTB7:PCBM blend organic solar cell. *Journal of Alloys and Compounds*, 748, 216-222.
- Ostroverkhova, O. (2018). *Handbook of Organic Materials for Electronic and Photonic Devices*: Woodhead Publishing.
- Park, S. H., Roy, A., Beaupré, S., Cho, S., Coates, N., Moon, J. S., . . . Heeger, A. J. (2009). Bulk heterojunction solar cells with internal quantum efficiency approaching 100%. *Nature photonics*, 3(5), 297-302.
- Proctor, C. M., Kuik, M., & Nguyen, T.-Q. (2013). Charge carrier recombination in organic solar cells. *Progress in Polymer Science*, 38(12), 1941-1960.
- Qi, B., & Wang, J. (2013). Fill factor in organic solar cells. *Physical Chemistry Chemical Physics*, 15(23), 8972-8982.
- Reese, M. O., Morfa, A. J., White, M. S., Kopidakis, N., Shaheen, S. E., Rumbles, G., & Ginley, D. S. (2008). Pathways for the degradation of organic photovoltaic P3HT:PCBM based devices. *Solar Energy Materials and Solar Cells*, 92(7), 746-752.
- Rehman, M. M., Siddiqui, G. U., Gul, J. Z., Kim, S.-W., Lim, J. H., & Choi, K. H. (2016). Resistive switching in all-printed, flexible and hybrid MoS₂-PVA nanocomposite based memristive device fabricated by reverse offset. *Scientific Reports*, 6(1), 1-10.
- Rehman, M. M., Yang, B.-S., Yang, Y.-J., Karimov, K. S., & Choi, K. H. (2017). Effect of device structure on the resistive switching characteristics of organic polymers fabricated through all printed technology. *Current Applied Physics*, 17(4), 533-540.
- Sariciftci, N. S., Braun, D., Zhang, C., Srdanov, V. I., Heeger, A. J., Stucky, G., & Wudl, F. (1993). Semiconducting polymer - buckminsterfullerene heterojunctions: Diodes, photodiodes, and photovoltaic cells. *Applied Physics Letters*, 62(6), 585-587.
- Schauer, F. (2005). Space-charge-limited currents for organic solar cells optimisation. *Solar Energy Materials and Solar Cells*, 87(1), 235-250.
- Shao, M., Keum, J., Chen, J., He, Y., Chen, W., Browning, J. F., . . . Xiao, K. (2014). The isotopic effects of deuteration on optoelectronic properties of conducting polymers. *Nature Communications*, 5(1), 1-11.

- Shrotriya, V., Ouyang, J., Tseng, R. J., Li, G., & Yang, Y. (2005). Absorption spectra modification in poly(3-hexylthiophene):methanofullerene blend thin films. *Chemical Physics Letters*, 411(1), 138-143.
- Smith, W. (1873). The action of light on selenium. *Telegraph Engineers, Journal of the Society of*, 2(4), 31-33.
- Spanggaard, H., & Krebs, F. C. (2004). A brief history of the development of organic and polymeric photovoltaics. *Solar Energy Materials and Solar Cells*, 83(2), 125-146.
- Taibi, I., Belghachi, A., & Abid, H. (2016). Effect of trapping and temperature on the performance of P3HT:PCBM organic solar cells. *Optik*, 127(20), 8592-8599.
- Tang, C. W. (1986). Two - layer organic photovoltaic cell. *Applied Physics Letters*, 48(2), 183-185.
- Triyana, K., Yasuda, T., Fujita, K., & Tsutsui, T. (2005). Tandem-type organic solar cells by stacking different heterojunction materials. *Thin Solid Films*, 477(1), 198-202.
- Tüzün Özmen, Ö. (2014). Effects of PCBM concentration on the electrical properties of the Au/P3HT:PCBM/n-Si (MPS) Schottky barrier diodes. *Microelectronics Reliability*, 54(12), 2766-2774.
- Tüzün Özmen, Ö., & Yağlıoğlu, E. (2014). Electrical and interfacial properties of Au/P3HT:PCBM/n-Si Schottky barrier diodes at room temperature. *Materials Science in Semiconductor Processing*, 26, 448-454.
- Vandewal, K., Himmelberger, S., & Salbeck, J. (2013). Structural factors that affect the performance of organic bulk heterojunction solar cells. *Macromolecules*, 46(16), 6379-6387.
- Vanlaeke, P., Swinnen, A., Haeldermans, I., Vanhoyland, G., Aernouts, T., Cheyns, D., . . . Manca, J. V. (2006). P3HT/PCBM bulk heterojunction solar cells: Relation between morphology and electro-optical characteristics. *Solar Energy Materials and Solar Cells*, 90(14), 2150-2158.
- Veysel Tunc, A., De Sio, A., Riedel, D., Deschler, F., Da Como, E., Parisi, J., & von Hauff, E. (2012). Molecular doping of low-bandgap-polymer:fullerene solar cells: Effects on transport and solar cells. *Organic Electronics*, 13(2), 290-296.
- Voroshazi, E., Verreet, B., Aernouts, T., & Heremans, P. (2011). Long-term operational lifetime and degradation analysis of P3HT:PCBM photovoltaic cells. *Solar Energy Materials and Solar Cells*, 95(5), 1303-1307.
- Wilken, S., Sandberg, O. J., Scheunemann, D., & Österbacka, R. (2020). Watching space charge build up in an organic solar cell. *Solar RRL*, 4(3), 1900505.
- Xiao, J., Jia, X. e., Duan, C., Huang, F., Yip, H.-L., & Cao, Y. (2021). Surpassing 13% efficiency for polythiophene organic solar cells processed from nonhalogenated solvent. *Advanced Materials*, 33(25), 2008158.